A NEW WIND-TUNNEL TECHNIQUE FOR THE MEASUREMENT OF VARIOUS AIRCRAFT STABILITY DERIVATIVES

A Thesis

Presented to

the Faculty of the Department of Engineering

University of Virginia

In Partial Fulfillment

of the Requirements for the Degree

Master of Applied Mechanics

by

Irving Abel

June 1968

APPROVAL SHEET

This thesis is submitted in partial fulfillment of

the requirements for the degree of

Master of Applied Mechanics

_____

Author

Approved:

_____

Faculty Advisor

_____

Dean, School of Engineering
and Applied Science

June 1968

TABLE OF CONTENTS

ABSTRACT

A new wind-tunnel technique for measuring various aerodynamic derivatives of an aeroelastic model is presented. The technique applies free-flight procedures to a model flown in the wind tunnel on the two-cable-mount system. The complete equations of motion are presented.

In the case of longitudinal motion, it is theoretically possible to uniquely determine each of the aerodynamic derivatives by measuring the model response to a steady-state sinusoidal oscillation of the horizontal tail. A comparison between free-flight and wind-tunnel equations shows that, due to the added mount system restraints, the equations can be solved for each derivative uniquely. However, introduction of an error into the model response investigated caused the solution to become ill-conditioned, resulting in equations similar to those used for determining the derivatives in free flight.

In the lateral equations of motion, a basic free-flight assumption of single-degree-of-freedom response in roll allows the experimental verification of the dynamic approach to derivative measurements. Experimental results obtained on an aeroelastically scaled model, tested both statically and dynamically in the wind tunnel, verify the application of this new testing procedure.

ACKNOWLEDGMENTS

The author wishes to express his appreciation to the many people who have contributed to this study. The research was supported by his employer, the National Aeronautics and Space Administration. Gratitude is expressed to his supervisors in the Aeroelasticity Branch, Dynamic Loads Division, for making available time and support for this work.

The advice and counsel of Professor R. T. Eppink has been of special value. The author wishes to thank his many colleagues in the Aeroelasticity Branch for their helpful suggestions.

Appreciation is expressed to Rossalyn Hampton, Edna Davidson, and Kay Eggleston for their care in typing the draft and final versions of the manuscript.

Finally, the author is pleased to acknowledge the support and encouragement of his wife, Susan, during the time it has taken to complete this work.

LIST OF FIGURES

LIST OF TABLES

LIST OF SYMBOLS

a	horizontal distance between model center of gravity and outer cable-tangency point on rear pulleys
b	wing span
$\bar{c}$	mean aerodynamic chord
C_D	drag coefficient, $\frac{\text{Drag}}{qS}$
C_l	rolling-moment coefficient, $\frac{\text{Rolling moment}}{qSb}$
C_L	lift coefficient, $\frac{\text{Lift}}{qS}$
C_{l_δ}	$\frac{\partial C_l}{\partial \delta_A}$
C_{L_δ}	$\frac{\partial C_L}{\partial \delta}$
C_m	pitching-moment coefficient, $\frac{\text{Pitching moment}}{qS\bar{c}}$
C_{m_δ}	$\frac{\partial C_m}{\partial \delta}$
C_n	yawing-moment coefficient, $\frac{\text{Yawing moment}}{qSb}$
C_y	side-force coefficient, $\frac{\text{Side force}}{qS}$
d	horizontal distance between model plane of symmetry and outer cable-tangency point on rear pulleys
e	horizontal distance between model center of gravity and outer cable-tangency point on front pulleys

g	acceleration due to gravity
h	vertical distance between model center of gravity and outer cable-tangency point on front pulleys
I_X, I_Y, I_Z	roll, pitch, yaw moment of inertia about x, y, z axes, respectively
I_{XZ}	product of inertia
K_{ij}	spring constant of mount support relating a force or moment in mode i due to a displacement in mode j
L, M, N	roll, pitch, and yaw moments about x, y, and z axes, respectively
$\bar{L}_A, \bar{M}_A, \bar{N}_A$	roll, pitch, and yaw aerodynamic moments
L_R, L_F	length of rear and forward cables, respectively, from wall attachment point to outer cable-tangency point on pulleys
L_t	distance from airplane center of gravity to tail aerodynamic center
m	mass of model including pulleys
q	dynamic pressure, $\frac{1}{2}\rho U^2$
S	wing area
T_R, T_F	support cable tension in rear and front cables, respectively
U	wind-tunnel flow velocity
$\vec{V}$	relative wind vector
x, y, z	displacement coordinates of model center of gravity
X, Y, Z	external forces on model in x, y, z coordinate directions, respectively

$\bar{Y}_A, \bar{Z}_A$	side and vertical translation aerodynamic forces, respectively
α	angle of attack, $\bar{\theta} + \frac{\dot{z}}{U}$
$\alpha_1, \alpha_2, \alpha_3$	phase angle between aileron displacement and roll, yaw, and side translation, respectively
β	angle of sideslip, $\frac{\dot{y}}{U} - \psi$
β_F	angle in vertical plane between x axis and forward cables
β_R	angle in horizontal plane between x axis and rear cables
δ	horizontal tail angle perturbation
δ_o	horizontal tail dynamic amplitude
δ_A	aileron angle
ζ_i	effective viscous damping ratio in mode i
θ	pitch angle perturbation about trim
θ_t	pitch angle for trim flight
$\bar{\theta}$	$\theta_t + \theta$, total pitch angle
ρ	mass density of wind-tunnel test medium
ϕ	roll angle
ϕ_1, ϕ_2	phase angle between tail forcing function and translation, pitch, respectively
ψ	yaw angle
ω	circular frequency

Aerodynamic derivative notation:

$$C_{L_\alpha} = \frac{\partial C_L}{\partial \alpha} \qquad C_{m_\alpha} = \frac{\partial C_m}{\partial \alpha} \qquad C_{m_{\dot{\alpha}}} = \frac{\partial C_m}{\partial\left(\frac{\dot{\alpha}\bar{c}}{2U}\right)}$$

$$C_{m_{\dot{\theta}}} = \frac{\partial C_m}{\partial\left(\frac{\dot{\theta}\bar{c}}{2U}\right)} \qquad C_{l_\beta} = \frac{\partial C_l}{\partial \beta} \qquad C_{y_\beta} = \frac{\partial C_y}{\partial \beta}$$

$$C_{n_\beta} = \frac{\partial C_n}{\partial \beta} \qquad C_{l_p} = \frac{\partial C_l}{\partial\left(\frac{\dot{\phi}b}{2U}\right)} \qquad C_{y_p} = \frac{\partial C_y}{\partial\left(\frac{\dot{\phi}b}{2U}\right)}$$

$$C_{n_p} = \frac{\partial C_n}{\partial\left(\frac{\dot{\phi}b}{2U}\right)} \qquad C_{l_r} = \frac{\partial C_l}{\partial\left(\frac{\dot{\psi}b}{2U}\right)} \qquad C_{y_r} = \frac{\partial C_y}{\partial\left(\frac{\dot{\psi}b}{2U}\right)}$$

$$C_{n_r} = \frac{\partial C_n}{\partial\left(\frac{\dot{\psi}b}{2U}\right)}$$

CHAPTER I

INTRODUCTION

In the study of aircraft stability and control a knowledge of the aerodynamic characteristics of the aircraft is of basic importance. The aerodynamic characteristics of a flexible airplane are difficult to measure or predict analytically, especially at transonic speeds. The purpose of this thesis is to present a new wind-tunnel testing technique for the measurement of certain aircraft aerodynamic characteristics known as the aerodynamic stability derivatives. An aerodynamic stability derivative indicates the rate of change of a force or moment acting on an airplane with the motion or variable causing the force or moment.

Structural components of an aircraft are often flexible enough to be considered as nonrigid. That is, such aeroelastic phenomena as flutter, divergence, and control surface effectiveness must be investigated. It is also realized that structural flexibility may have appreciable influence on the aerodynamic derivatives and thereby affect the overall flying qualities of the aircraft. Aerodynamic considerations of structural flexibility occurring in the transonic speed region can be especially difficult since no dependable aerodynamic theories are available. Consequently, the necessity for measuring the aerodynamic derivatives of a flexible aircraft is apparent.

Within recent years a mount system has been developed (Ref. 4) which permits the "free-flight" behavior of an aircraft to be simulated

in the wind tunnel. This mount system, referred to as the two-cable mount, is shown schematically in Figure 1 (p. 7). The model is held by two mutually perpendicular cables passing through pulleys in the fuselage and attached to the tunnel walls. The cables are kept under tension by stretching a soft spring in the rear cable. Remotely operated trim controls are provided on the model. The mount system was originally designed for the testing of aeroelastic effects such as flutter. Since the equations governing motion on the mount system are quite similar to those of flight, it was soon realized that the mount offers a potential for measuring aerodynamic derivatives of a flexible model in the wind tunnel.

The equations governing model behavior in the wind tunnel are essentially the free-flight equations modified by the addition of mount system restraints. It is therefore possible to apply test techniques similar to those presently used to obtain free-flight data. The technique selected for investigation involves measuring the model response to a sinusoidal steady-state excitation provided by the model control surfaces.

The equations governing model motion on the two-cable-mount system are derived in terms of model mass properties, linearized mount restraints, and unknown aerodynamic derivatives. Since fore and aft motion is not provided by the mount configuration analyzed, the equations of motion are presented in five degrees of freedom. The equations are simplified by separating them into two independent groups.

The longitudinal equations include vertical translation and pitching motions. The lateral equations include side translation, roll, and yawing motions. Each of these sets of equations is treated separately.

A technique for measuring the longitudinal aerodynamic derivatives is presented. The longitudinal equations are expressed in two degrees of freedom. A sinusoidal steady-state forcing function generated by the horizontal tail is introduced into the equations of motion. A steady-state sinusoidal response is assumed, and the resultant equations are expanded in terms of measurable model response and the unknown stability derivatives. It is assumed that the derivatives are independent of frequency; therefore, the equations of motion are valid at each discrete excitation frequency. From the model response measurements at several frequencies, a set of redundant equations is generated which can be solved for the unknown derivatives. A least-squares solution is used to obtain the derivatives from the set of redundant equations.

Since no experimental data are available for longitudinal motion, a numerical example is given to determine the effect of measurement errors on the derivatives. Equations for the two-cable mount show that it is theoretically possible to separate the results into uniquely determined stability derivatives. Greenburg (Ref. 2) states that results obtained by the dynamic technique from free-flight measurements appear as linear combinations of the aerodynamic derivatives caused by a dependency on the aircraft response. A comparison between flight and wind-tunnel equations shows that the mount system restraints allow separation of the unknown derivatives. In practice, however, the magnitude of this

restraint term is overshadowed by small errors in response measurements, which result in an ill-conditioned problem when solving for each of the derivatives uniquely.

The problem of determining each of the aerodynamic derivatives appearing in the lateral equations is more complex than that of the longitudinal case because of the added degree of freedom and its associated derivatives. However, Etkin (Ref. 1) states that for many conventional airplane configurations the roll equation in flight can be simplified and treated as a single degree of freedom.

In order to verify the basic dynamic approach to derivative measurements, an experimental technique for measuring aileron effectiveness and damping-in-roll stability derivatives is presented. Modified flight techniques are applied to the wind-tunnel tests. The experimental technique involves the measurement of model response to a sinusoidal steady-state forcing function generated by the ailerons. In order to satisfy free-flight requirements (single degree-of-freedom response), a parametric study of the two-cable-mount system was run in an effort to force the model to behave, essentially, as a single degree of freedom in roll. If the aerodynamic derivatives are independent of frequency, the roll equation is valid at each discrete aileron frequency. Measuring the model response as a function of aileron frequency generates a set of redundant equations which are solved for the unknown derivatives. In this manner both the aileron effectiveness (C_{l_δ}) and damping-in-roll derivative (C_{l_p}) are determined.

Experimental results are presented for a 1/19-size aeroelastic scaled model of a large, subsonic, multijet cargo airplane. Experimental results are obtained dynamically, as described, to determine C_{l_δ} and C_{l_p} and statically to determine C_{l_δ}. A brief description of the static mount and test procedure is given. A comparison between static and dynamic tests shows good agreement within the basic assumptions made.

Based on these results, the application of flight techniques to scaled models flown in the wind tunnel on the two-cable mount offers a potential for making quantitative measurements of the effect of flexibility on aircraft stability derivatives. This new testing procedure offers the aircraft designer early estimates of the stability and control characteristics of future aircraft configurations.

CHAPTER II

EQUATIONS OF MOTION

2.1 Introduction

In this Chapter the equations of motion governing model behavior on the two-cable-mount system are developed. Cable restraints are presented as stiffness influence coefficients. The assumption of small perturbations from trimmed flight makes the equations of motion linear and allows them to be separated into longitudinal and lateral degrees of freedom.

The mount configuration shown schematically in Figure 1 is analyzed. The model is held by two cable loops; the upstream cable is in the vertical plane, and the downstream cable in the horizontal plane. A soft spring in the rear cable keeps the system under tension. The x, y, z axes form a fixed right-hand coordinate system with its origin at the model center of gravity. The x axis is directed upstream in the tunnel, and the z axis is in the direction of gravity. The equations of motion are limited to five degrees of rigid-body freedom since fore and aft motion is not provided by the mount configuration analyzed.

Assuming positive displacements as shown in Figure 1, the dynamic equations of motion can be written as follows:

Vertical translation:

Summation of forces in the z direction

$$Z_A + Z_C + mg = m\ddot{z} \tag{1a}$$

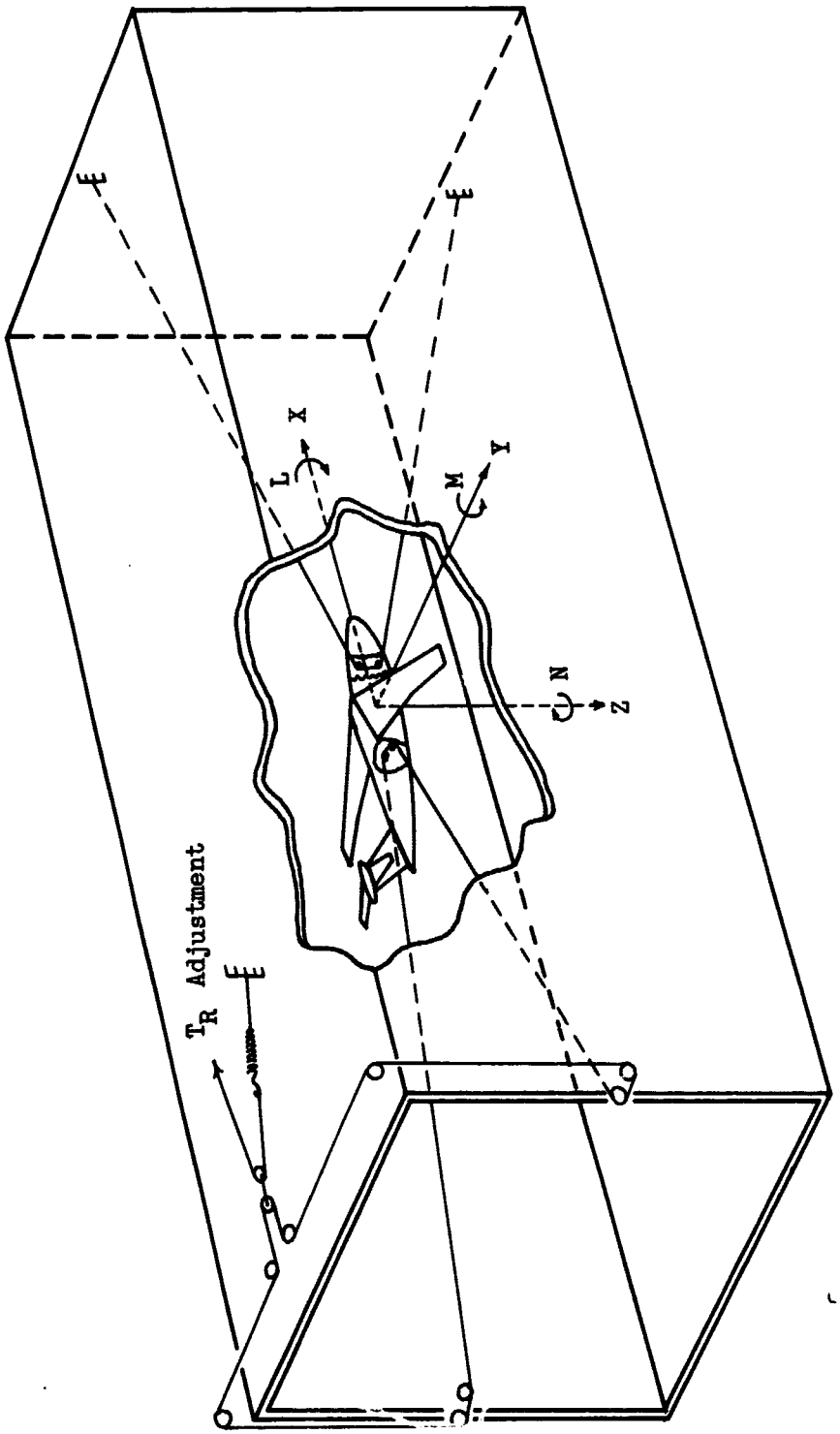

Figure 1.- Two-cable-mount system.

Pitch:

Summation of moments about the y axis

$$M_A + M_C = I_Y\ddot{\theta} \tag{1b}$$

Side translation:

Summation of forces in the y direction

$$Y_A + Y_C = m\ddot{y} \tag{1c}$$

Roll:

Summation of moments about the x axis

$$L_A + L_C = I_X\ddot{\phi} - I_{XZ}\ddot{\psi} \tag{1d}$$

Yaw:

Summation of moments about the z axis

$$N_A + N_C = I_Z\ddot{\psi} - I_{XZ}\ddot{\phi} \tag{1e}$$

where

z = vertical translation of model center of gravity

θ = rotation about y axis

y = lateral translation of model center of gravity

ϕ = rotation about x axis

ψ = rotation about z axis

and

L,M,N are moments about the x, y, z axes, respectively

Z,Y are forces along the z and y axes, respectively

The subscripts A refer to aerodynamic forces and moments; the subscripts C, to forces and moments generated by the mount restraints.

Etkin (Ref. 1) shows through the use of small perturbation theory and other assumptions that the complete set of equations of motion in flight can be separated into two independent groups. These two groups are referred to as the longitudinal and lateral equations of motion. The equations for longitudinal motion include fore and aft motion, vertical translation, and pitch. The equations for lateral motion include side translation, roll, and yaw. The basic longitudinal and lateral equations of motion for the two-cable-mount system will be presented in the following sections.

2.2 Derivation of Equations of Motion

2.2.1 Aerodynamic Force Components

2.2.1.1 Longitudinal Forces.- Lift and drag forces (L and D) are defined to have directions normal and parallel, respectively, to the relative wind vector $\vec{V}$, as shown in Figure 2. We have the following:

$$\vec{V} = \vec{V}_o + \dot{z}$$

$$\alpha = \bar{\theta} + \frac{\dot{z}}{U} \qquad \text{for } \dot{z} << U$$

$$U = \left|\vec{V}_o\right|$$

$$\bar{\theta} = \theta_t + \theta$$

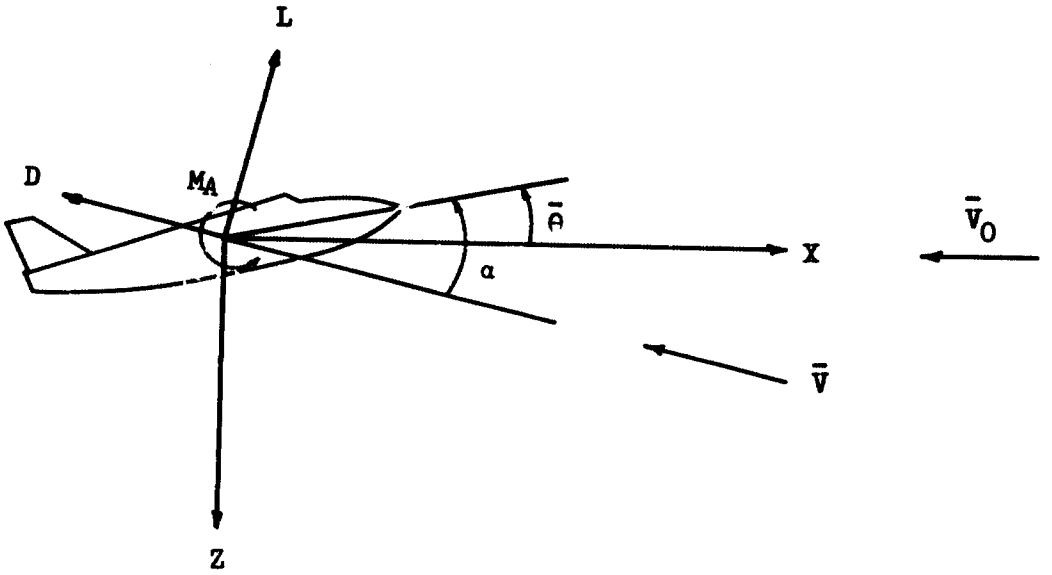

Figure 2.- Longitudinal aerodynamic forces.

where

$\vec{V}$ = relative wind vector of the airplane

$\vec{V}_o$ = wind vector along x axis

U = wind-tunnel flow velocity

θ_t = pitch angle for trimmed flight

θ = pitch angle perturbation about trim

Vertical translation:

Referring to Figure 2, the sum of the aerodynamic forces in the z direction results in

$$Z_A = -L \cos(\alpha - \bar{\theta}) - D \sin(\alpha - \bar{\theta})$$

Since it is assumed that $\dot{z} << U$, then

$$Z_A = -L - D(\alpha - \bar{\theta}) \tag{2}$$

The aerodynamic forces are normally expressed in terms of their coefficients

$$L = qSC_L$$

$$D = qSC_D$$

The nondimensional coefficients, C_L and C_D, represent the lift and drag generated on an airplane for a given dynamic pressure q and representative wing area S. (Dynamic pressure q is defined as $q = \frac{1}{2}\rho U^2$, where ρ is the testing medium density.)

Equation (2) can be written as

$$Z_A = -qS\left[C_L + C_D \frac{\dot{z}}{U}\right] \tag{3}$$

Making the basic assumption that the lift coefficient C_L is a linear function of angle of attack α and tail angle δ, we can express C_L as a Taylor series about the trim point θ_t. Therefore,

$$C_L = C_{L_o} + \frac{\partial C_L}{\partial \alpha} \Delta\alpha + \frac{\partial C_L}{\partial \delta} \Delta\delta$$

where

C_{L_o} = lift coefficient at trim θ_t

$\Delta\alpha = \alpha$ (angle of attack perturbation)

$\Delta\delta = \delta$ (tail angle perturbation)[1]

Let

$$\frac{\partial C_L}{\partial \alpha} = C_{L_\alpha}$$

Therefore, equation (3) can be written as

$$Z_A = Z_{A_o} - qS\left[C_{L_\alpha}\alpha + C_D \frac{\dot{z}}{U}\right] - qSC_{L_\delta}\delta$$

---

[1]Sign convention used is $+\delta$ is a trailing edge up which generates a negative lift.

or

$$Z_A = Z_{A_o} - qS\left[C_{L_\alpha}\left(\theta + \frac{\dot{z}}{U}\right) + C_D\frac{\dot{z}}{U}\right] + \bar{Z}_A \tag{4}$$

where

$$Z_{A_o} = \text{trim aerodynamic forces}$$
$$\bar{Z}_A = -qSC_{L_\delta}\delta \tag{4a}$$

Pitching motion:

The aerodynamic pitching moment is normally expressed as

$$M_A = qS\bar{c}C_m \tag{5a}$$

C_m is a nondimensional coefficient representing the moment generated for a given dynamic pressure, wing area, and a representative length $\bar{c}$. ($\bar{c}$ is the mean aerodynamic chord.[1]) Seckel (Ref. 5) shows that the aerodynamic moment can be expressed in a Taylor series expansion about θ_t as

$$M_A = M_{A_o} + \frac{\partial M_A}{\partial \alpha}\Delta\alpha + \frac{\partial M_A}{\partial \dot{\alpha}}\Delta\dot{\alpha} + \frac{\partial M_A}{\partial \dot{\theta}}\Delta\dot{\theta} + \frac{\partial M_A}{\partial \delta}\Delta\delta \tag{5b}$$

---

[1]The mean aerodynamic chord is defined by the formula $\frac{2}{S}\int_o^{b/2} C^2 dy$ where C is the local chord, b is the span, S is the wind area, and y is the lateral coordinate.

where

M_{A_o} = static trim condition

$\Delta\alpha = \alpha$, angle-of-attack perturbation

$\Delta\dot{\alpha} = \dot{\alpha}$, rate of angle-of-attack perturbation

$\Delta\dot{\theta} = \dot{\theta}$, rate of pitch-angle perturbation

$\Delta\delta = \delta$, tail-angle perturbation

Substituting equation (5a) into (5b) results in,

$$M_A = M_{A_o} + qS\bar{c}\left[\frac{\partial C_m}{\partial \alpha}\alpha + \frac{\partial C_m}{\partial \dot{\alpha}}\dot{\alpha} + \frac{\partial C_m}{\partial \dot{\theta}}\dot{\theta} + \frac{\partial C_m}{\partial \delta}\delta\right] \tag{6}$$

In order to handle the aerodynamic terms more conveniently, it is common practice to nondimensionalize the aerodynamic derivatives in the following manner:

$$\frac{\partial C_m}{\partial \alpha} = C_{m_\alpha}$$

$$\frac{\partial C_m}{\partial \dot{\theta}} = \frac{\bar{c}}{2U}\frac{\partial C_m}{\partial\left(\frac{\dot{\theta}\bar{c}}{2U}\right)} = \frac{\bar{c}}{2U}C_{m_{\dot{\theta}}}$$

$$\frac{\partial C_m}{\partial \dot{\alpha}} = \frac{\bar{c}}{2U}\frac{\partial C_m}{\partial\left(\frac{\dot{\alpha}\bar{c}}{2U}\right)} = \frac{\bar{c}}{2U}C_{m_{\dot{\alpha}}}$$

Substituting the preceding terms into equation (6) and expanding the expressions results in

$$M_A = M_{A_o} + qS\bar{c}\left[C_{m_\alpha}\theta + C_{m_{\dot\alpha}}\frac{\dot z}{U} + \frac{\bar c}{2U}C_{m_{\dot\alpha}}\frac{\ddot z}{U} + \frac{\bar c}{2U}(C_{m_{\dot\alpha}} + C_{m_{\dot\theta}})\dot\theta\right] + \bar M_A \tag{7}$$

where

$$\bar M_A = qS\bar c C_{m_\delta}\delta \tag{7a}$$

2.2.1.2 Lateral Forces.- The lateral aerodynamics are determined in a manner similar to that in which the longitudinal aerodynamics are derived. The lateral aerodynamic equations can be written as follows (Ref. 4):

$$L_A = qSbC_l$$

$$N_A = qSbC_n$$

$$Y_A = qSC_y$$

where

C_l = rolling-moment coefficient

C_n = yawing-moment coefficient

C_y = side-force coefficient

The representative length for the lateral equations is the wing span b. The angle of sideslip β is defined as $\frac{\dot y}{U} - \psi$. The lateral aerodynamic equations can now be written as follows:

$$L_A = qSb\left(C_{l_\beta}\frac{\dot y}{U} + C_{l_p}\frac{b}{2U}\dot\phi - C_{l_\beta}\psi + C_{l_r}\frac{b}{2U}\dot\psi\right) + \bar L_A \tag{8}$$

$$N_A = qSb\left(C_{n_\beta}\frac{\dot{y}}{U} + C_{n_p}\frac{b}{2U}\dot{\phi} - C_{n_\beta}\psi + C_{n_r}\frac{b}{2U}\dot{\psi}\right) + \bar{N}_A \tag{9}$$

$$Y_A = qS\left[(C_{y_\beta} - C_D)\frac{\dot{y}}{U} + C_L\phi + C_{y_p}\frac{b}{2U}\dot{\phi} - C_{y_\beta}\psi + C_{y_r}\frac{b}{2U}\dot{\psi}\right] + \bar{Y}_A \tag{10}$$

where

$$\left.\begin{aligned} \bar{L}_A &= qSbC_{l_{\delta_A}}\delta_A \\ \bar{N}_A &= qSbC_{n_{\delta_A}}\delta_A \\ \bar{Y}_A &= qSbC_{y_{\delta_A}}\delta_A \end{aligned}\right\} \text{Rudder fixed}$$

δ_A = aileron angle perturbation

The expressions for $\bar{L}_A$, $\bar{N}_A$, and $\bar{Y}_A$ are simplified forms corresponding to a fixed rudder configuration which is utilized in wind-tunnel testing procedure. The aerodynamic derivatives are nondimensionalized as follows:

$$\frac{\partial C_l}{\partial \beta} = C_{l_\beta} \qquad \frac{\partial C_l}{\partial \dot{\phi}} = \frac{b}{2U}\frac{\partial C_l}{\partial\left(\frac{\dot{\phi}b}{2U}\right)} = \frac{b}{2U}C_{l_p} \qquad \frac{\partial C_l}{\partial \dot{\psi}} = \frac{b}{2U}\frac{\partial C_l}{\partial\left(\frac{\dot{\psi}b}{2U}\right)} = \frac{b}{2U}C_{l_r}$$

$$\frac{\partial C_n}{\partial \beta} = C_{n_\beta} \qquad \frac{\partial C_n}{\partial \dot{\phi}} = \frac{b}{2U}\frac{\partial C_n}{\partial\left(\frac{\dot{\phi}b}{2U}\right)} = \frac{b}{2U}C_{n_p} \qquad \frac{\partial C_n}{\partial \dot{\psi}} = \frac{b}{2U}\frac{\partial C_n}{\partial\left(\frac{\dot{\psi}b}{2U}\right)} = \frac{b}{2U}C_{n_r}$$

$$\frac{\partial C_y}{\partial \beta} = C_{y_\beta} \qquad \frac{\partial C_y}{\partial \phi} = \frac{b}{2U}\frac{\partial C_y}{\partial\left(\frac{\dot{\phi} b}{2U}\right)} = \frac{b}{2U} C_{y_p} \qquad \frac{\partial C_y}{\partial \dot{\psi}} = \frac{b}{2U}\frac{\partial C_y}{\partial\left(\frac{\dot{\psi} b}{2U}\right)} = \frac{b}{2U} C_{y_r}$$

$$\frac{\partial C_l}{\partial \delta_A} = C_{l_{\delta_A}} \qquad \frac{\partial C_n}{\partial \delta_A} = C_{n_{\delta_A}} \qquad \frac{\partial C_y}{\partial \delta_A} = C_{y_{\delta_A}}$$

2.2.2 Mount Restraint Force Components

The two-cable-mount configuration used during this investigation is presented in Figure 3. The linearized cable restraint forces for the longitudinal degrees of freedom are derived in Appendix A. Equations are developed to determine the longitudinal spring constants in terms of mount system geometry, tension, etc. The longitudinal and lateral cable restraint forces can be expressed as follows:

$$Z_C = Z_{C_o} - K_{Z\theta}\theta - K_{ZZ}z \tag{11a}$$

$$M_C = M_{C_o} - K_{\theta Z}z - K_{\theta\theta}\theta \tag{11b}$$

$$L_C = -K_{\phi Y}y - K_{\phi\phi}\phi - K_{\phi\psi}\psi \tag{11c}$$

$$N_C = -K_{\psi Y}y - K_{\psi\phi}\phi - K_{\psi\psi}\psi \tag{11d}$$

$$Y_C = -K_{YY}y - K_{Y\phi}\phi - K_{Y\psi}\psi \tag{11e}$$

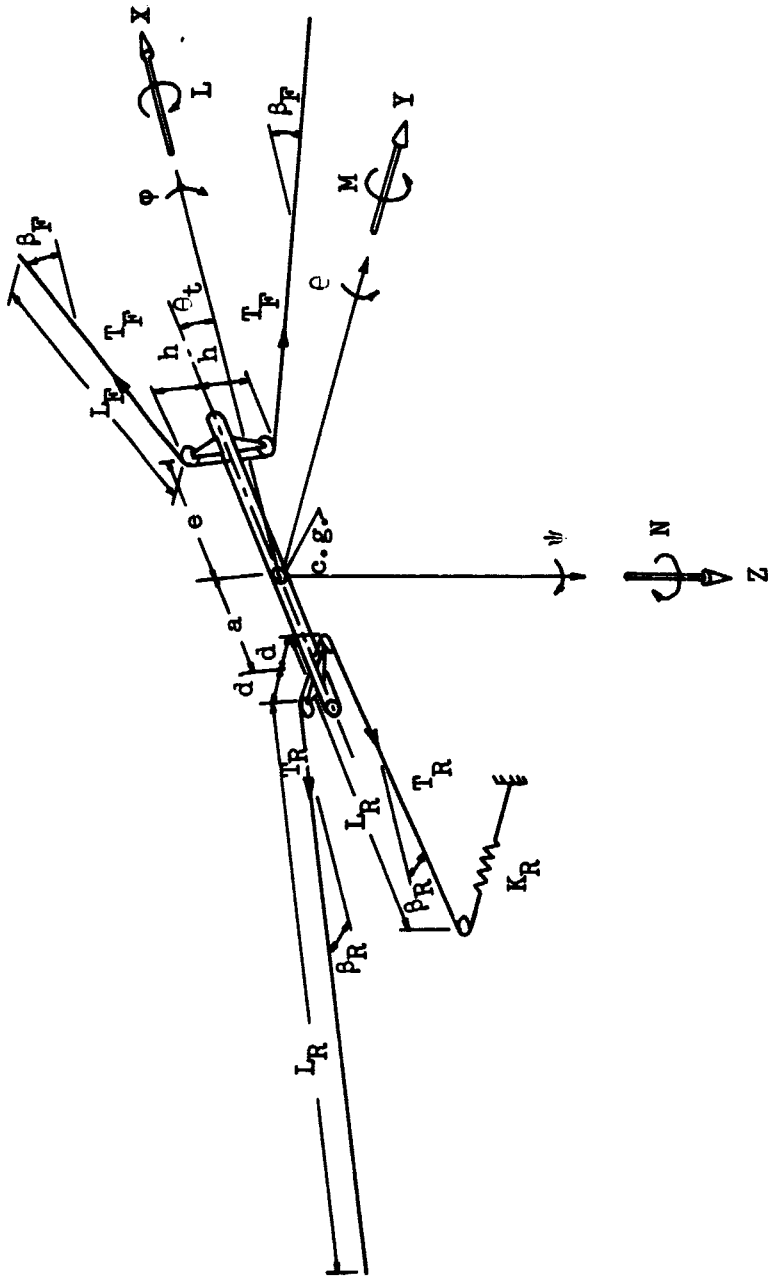

Figure 3.- Cable-mount configuration.

where K_{ij} is the spring constant relating a force or moment in mode i due to a displacement in mode j.

For the configuration under investigation (Appendix A) the stiffness influence coefficients are as follows:

Longitudinal stiffness influence coefficients

$$K_{ZZ} = 2\left[\frac{T_F}{L_F}\cos^2\beta_F + \frac{T_R}{L_R}\right]$$

$$K_{Z\theta} = 2\left[a\frac{T_R}{L_R} - \frac{T_F}{L_F}h\cos\beta_F\sin\beta_F - \frac{T_F}{L_F}e\cos^2\beta_F\right]$$

$$Z_{C_o} = -K_{Z\theta}\theta_t$$

$$K_{\theta Z} = K_{Z\theta}$$

$$K_{\theta\theta} = 2a^2\frac{T_R}{L_R} + 2aT_R\cos\beta_R + 2T_F\left[h\sin\beta_F + e\cos\beta_F + \frac{1}{L_F}(e\cos\beta_F + h\sin\beta_F)^2\right]$$

Lateral stiffness influence coefficients

$$K_{YY} = 2\frac{T_F}{L_F} + 2\frac{T_R}{L_R}\cos^2\beta_R$$

$$K_{Y\phi} = 0$$

$$K_{Y\psi} = 2\frac{T_F}{L_F}e - 2\frac{T_R}{L_R}\cos\beta_R(d\sin\beta_R + a\cos\beta_R)$$

$$K_{\phi Y} = K_{Y\phi} = 0$$

$$K_{\phi\phi} = 2hT_F\left(\frac{h}{L_F} + \sin\beta_F\right) + 2dT_R\left(\frac{d}{L_R} + \sin\beta_R\right)$$

$$K_{\phi\psi} = 0$$

$$K_{\psi\phi} = K_{\phi\psi} = 0$$

$$K_{\psi Y} = K_{Y\psi}$$

$$K_{\psi\psi} = 2eT_F\left(\frac{e}{L_F} + \cos\beta_F\right) + 2T_R\left[a\cos\beta_R + d\sin\beta_R + \frac{1}{L_R}(a\cos\beta_R + d\sin\beta_R)^2\right]$$

2.2.3 Complete Equations of Motion

Having developed the aerodynamic and mount forces, equations (4), (7), (8), (9) (10), (11a) through (11e) are substituted into equations (1a) through (1e) resulting in the following equations of motion:

Vertical translation:

$$\bar{Z}_A + Z_{A_o} - qS\left[C_{L_\alpha}\left(\theta + \frac{\dot{z}}{U}\right) + C_D \frac{\dot{z}}{U}\right] + Z_{C_o} - K_{Z\theta}\theta - K_{ZZ}z + mg = m\ddot{z} \tag{12a}$$

Pitch:

$$\bar{M}_A + M_{A_o} + qS\bar{c}\left[C_{m_\alpha}\theta + C_{m_\alpha}\frac{\dot{z}}{U} + \frac{\bar{c}}{2U} C_{m_{\dot{\alpha}}}\frac{\dot{z}}{U} + \frac{\bar{c}}{2U}(C_{m_{\dot{\alpha}}} + C_{m_{\dot{\theta}}})\dot{\theta}\right]$$

$$+ M_{C_o} - K_{\theta Z}z - K_{\theta\theta}\theta = I_Y\ddot{\theta} \tag{12b}$$

Side translation:

$$\bar{Y}_A + qS\left[(C_{y_\beta} - C_D)\frac{\dot{y}}{U} + C_L\phi + C_{y_p}\frac{b}{2U}\dot{\phi} - C_{y_\beta}\psi + C_{y_r}\frac{b}{2U}\dot{\psi}\right]$$

$$- K_{YY}y - K_{Y\phi}\phi - K_{Y\psi}\psi = m\ddot{y} \tag{12c}$$

Roll:

$$\bar{L}_A + qSb\left[C_{l_\beta}\frac{\dot{y}}{U} + C_{l_p}\frac{b}{2U}\dot{\phi} - C_{l_\beta}\psi + C_{l_r}\frac{b}{2U}\dot{\psi}\right] - K_{\phi Y}y - K_{\phi\phi}\phi$$

$$- K_{\phi\psi}\psi = I_X\ddot{\phi} - I_{XZ}\ddot{\psi} \tag{12d}$$

Yaw:

$$\bar{N}_A + qSb\left[C_{n_\beta}\frac{\dot{y}}{U} + C_{n_p}\frac{b}{2U}\dot{\phi} - C_{n_\beta}\psi + C_{n_r}\frac{b}{2U}\dot{\psi}\right] - K_{\psi Y}y - K_{\psi\phi}\phi$$

$$- K_{\psi\psi}\psi = I_Z\ddot{\psi} - I_{XZ}\ddot{\phi} \tag{12e}$$

The longitudinal equations can be simplified further by considering the static trim condition θ_t. At θ_t let $\theta = \dot{\theta} = z = \dot{z} = \ddot{z} = 0$; $\delta = \delta_o$. Therefore,

$$\left.\begin{aligned} -qSC_{L_\delta}\delta_o + Z_{A_o} + Z_{C_o} + mg = 0 \\ qS\bar{c}C_{m_\delta}\delta_o + M_{A_o} + M_{C_o} = 0 \end{aligned}\right\} \text{Static trim equations}$$

The dynamic longitudinal equations of motion for small perturbations about the trim point θ_t become the following:

Vertical translation:

$$\bar{Z}_A - qS\left[C_{L_\alpha}\left(\theta + \frac{\dot{z}}{U}\right) + C_D\frac{\dot{z}}{U}\right] - K_{Z\theta}\theta - K_{ZZ}z = m\ddot{z} \tag{13a}$$

Pitch:

$$\bar{M}_A + qS\bar{c}\left[C_{m_\alpha}\theta + C_{m_\alpha}\frac{\dot{z}}{U} + \frac{\bar{c}}{2U}C_{m_{\dot{\alpha}}}\frac{\ddot{z}}{U} + \frac{\bar{c}}{2U}(C_{m_{\dot{\alpha}}} + C_{m_{\dot{\theta}}})\dot{\theta}\right] - K_{\theta Z}z - K_{\theta\theta}\theta = I_Y\ddot{\theta} \tag{13b}$$

The equations of motion are linear second-order differential equations with constant coefficients. The analysis does not include the dynamic properties of the mount itself such as cable inertia and pulley damping. A simplified approach is to neglect cable inertia and add viscous damping terms proportional to displacement rates in each mode. The terms $C_Z\dot{z}$, $C_\theta\dot{\theta}$, $C_Y\dot{y}$, $C_\psi\dot{\psi}$, and $C_\phi\dot{\phi}$ are added to each of the equations of motion, respectively. Where

$$C_Z = 2\zeta_Z m\omega_{ZZ} \qquad \omega_{ZZ} = \sqrt{\frac{K_{ZZ}}{m}}$$

$$C_\theta = 2\zeta_\theta I_Y\omega_{\theta\theta} \qquad \omega_{\theta\theta} = \sqrt{\frac{K_{\theta\theta}}{I_Y}}$$

$$C_Y = 2\zeta_Y m\omega_{YY} \qquad \omega_{YY} = \sqrt{\frac{K_{YY}}{m}}$$

$$C_\psi = 2\zeta_\psi I_Z\omega_{\psi\psi} \qquad \omega_{\psi\psi} = \sqrt{\frac{K_{\psi\psi}}{I_Z}}$$

$$C_\phi = 2\zeta_\phi I_X\omega_{\phi\phi} \qquad \omega_{\phi\phi} = \sqrt{\frac{K_{\phi\phi}}{I_X}}$$

The damping factors ζ_Z, ζ_θ, ζ_Y, ζ_ψ, and ζ_ϕ are estimated for the pulley configuration being investigated. Substituting these terms into equations (12c), (12d), (12e), (13a), (13b), and rearranging, results in the following equations:

Vertical translation:

$$m\ddot{z} + \left[\frac{qS}{U}(C_{L_\alpha} + C_D) + 2\zeta_Z m\omega_{ZZ}\right]\dot{z} + K_{ZZ}z + (K_{Z\theta} + qSC_{L_\alpha})\theta = \bar{Z}_A \tag{14a}$$

Pitch:

$$I_Y\ddot{\theta} - \left[\frac{qS\bar{c}^2}{2U}(C_{m_{\dot{\alpha}}} + C_{m_{\dot{\theta}}}) - 2\zeta_\theta I_Y\omega_{\theta\theta}\right]\dot{\theta} + (K_{\theta\theta} - qS\bar{c}C_{m_\alpha})\theta$$

$$- \frac{qS\bar{c}^2}{2U^2}C_{m_{\dot{\alpha}}}\ddot{z} - \frac{qS\bar{c}}{U}C_{m_\alpha}\dot{z} + K_{\theta Z}z = \bar{M}_A \tag{14b}$$

Side translation:

$$m\ddot{y} - \left[\frac{qS}{U}(C_{y_\beta} - C_D) - 2\zeta_Y m\omega_{YY}\right]\dot{y} + K_{YY}y - \frac{qSb}{2U}C_{y_p}\dot{\phi} + (K_{Y\phi} - qSC_L)\phi$$

$$- \frac{qSb}{2U}C_{y_r}\dot{\psi} + (qSC_{y_\beta} + K_{Y\psi})\psi = \bar{Y}_A \tag{14c}$$

Roll:

$$I_X\ddot{\phi} - \left(\frac{qSb^2}{2U}C_{l_p} - 2\zeta_\phi I_X\omega_{\phi\phi}\right)\dot{\phi} + K_{\phi\phi}\phi - I_{XZ}\ddot{\psi} - \frac{qSb^2}{2U}C_{l_r}\dot{\psi}$$

$$+ (qSbC_{l_\beta} + K_{\phi\psi})\psi - \frac{qSb}{U}C_{l_\beta}\dot{y} + K_{\phi Y}y = \bar{L}_A \tag{14d}$$

Yaw:

$$I_Z\ddot{\psi} - \left(\frac{qSb^2}{2U} C_{n_r} - 2\zeta_\psi I_Z \omega_{\psi\psi}\right)\dot{\psi} + (qSbC_{n_\beta} + K_{\psi\psi})\psi - \frac{qSb}{U} C_{n_\beta}\dot{y}$$

$$+ K_{\psi Y}y - I_{XZ}\ddot{\phi} - \frac{qSb^2}{2U} C_{n_p}\dot{\phi} + K_{\psi\phi}\phi = \bar{N}_A \qquad (14e)$$

Equations (14a) through (14e) completely describe, within the framework of the assumptions made, both the longitudinal and lateral motion of the model in the wind tunnel. The equations are expressed in terms of model mass properties, tunnel test conditions, mount properties, and aerodynamic derivatives.

CHAPTER III

TECHNIQUE FOR MEASURING LONGITUDINAL AERODYNAMIC DERIVATIVES

The equations of motion governing model behavior in the wind tunnel are quite similar to the free-flight equations modified by the addition of mount system constraints. Hence, it is possible to apply test techniques similar to those used to obtain aerodynamic derivatives from free-flight tests. The technique selected involves measuring the dynamic response of the model to a sinusoidal excitation. In this thesis, the excitation is provided by a sinusoidal movement of the horizontal tail. Greenburg (Ref. 2) presents this technique for the free-flight case.

3.1 Derivation

For simplicity, it is assumed the pulley damping and cross-coupled mount stiffnesses in equations (14a) and (14b) are zero (i.e., $\zeta_\theta = \zeta_Z = K_{\theta Z} = K_{Z\theta} = 0$). The equations of motion become

$$m\ddot{z} + \frac{qS}{U}(C_{L_\alpha} + C_D)\dot{z} + K_{ZZ}z + qSC_{L_\alpha}\theta = \bar{Z}_A \qquad (15a)$$

$$I_Y\ddot{\theta} - \frac{q\bar{S}\bar{c}^2}{2U}(C_{m_{\dot{\alpha}}} + C_{m_{\dot{\theta}}})\dot{\theta} + (K_{\theta\theta} - q\bar{S}\bar{c}C_{m_\alpha})\theta - \frac{q\bar{S}\bar{c}^2}{2U^2}C_{m_{\dot{\alpha}}}\ddot{z}$$

$$- \frac{q\bar{S}\bar{c}}{U}C_{m_\alpha}\dot{z} = \bar{M}_A \qquad (15b)$$

In order to provide a dynamic forcing function, let the tail deflection be $\delta = \delta_o e^{i\omega t}$. A sinusoidal deflection of the tail will provide translation and pitch forcing functions of the form:

$$\bar{Z}_A(t) = -qSC_{L_\delta}\delta_o e^{i\omega t} \tag{16a}$$

$$\bar{M}_A(t) = qS\bar{c}C_{m_\delta}\delta_o e^{i\omega t} \tag{16b}$$

Substitution of the forcing functions in the form $\bar{Z}_A(t)$, $\bar{M}_A(t)$ into equations (15a) and (15b) results in,

$$m\ddot{z} + \frac{qS}{U}(C_{L_\alpha} + C_D)\dot{z} + K_{ZZ}z + qSC_{L_\alpha}\theta = -qSC_{L_\delta}\delta_o e^{i\omega t} \tag{17a}$$

$$I_Y\ddot{\theta} - \frac{qS\bar{c}^2}{2U}(C_{m_{\dot\alpha}} + C_{m_{\dot\theta}})\dot{\theta} + (K_{\theta\theta} - qS\bar{c}C_{m_\alpha})\theta - \frac{qS\bar{c}^2}{2U^2}C_{m_{\dot\alpha}}\ddot{z}$$

$$- \frac{qS\bar{c}}{U}C_{m_\alpha}\dot{z} = qS\bar{c}C_{m_\delta}\delta_o e^{i\omega t} \tag{17b}$$

For sinusoidal motion, the steady-state response becomes:

$$z = z_o e^{i(\omega t+\phi_1)} \qquad \theta = \theta_o e^{i(\omega t+\phi_2)}$$

$$\dot{z} = i\omega z_o e^{i(\omega t+\phi_1)} \qquad \dot{\theta} = i\omega\theta_o e^{i(\omega t+\phi_2)}$$

$$\ddot{z} = -\omega^2 z_o e^{(\omega t+\phi_1)} \qquad \ddot{\theta} = -\omega^2\theta_o e^{i(\omega t+\phi_2)}$$

ϕ_1 and ϕ_2 are the phase angles between tail and model displacements. Substituting the response functions into (17a) and (17b) results in the following equations:

Vertical translation:

$$C_{L_\alpha}\left(qS\theta_o e^{i\phi_2} + i\omega \frac{qS}{U} z_o e^{i\phi_1}\right) + C_D\left(i\omega \frac{qS}{U} z_o e^{i\phi_1}\right)$$

$$+ C_{L_\delta}(+qS\delta_o) = (m\omega^2 - K_{ZZ})z_o e^{i\phi_1} \qquad (18a)$$

Pitch:

$$C_{m_{\dot\theta}}\left[-\frac{qS\bar{c}^2}{2U} i\omega\theta_o e^{i\phi_2}\right] + C_{m_{\dot\alpha}}\left[-i\omega \frac{qS\bar{c}^2}{2U} \theta_o e^{i\phi_2} + \frac{qS\bar{c}^2}{2U^2} \omega^2 z_o e^{i\phi_1}\right]$$

$$+ C_{m_\alpha}\left[-qS\bar{c}\theta_o e^{i\phi_2} - i\omega \frac{qS\bar{c}}{U} z_o e^{i\phi_1}\right] + C_{m_\delta}\left[-qS\bar{c}\delta_o\right]$$

$$= (I_Y\omega^2 - K_{\theta\theta})\theta_o e^{i\phi_2} \qquad (18b)$$

If the aerodynamic derivatives C_{L_α}, C_D, C_{L_δ}, $C_{m_{\dot\theta}}$, $C_{m_{\dot\alpha}}$, C_{m_α}, and C_{m_δ} are assumed to be independent of frequency, each of the equations of motion can be used to generate a set of redundant equations which can be solved, using a least-squares method of solution (refer to Appendix B) for each of the aerodynamic derivatives. The least-squares method of solution presented in Appendix B is a mathematical procedure

for solving a set of redundant equations. Equation (18a) can be expressed as a function of frequency in the following form:

$$C_{L_\alpha}\left[qS\theta_o e^{i\phi_2} + i\omega\frac{qS}{U}z_o e^{i\phi_1}\right]_{\omega=\omega_j} + C_D\left[i\omega\frac{qS}{U}z_o e^{i\phi_1}\right]_{\omega=\omega_j} + C_{L_\delta}\left[qS\delta_o\right]$$

$$= \left[(m\omega^2 - K_{ZZ})z_o e^{i\phi_1}\right]_{\omega=\omega_j}$$

$$j = 1,2,3, \ldots N \qquad (19a)$$

θ_o, z_o, ϕ_1, and ϕ_2 are measured from model response as a function of the tail frequency ω. Similarly, equation (18b) can be written as

$$C_{m_{\dot\theta}}\left[-\frac{qS\bar{c}^2}{2U}i\omega\theta_o e^{i\phi_2}\right]_{\omega=\omega_j} + C_{m_{\dot\alpha}}\left[-i\omega\frac{qS\bar{c}^2}{2U}\theta_o e^{i\phi_2} + \frac{qS\bar{c}^2}{2U^2}\omega^2 z_o e^{i\phi_1}\right]_{\omega=\omega_j}$$

$$+ C_{m_\alpha}\left[-qS\bar{c}\theta_o e^{i\phi_2} - i\omega\frac{qS\bar{c}}{U}z_o e^{i\phi_1}\right]_{\omega=\omega_j} + C_{m_\delta}\left[-qS\bar{c}\delta_o\right]$$

$$= \left[(I_Y\omega^2 - K_{\theta\theta})\theta_o e^{i\phi_2}\right]_{\omega=\omega_j}$$

$$j = 1,2,3, \ldots N \qquad (19b)$$

Equation for vertical translation:

Equation (19a) can be rewritten in the form,

$$A_{j1}C_{L_\alpha} + A_{j2}C_D + A_{j3}C_{L_\delta} = b_j \qquad (19c)$$

where

$$A_{j1} = qS\left[\theta_o e^{i\phi_2} + i\omega \frac{z_o}{U} e^{i\phi_1}\right]_{\omega=\omega_j}$$

$$A_{j2} = i \frac{qS}{U}\left[\omega z_o e^{i\phi_1}\right]_{\omega=\omega_j}$$

$$A_{j3} = +qS\delta_o$$

$$b_j = \left[(m\omega^2 - K_{ZZ})z_o e^{i\phi_1}\right]_{\omega=\omega_j} \qquad j = 1,2,3, \ldots N$$

Applying a least-squares solution to equation (19c) results in the following (Appendix B):

$$\begin{bmatrix} 2\sum_{j=1}^{N}\left|A_{j1}\right|^2 & \sum_{j=1}^{N}(A^*_{j1}A_{j2} + A_{j1}A^*_{j2})^1 & \sum_{j=1}^{N}(A^*_{j1}A_{j3} + A_{j1}A^*_{j3}) \\ \sum_{j=1}^{N}(A^*_{j1}A_{j2} + A_{j1}A^*_{j2}) & 2\sum_{j=1}^{N}\left|A_{j2}\right|^2 & \sum_{j=1}^{N}(A^*_{j2}A_{j3} + A_{j2}A^*_{j3}) \\ \sum_{j=1}^{N}(A^*_{j1}A_{j3} + A_{j1}A^*_{j3}) & \sum_{j=1}^{N}(A^*_{j2}A_{j3} + A_{j2}A^*_{j3}) & 2\sum_{j=1}^{N}\left|A_{j3}\right|^2 \end{bmatrix} \begin{bmatrix} C_{L_\alpha} \\ C_D \\ C_{L_\delta} \end{bmatrix} =$$

[1]*Complex conjugate of the term (defined in Appendix B).

$$\begin{bmatrix} \sum_{j=1}^{N} (b_j^* A_{j1} + b_j A_{j1}^*) \\ \sum_{j=1}^{N} (b_j^* A_{j2} + b_j A_{j2}^*) \\ \sum_{j=1}^{N} (b_j^* A_{j3} + b_j A_{j3}^*) \end{bmatrix} \tag{20}$$

Substituting the expressions for A_{j1}, A_{j2}, A_{j3}, and b_j into (20) results in three simultaneous equations which are solved for C_{L_α}, C_D, and C_{L_δ}. The algebraic expressions necessary to calculate the aerodynamic derivatives are presented in terms of measured response data.

$$\sum_{j=1}^{N} |A_{j1}|^2 = (qS)^2 \sum_{j=1}^{N} \left[\theta_o^2 + \left(\frac{\omega z_o}{U} \right)^2 + \frac{2\omega z_o \theta_o}{U} \sin(\phi_2 - \phi_1) \right]_{\omega=\omega_j}$$

$$\sum_{j=1}^{N} |A_{j2}|^2 = \left(\frac{qS}{U} \right)^2 \sum_{j=1}^{N} (\omega z_o)^2_{\omega=\omega_j}$$

$$\sum_{j=1}^{N} |A_{j3}|^2 = (qS\delta_o)^2 N$$

$$\sum_{j=1}^{N} (A_{j1}^* A_{j2} + A_{j1} A_{j2}^*) = \frac{2(qS)^2}{U} \sum_{j=1}^{N} \left[\frac{(\omega z_o)^2}{U} + \omega \theta_o z_o \sin(\phi_2 - \phi_1) \right]_{\omega=\omega_j}$$

$$\sum_{j=1}^{N} (A_{j1}^* A_{j3} + A_{j1} A_{j3}^*) = 2q^2 S^2 \delta_o \sum_{j=1}^{N} \left[\theta_o \cos \phi_2 - \frac{\omega z_o}{U} \sin \phi_1 \right]_{\omega=\omega_j}$$

$$\sum_{j=1}^{N} (A_{j2}^* A_{j3} + A_{j2} A_{j3}^*) = \frac{-2q^2 S^2 \delta_o}{U} \sum_{j=1}^{N} \left[\omega z_o \sin \phi_1 \right]_{\omega=\omega_j}$$

$$\sum_{j=1}^{N} (b_j^* A_{j1} + b_j A_{j1}^*) = 2qS \sum_{j=1}^{N} \left[(m\omega^2 - K_{ZZ}) z_o \theta_o \cos(\phi_2 - \phi_1) \right]_{\omega=\omega_j}$$

$$\sum_{j=1}^{N} (b_j^* A_{j2} + b_j A_{j2}^*) = 0$$

$$\sum_{j=1}^{N} (b_j^* A_{j3} + b_j A_{j3}^*) = 2qS\delta_o \sum_{j=1}^{N} \left[(m\omega^2 - K_{ZZ}) z_o \cos \phi_1 \right]_{\omega=\omega_j}$$

Equation for pitching motion:

Equation (19b) can be rewritten in the form,

$$g_{j1} C_{m_{\dot{\theta}}} + g_{j2} C_{m_{\dot{\alpha}}} + g_{j3} C_{m_\alpha} + g_{j4} C_{m_\delta} = h_j \qquad (19d)$$

where

$$g_{j1} = -i \frac{qS\bar{c}^2}{2U}\left[\omega\theta_o e^{i\phi_2}\right]_{\omega=\omega_j}$$

$$g_{j2} = -\frac{qS\bar{c}^2}{2U}\left[i\omega\theta_o e^{i\phi_2} - \frac{\omega^2 z_o}{U} e^{i\phi_1}\right]_{\omega=\omega_j}$$

$$g_{j3} = -qS\bar{c}\left[\theta_o e^{i\phi_2} + \frac{i\omega z_o}{U} e^{i\phi_1}\right]_{\omega=\omega_j}$$

$$g_{j4} = -qS\bar{c}\delta_o$$

$$h_j = \left[(I_Y\omega^2 - K_{\theta\theta})\theta_o e^{i\phi_2}\right]_{\omega=\omega_j} \qquad j = 1,2,3, \ldots N$$

Applying a least-squares solution to equation (19d) results in the following:

$$
\begin{bmatrix}
2\sum_{j=1}^{N} |g_{j1}|^2 & \sum_{j=1}^{N} (g^*_{j1}g_{j2} + g_{j1}g^*_{j2}) & \sum_{j=1}^{N} (g^*_{j1}g_{j3} + g_{j1}g^*_{j3}) & \sum_{j=1}^{N} (g^*_{j1}g_{j4} + g_{j1}g^*_{j4}) \\
\sum_{j=1}^{N} (g^*_{j1}g_{j2} + g_{j1}g^*_{j2}) & 2\sum_{j=1}^{N} |g_{j2}|^2 & \sum_{j=1}^{N} (g^*_{j2}g_{j3} + g_{j2}g^*_{j3}) & \sum_{j=1}^{N} (g^*_{j2}g_{j4} + g_{j2}g^*_{j4}) \\
\sum_{j=1}^{N} (g^*_{j1}g_{j3} + g_{j1}g^*_{j3}) & \sum_{j=1}^{N} (g^*_{j2}g_{j3} + g_{j2}g^*_{j3}) & 2\sum_{j=1}^{N} |g_{j3}|^2 & \sum_{j=1}^{N} (g^*_{j3}g_{j4} + g_{j3}g^*_{j4}) \\
\sum_{j=1}^{N} (g^*_{j1}g_{j4} + g_{j1}g^*_{j4}) & \sum_{j=1}^{N} (g^*_{j2}g_{j4} + g_{j2}g^*_{j4}) & \sum_{j=1}^{N} (g^*_{j3}g_{j4} + g_{j3}g^*_{j4}) & 2\sum_{j=1}^{N} |g_{j4}|^2
\end{bmatrix}
\begin{bmatrix} C_{m_{\dot{\theta}}} \\ C_{m_{\dot{\alpha}}} \\ C_{m_{\alpha}} \\ C_{m_{\delta}} \end{bmatrix} =
$$

$$\begin{bmatrix} \sum_{j=1}^{N} (h_j^* g_{j1} + h_j g_{j1}^*) \\ \sum_{j=1}^{N} (h_j^* g_{j2} + h_j g_{j2}^*) \\ \sum_{j=1}^{N} (h_j^* g_{j3} + h_j g_{j3}^*) \\ \sum_{j=1}^{N} (h_j^* g_{j4} + h_j g_{j4}^*) \end{bmatrix} \tag{21}$$

Substituting the expressions for g_{j1}, g_{j2}, g_{j3}, g_{j4}, and h_j into (21) results in four simultaneous equations which are solved for $C_{m_{\dot{\theta}}}$, $C_{m_{\dot{\alpha}}}$, $C_{m_{\alpha}}$, and $C_{m_{\delta}}$. The algebraic expressions necessary to calculate the aerodynamic derivatives are presented in terms of measured response data.

$$\sum_{j=1}^{N} |g_{j1}|^2 = \left(\frac{qS\bar{c}^2}{2U}\right)^2 \sum_{j=1}^{N} [a\theta_o]_{\omega=\omega_j}$$

$$\sum_{j=1}^{N} |g_{j2}|^2 = \left(\frac{qS\bar{c}^2}{2U}\right)^2 \sum_{j=1}^{N} \left[\theta_o^2 + \left(\frac{\omega z_o}{U}\right)^2 + \frac{2\theta_o z_o \omega}{U} \sin(\phi_2 - \phi_1)\right]_{\omega=\omega_j} (\omega_j)^2$$

$$\sum_{j=1}^{N} \left|g_{j3}\right|^2 = (qS\bar{c})^2 \sum_{j=1}^{N} \left[\theta_o^2 + \left(\frac{\omega z_o}{U}\right)^2 + \frac{2\theta_o z_o \omega}{U} \sin(\phi_2 - \phi_1)\right]_{\omega=\omega_j}$$

$$\sum_{j=1}^{N} \left|g_{j4}\right|^2 = (qS\bar{c}\delta_o)^2 N$$

$$\sum_{j=1}^{N} (g_{j1}^* g_{j2} + g_{j1} g_{j2}^*) = 2\left(\frac{qS\bar{c}^2}{2U}\right)^2 \sum_{j=1}^{N} \left[\theta_o^2 + \frac{\omega\theta_o z_o}{U} \sin(\phi_2 - \phi_1)\right]_{\omega=\omega_j} (\omega_j)^2$$

$$\sum_{j=1}^{N} (g_{j1}^* g_{j3} + g_{j1} g_{j3}^*) = \frac{2q^2 S^2 \bar{c}^3}{2U^2} \sum_{j=1}^{N} \left[\omega^2 \theta_o z_o \cos(\phi_1 - \phi_2)\right]_{\omega=\omega_j}$$

$$\sum_{j=1}^{N} (g_{j1}^* g_{j4} + g_{j1} g_{j4}^*) = -\frac{2q^2 S^2 \bar{c}^3 \delta_o}{2U} \sum_{j=1}^{N} \left[\omega\theta_o \sin\phi_2\right]_{\omega=\omega_j}$$

$$\sum_{j=1}^{N} (g_{j2}^* g_{j3} + g_{j2} g_{j3}^*) = 0$$

$$\sum_{j=1}^{N} (g_{j2}^* g_{j4} + g_{j2} g_{j4}^*) = -\frac{2q^2 S^2 \bar{c}^3 \delta_o}{2U} \sum_{j=1}^{N} \left[\omega\theta_o \sin\phi_2 + \frac{\omega^2 z_o}{U} \cos\phi_1\right]_{\omega=\omega_j}$$

$$\sum_{j=1}^{N} (g_{j3}^* g_{j4} + g_{j3} g_{j4}^*) = 2q^2 S^2 \bar{c}^2 \delta_o \sum_{j=1}^{N} \left[\theta_o \cos\phi_2 - \frac{\omega z_o}{U} \sin\phi_1\right]_{\omega=\omega_j}$$

$$\sum_{j=1}^{N} (h_j^* g_{j1} + h_j g_{j1}^*) = 0$$

$$\sum_{j=1}^{N} (h_j^* g_{j2} + h_j g_{j2}^*) = \frac{2qS\bar{c}^2}{2U^2} \sum_{j=1}^{N} \left[(I_Y\omega^2 - K_{\theta\theta})\omega^2 z_o\theta_o \cos(\phi_2 - \phi_1)\right]_{\omega=\omega_j}$$

$$\sum_{j=1}^{N} (h_j^* g_{j3} + h_j g_{j3}^*) = -2qS\bar{c} \sum_{j=1}^{N} \left[(I_Y\omega^2 - K_{\theta\theta})\left[\theta_o^2 + \frac{\omega z_o\theta_o}{U} \sin(\phi_2 - \phi_1)\right]\right]_{\omega=\omega_j}$$

$$\sum_{j=1}^{N} (h_j^* g_{j4} + h_j g_{j4}^*) = -2qS\bar{c}\delta_o \sum_{j=1}^{N} \left[(I_Y\omega^2 - K_{\theta\theta})\theta_o \cos \phi_2\right]_{\omega=\omega_j}$$

The aerodynamic derivatives are determined by solving equations (20) and (21). The data required are obtained from wind-tunnel tests.

At a test point (tunnel conditions fixed) the horizontal tail surface is oscillated at a known amplitude through a range of frequencies. At each discrete frequency $\omega = \omega_j$ ($j = 1,2,3, \ldots N$; $N > 4$) the model motion is monitored to determine z_o, θ_o, ϕ_1, and ϕ_2. Cable tensions are monitored at each test point to calculate mount stiffnesses from the equations presented in Appendix A. The data collected at N different frequencies are used to evaluate the algebraic terms which comprise equations (20) and (21). Each equation is then solved for the associated aerodynamic derivatives.

3.2 Error Analysis

3.2.1 Error Analysis Computation

An error analysis is provided to determine the accuracy with which the model response z_o, θ_o, ϕ_1, and ϕ_2 needs to be measured in order to obtain meaningful results. A numerical error analysis is presented to determine the error in the calculated aerodynamic derivatives due to an error in measuring model response. Since no experimental data are available, a set of amplitudes and phase angles is obtained by solving the equations of motion (eqs. (17a) and (17b)) for an assumed tunnel test point and representative values of th aerodynamic derivatives.[1] This analysis assumes that the governing equations of motion are correct as presented in equations (17a) and (17b). All parameters other than model response are assumed to be correct.

Errors are now introduced into the response data, and the aerodynamic derivatives based on the new response are calculated using equations (20) and (21). The new aerodynamic derivatives can be expressed in a Taylor series in the following manner:

$$C_{\epsilon \neq 0} = C_{\epsilon=0} + \frac{\partial C}{\partial \epsilon_Z} \Delta\epsilon_z + \frac{\partial C}{\partial \epsilon_\theta} \Delta\epsilon_\theta + \frac{\partial C}{\partial \epsilon_{\phi_1}} \Delta\epsilon_{\phi_1} + \frac{\partial C}{\partial \epsilon_{\phi_2}} \Delta\epsilon_{\phi_2} \qquad (22)$$

---

[1]The aerodynamic derivatives selected are those of a large multijet cargo airplane.

where

$C_{\epsilon \neq 0}$ = numerical value of aerodynamic derivative with error

$C_{\epsilon=0}$ = numerical value of aerodynamic derivative without error

$\Delta\epsilon$ = incremental error in measurement

$\frac{\partial C}{\partial \epsilon}$ = rate of change of the aerodynamic derivative with respect to the error

Appendix C describes the computer programs used in this analysis.

The model properties, test conditions, and aerodynamic derivatives assumed for the numerical error analysis are as follows:

$U = 500$ ft/sec	$\omega = 1,2,3, \ldots 30$ rad/sec
$q = 100$ lb/ft^2	$C_{L_\alpha} = 5.00$/rad
$S = 10$ ft^2	$C_D = 0.02$
$m = 2.0$ slugs	$C_{m_\alpha} = -1.00$/rad
$\bar{c} = 1.0$ ft	$C_{m_{\dot{\alpha}}} = -4.00$/rad
$I_Y = 3.0$ slug-ft^2	$C_{m_{\dot{\theta}}} = -15.0$/rad
$\delta_o = 0.00698$ rad	$C_{L_\delta} = -0.40$/rad
$K_{ZZ} = 20.0$ lb/ft	$C_{m_\delta} = 1.2$/rad
$K_{\theta\theta} = 500$ ft-lb/rad	

These parameters are substituted into equations (C-1) and (C-2) to evaluate the model response Z_o, θ_o, ϕ_1, and ϕ_2 as a function of the tail frequency ω. The model response for this example is presented in Figure 4. The peak responses occur at the damped natural frequencies of the system.

Errors are now introduced into each term of the response data, and the aerodynamic derivatives with response errors are calculated using equations (20) and (21). Appendix C presents equations (20) and (21) as equations (C-3) and (C-4), where

$$B(1,1) = \sum_{j=1}^{N} \left|A_{j1}\right|^2$$

$$B(1,2) = \frac{1}{2} \sum_{j=1}^{N} (A^*_{j1}A_{j2} + A_{j1}A^*_{j2})$$

$$B(1,3) = \frac{1}{2} \sum_{j=1}^{N} (A^*_{j1}A_{j3} + A_{j1}A^*_{j3}), \text{ etc.}$$

$$A(1,1) = \sum_{j=1}^{N} \left|g_{j1}\right|^2$$

$$A(1,2) = \frac{1}{2} \sum_{j=1}^{N} (g^*_{j1}g_{j2} + g_{j1}g^*_{j2})$$

$$A(1,3) = \frac{1}{2} \sum (g^*_{j1}g_{j3} + g_{j1}g^*_{j3}), \text{ etc.}$$

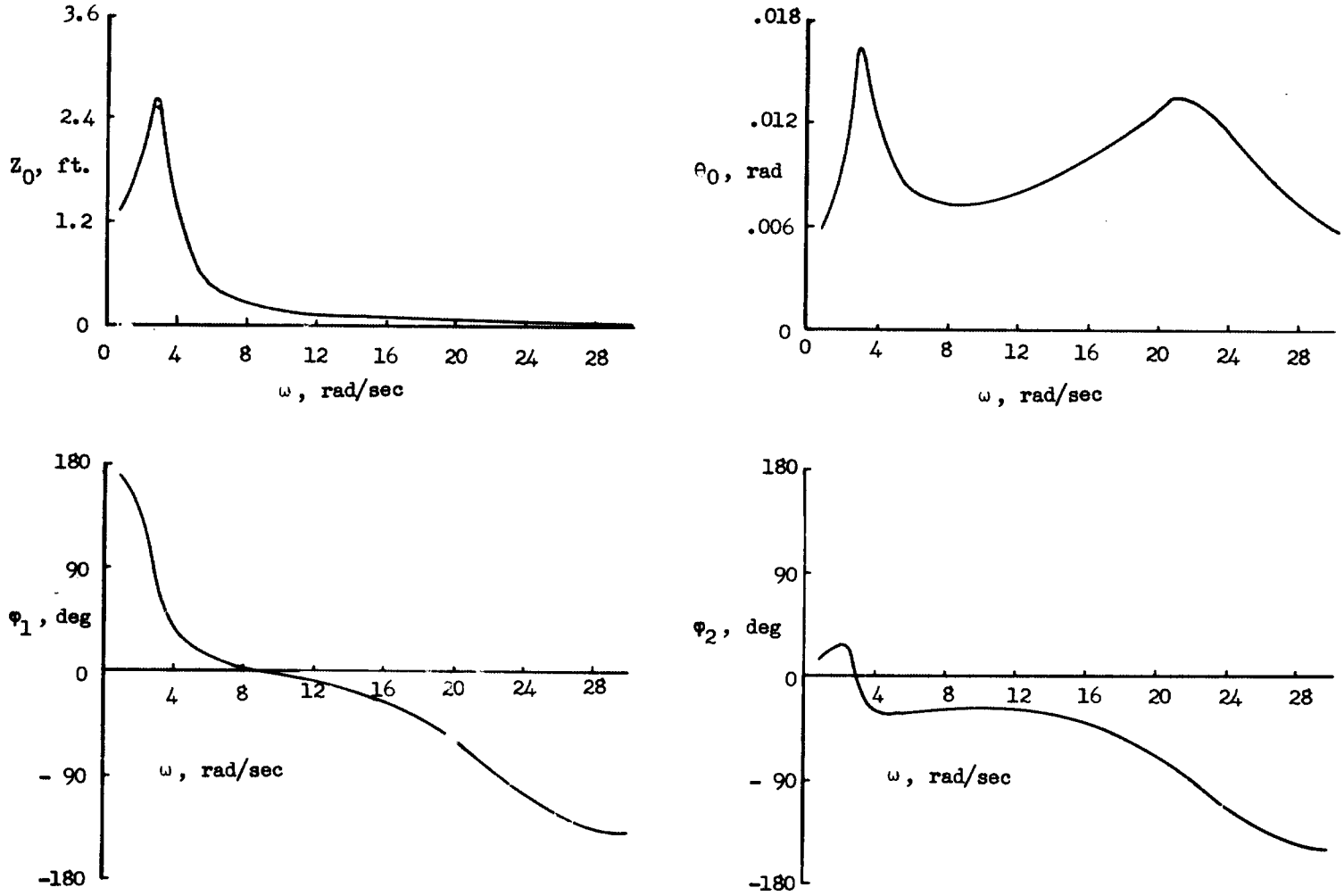

Figure 4.- Longitudinal response as a function of tail frequency.

Based on equation (22), a numerical comparison of the aerodynamic derivatives, with and without response errors, is used to calculate $\frac{\partial C}{\partial \epsilon}$ and the per cent error. In general, equation (22) is written

$$C_{\epsilon \neq 0} = C_{\epsilon=0} + \frac{\partial C}{\partial \epsilon_1} \Delta\epsilon_1 + \frac{\partial C}{\partial \epsilon_2} \Delta\epsilon_2 + \frac{\partial C}{\partial \epsilon_3} \Delta\epsilon_3 + \cdots \frac{\partial C_m}{\partial \epsilon_m} \Delta\epsilon_m$$

Considering each of the error functions separately ($\Delta\epsilon_1 \neq 0$; $\Delta\epsilon_2 = \Delta\epsilon_3 \cdots = \Delta\epsilon_m = 0$) results in the following expressions for the rate of change of the aerodynamic derivatives with respect to the response errors:

$$\frac{\partial C}{\partial \epsilon_1} = \frac{C_{\epsilon_1 \neq 0} - C_{\epsilon=0}}{\Delta\epsilon_1} \qquad \frac{\partial C}{\partial \epsilon_2} = \frac{C_{\epsilon_2 \neq 0} - C_{\epsilon=0}}{\Delta\epsilon_2} \tag{23}$$

We can also define

$$\text{Per cent error} = \frac{C_{\epsilon \neq 0} - C_{\epsilon=0}}{C_{\epsilon=0}} \times 100 \tag{24}$$

A numerical calculation of the aerodynamic derivatives with and without response errors is presented in Table I. Errors ranging in amplitude from 0 to 5 per cent and in-phase angle of 1°, 2°, and 3° are presented. The derivatives are obtained numerically by considering an error in one response function while the others are held constant.

Tables II and III present the calculated data in terms of the rate of change of the aerodynamic derivatives with respect to response error and the per cent error in the aerodynamic derivatives, respectively.

TABLE I.- CALCULATED AERODYNAMIC DERIVATIVES WITH RESPONSE ERROR

ϵ_z, % error	C_{L_α} / rad	C_D	C_{L_δ} / rad	C_{m_α} / rad	$C_{m_{\dot\alpha}}$ / rad	$C_{m_{\dot\theta}}$ / rad	C_{m_δ} / rad	$C_{m_{\dot\alpha}} + C_{m_{\dot\theta}}$ / rad
0	5.00	0.02	-0.400	-1.00	-4.00	-15.00	1.20	-19.00
1	5.05	-0.03	-0.404	-1.00	-3.75	-15.05	1.197	-18.80
2	5.10	-0.08	-0.408	-1.00	-3.42	-15.17	1.194	-18.59
3	5.15	-0.13	-0.412	-0.99	-3.01	-15.37	1.191	-18.38
4	5.20	-0.18	-0.416	-0.99	-2.54	-15.63	1.185	-18.17
5	5.25	-0.23	-0.420	-0.99	-2.00	-15.97	1.182	-17.97
ϵ_θ, % error								
1	4.95	0.07	-0.400	-1.00	-4.17	-15.03	1.215	-19.20
2	4.90	0.12	-0.400	-1.00	-4.26	-15.14	1.230	-19.40
3	4.85	0.17	-0.400	-1.00	-4.27	-15.32	1.245	-19.59
4	4.81	0.21	-0.400	-1.00	-4.20	-15.58	1.260	-19.78
5	4.76	0.26	-0.400	-1.00	-4.06	-15.91	1.275	-19.97
ϵ_{ϕ_1}, deg								
1	5.00	0.09	-0.328	-0.98	0.96	-19.89	1.194	-18.93
2	5.00	0.17	-0.255	-0.96	5.78	-24.61	1.191	-18.83
3	5.00	0.24	-0.182	-0.94	10.46	-29.14	1.188	-18.68
ϵ_{ϕ_2}, deg								
1	5.00	-0.06	-0.473	-1.04	-7.53	-11.43	1.209	-18.96
2	5.00	-0.14	-0.544	-1.09	-18.86	0.04	1.218	-18.82
3	5.00	-0.22	-0.615	-1.13	-26.25	7.64	1.227	-18.61

TABLE II.- RATE OF CHANGE OF AERODYNAMIC DERIVATIVES WITH RESPONSE ERROR

$\Delta\epsilon_z$, % error	$\frac{\partial C_{I_\alpha}}{\partial \epsilon}$	$\frac{\partial C_D}{\partial \epsilon}$	$\frac{\partial C_{I_\delta}}{\partial \epsilon}$	$\frac{\partial C_{m_\alpha}}{\partial \epsilon}$	$\frac{\partial C_{m_{\dot\alpha}}}{\partial \epsilon}$	$\frac{\partial C_{m_{\dot\theta}}}{\partial \epsilon}$	$\frac{\partial C_{m_\delta}}{\partial \epsilon}$	$\frac{\partial (C_{m_{\dot\alpha}} + C_{m_{\dot\theta}})}{\partial \epsilon}$
1	5.0	-5.0	-0.40	0	25.0	-5.0	-0.30	20.0
2	5.0	-5.0	-0.40	0	29.0	-8.5	-0.30	20.5
3	5.0	-5.0	-0.40	0.33	33.0	-12.3	-0.30	20.7
4	5.0	-5.0	-0.40	0.25	36.5	-15.6	-0.39	20.8
5	5.0	-5.0	-0.40	0.20	40.0	-19.4	-0.36	20.6
$\Delta\epsilon_\theta$, % error								
1	-5.0	5.0	0	0	-17.0	-3.0	1.5	-20.0
2	-5.0	5.0	0	0	-13.0	-7.0	1.5	-20.0
3	-5.0	5.0	0	0	-9.0	-10.8	1.5	-19.7
4	-4.8	4.8	0	0	-5.0	-14.5	1.5	-19.5
5	-4.8	4.8	0	0	-1.2	-18.2	1.5	-19.4
$\Delta\epsilon\phi_1$, deg								
1	0	0.07	0.072	0.02	4.96	-4.89	-0.006	0.07
2	0	0.08	0.073	0.02	4.89	-4.81	-0.006	0.08
3	0	0.07	0.073	0.02	4.82	-4.71	-0.003	0.11
$\Delta\epsilon\phi_2$, deg								
1	0	-0.08	-0.073	-0.04	-3.53	3.56	0.009	0.04
2	0	-0.08	-0.072	-0.05	-7.43	7.48	0.009	0.09
3	0	-0.08	-0.072	-0.04	-7.42	7.55	0.009	0.13

TABLE III.- PER CENT ERROR OF AERODYNAMIC DERIVATIVES

$\Delta\epsilon_z$, % error	C_{L_α}	C_D	C_{L_δ}	C_{m_α}	$C_{m_{\dot\alpha}}$	$C_{m_{\dot\theta}}$	C_{m_δ}	$C_{m_{\dot\alpha}} + C_{m_{\dot\theta}}$
1	1.0	-250	1.0	0	-6.3	0.3	-0.25	-1.1
2	2.0	-500	2.0	0	-13.5	1.1	-0.50	-2.2
3	3.0	-750	3.0	-1.0	-24.8	2.5	-0.75	-3.3
4	4.0	-1000	4.0	-1.0	-36.5	4.2	-1.25	-4.4
5	5.0	-1250	5.0	-1.0	-50.0	6.7	-1.50	-5.4
$\Delta\epsilon_\theta$, % error								
1	-1.0	250	0	0	4.3	0.2	1.3	1.1
2	-2.0	500	0	0	6.5	0.9	2.5	2.2
3	-3.0	75[illegible]	0	0	6.8	2.1	3.8	3.1
4	-3.8	900	0	0	5.0	3.9	5.0	4.1
5	-4.8	1200	0	0	2.0	6.1	6.3	5.1
$\Delta\epsilon\phi_1$, deg								
1	0	350	-18.0	-2.0	-124.0	33.0	-0.50	-0.37
2	0	750	-36.0	-4.0	-245.0	64.0	-0.75	-0.90
3	0	1100	-54.5	-6.0	-362.0	94.0	-1.00	-1.70
$\Delta\epsilon\phi_2$, deg								
1	0	-400	18.3	4.0	88.0	-24.0	0.75	-0.21
2	0	-800	36.0	9.0	374.0	-100.0	1.50	-0.95
3	0	-1200	53.8	13.0	556.0	-151.0	2.25	-2.10

These Tables are obtained by applying equations (23) and (24) to the results presented in Table I. Error intervals are included to establish the linearity of the functions. Table II is presented so that equation (22) can be used to establish the effect of errors in several of the variables on each aerodynamic derivative.

3.2.2 Results and Discussion

The results given are for a particular example; therefore, they should not be generalized. Since the dynamics of the problem are dependent on the system parameters and the test point, it is necessary that each case be analyzed separately.

(1) C_{L_α}

Referring to Tables I and III, notice that C_{L_α} appears to behave favorably in the dynamic analysis. That is, C_{L_α} is not significantly affected by errors. This term is one of the more important derivatives and is normally measured statically. Numerical values of this derivative, with errors in response amplitudes, tend to give linear results with error in the derivative on the same order of magnitude as the error in the response. Table I shows that errors in the phase angles ϕ_1 and ϕ_2 do not affect this derivative.

(2) C_D

Referring to Table I, large errors in the drag coefficient are evident for all values of response error. The reason for this is apparent from equation (15a). The drag coefficient appears in combination with C_{L_α} in the form $(C_{L_\alpha} + C_D)$. For most configurations $C_{J_\alpha} >> C_D$, and as our results show, the drag coefficient cannot be separated when a response error is introduced.

Although the drag coefficient, then, should not be measured using the dynamic technique, it is still possible to obtain C_D statically on the mount system. If the static equations of equilibrium are written in the x direction (refer to Fig. 3), the front and rear cables differ in tension as a function of geometry and model drag in the following approximate manner:

$$2T_F \cos \beta_F = 2T_R \cos \beta_R + qSC_D$$

hence

$$C_D = \frac{2(T_F \cos \beta_F - T_R \cos \beta_R)}{qS}$$

Load cells on the front and rear cables provide T_F and T_R.

(3) C_{L_δ}

Referring to Table III, note that amplitude errors affect the magnitude of C_{L_δ} slightly, ranging from zero to about 5 per cent. Errors in phase affect this term appreciably. Errors of 3^o in either ϕ_1 or ϕ_2 result in magnitude errors of over 50 per cent.

The reason for this result is that for conventional airplane configurations the tail lift is almost negligible. The primary forcing function obtained from the tail is the aerodynamic moment $\bar{M}_A$. This moment is physically generated by the tail lift $\bar{Z}_A$ acting a distance L_t rearward of the model center of gravity. (L_t is the distance between the tail aerodynamic center and the aircraft center of gravity.) Etkin (Ref. 1) shows that the aerodynamic moment can be approximated by the equation $\bar{M}_A = -L_t \bar{Z}_A$.

Hence

$$qS\bar{c}C_{m_\delta}\delta = -L_t qSC_{L_\delta}\delta$$

or

$$C_{L_\delta} = -\frac{C_{m_\delta}\bar{c}}{L_t}$$

For our example $L_t = 3.0$ ft since $\bar{c} = 1.0$ ft, $C_{m_\delta} = 1.2$/rad, and $C_{L_\delta} = -0.4$/rad. We can therefore assume that C_{L_δ} can be determined from the values obtained for C_{m_δ}.

(4) C_{m_δ}

Referring to Table III, notice that C_{m_δ} behaves favorably in the dynamic analysis. Amplitude errors affect the magnitude of C_{m_δ} slightly, ranging from near zero to about 6 per cent. Error in phase angle affects C_{m_δ} even less.

(5) C_{m_α}

Another of the important derivatives, which is normally measured statically, appears from Tables I and III to behave quite well in the dynamic analysis. The effect of amplitude errors on C_{m_α} is quite small. Errors in phase angle affect this term the most, resulting in a 13 per cent error due to an error of 3° in ϕ_2.

(6) $C_{m_{\dot{\alpha}}}$, $C_{m_{\dot{\theta}}}$, $(C_{m_{\dot{\alpha}}} + C_{m_{\dot{\theta}}})$

Tables I and III show that errors in both amplitude and phase measurements result in extremely large errors when $C_{m_{\dot{\alpha}}}$ and $C_{m_{\dot{\theta}}}$ are calculated separately. For the test condition analyzed, errors of over 500 per cent are evident for small errors in phase.

Notice, however, that the sum of these terms ($C_{m_{\dot{\alpha}}} + C_{m_{\dot{\theta}}}$) behaves quite well for both amplitude and phase errors. Numerical results presented in Table III show that the sum ($C_{m_{\dot{\alpha}}} + C_{m_{\dot{\theta}}}$) varies almost linearly with amplitude errors while phase affects the results a maximum of about 2 per cent. In view of these results, it appears that the sum of ($C_{m_{\dot{\alpha}}} + C_{m_{\dot{\theta}}}$) can be measured accurately in the dynamic analysis, but unique solutions for each of the derivatives cannot be determined. The following section will further interpret this problem.

3.2.3 Comparison of Free-Flight and Two-Cable-Mount Equations of Motion

In order to fully understand the problems which arise in determining unique solutions for each of the aerodynamic derivatives, a comparison of free-flight and mount equations is presented. Greenburg (Ref. 2) shows that for the free-flight case a linear dependency exists in the dynamic response, so that the aerodynamic derivatives in the pitch equation cannot be solved uniquely. Neglecting the drag coefficient C_D the free-flight lift equation (eq. (15a), $K_{ZZ} = 0$) can be written as follows:

$$m\ddot{z} + qSC_{L_\alpha}\frac{\dot{z}}{U} + qSC_{L_\alpha}\theta = -qSC_{L_\delta}\delta \tag{25}$$

Since $\alpha = \theta + \frac{\dot{z}}{U}$, equation (25) can be written as

$$mU\dot{\alpha} - mU\dot{\theta} + L_\alpha\alpha + L_\delta\delta = 0 \tag{26}$$

where

$$L_\alpha = qSC_{L_\alpha}$$

$$L_\delta = qSC_{L_\delta}$$

Similarly the free-flight pitch equation becomes

$$I_Y\ddot{\theta} - \frac{qS\bar{c}^2}{2U}(C_{m_{\dot{\alpha}}} + C_{m_{\dot{\theta}}})\dot{\theta} - qS\bar{c}C_{m_\alpha}\theta - \frac{qS\bar{c}^2}{2U^2}C_{m_{\dot{\alpha}}}\ddot{z} - \frac{qS\bar{c}}{U}C_{m_\alpha}\dot{z} = qS\bar{c}C_{m_\delta}\delta$$

or

$$I_Y\ddot{\theta} - M_\alpha\alpha - M_{\dot{\alpha}}\dot{\alpha} - M_{\dot{\theta}}\dot{\theta} = M_\delta\delta \qquad (27)$$

Where

$$M_\alpha = qS\bar{c}C_{m_\alpha}$$

$$M_{\dot{\alpha}} = \frac{qS\bar{c}^2}{2U}C_{m_{\dot{\alpha}}}$$

$$M_{\dot{\theta}} = \frac{qS\bar{c}^2}{2U}C_{m_{\dot{\theta}}}$$

$$M_\delta = qS\bar{c}C_{m_\delta}$$

Solving equation (26) for $\dot{\theta}$ results in

$$\dot{\theta} = \frac{L_\alpha\alpha + L_\delta\delta}{mU} + \dot{\alpha}$$

Substituting this expression into equation (27) results in the following:

$$I_Y\ddot{\theta} - \alpha\left(M_\alpha + \frac{M_{\dot{\theta}}L_\alpha}{mU}\right) - \dot{\alpha}(M_{\dot{\alpha}} + M_{\dot{\theta}}) - \delta\left(M_\delta + \frac{M_{\dot{\theta}}L_\delta}{mU}\right) = 0 \qquad (28)$$

Due to the relation expressed in equation (26), equation (28) can be solved for the following combination of derivatives:

$$M_\alpha + \frac{M_{\dot{\theta}}L_\alpha}{mU}$$

$$M_\delta + \frac{M_{\dot{\theta}}L_\delta}{mU}$$

$$M_{\dot{\alpha}} + M_{\dot{\theta}}$$

Greenburg (Ref. 2) states that for most conventional configurations this indeterminacy affects only the separation of the damping derivatives $(C_{m_{\dot{\alpha}}} + C_{m_{\dot{\theta}}})$ because they are of the same order of magnitude. For most configurations the terms $M_\alpha + \frac{M_{\dot{\theta}}L_\alpha}{mU}$ and $M_\delta + \frac{M_{\dot{\theta}}L_\delta}{mU}$ are approximately M_α and M_δ, respectively, to within 5 per cent. Only if $M_{\dot{\theta}}$ or $M_{\dot{\alpha}}$ can be determined separately by some other method can the damping derivatives be separated uniquely.

The equations equivalent to (26) and (27) on the mount system can be written as follows:

$$mU\dot{\alpha} - mU\dot{\theta} + L_\alpha\alpha + L_\delta\delta + K_{ZZ}z = 0 \qquad (29)$$

$$I_Y\ddot{\theta} - M_\alpha\alpha - M_{\dot{\alpha}}\dot{\alpha} - M_{\dot{\theta}}\dot{\theta} + K_{\theta\theta}\theta = M_\delta\delta \tag{30}$$

Solving equation (29) for $\dot{\theta}$ results in

$$\dot{\theta} = \frac{L_\alpha\alpha + L_\delta\delta + K_{ZZ}z}{mU} + \dot{\alpha}$$

Substituting this expression for $\dot{\theta}$ into equation (30) results in

$$I_Y\ddot{\theta} + K_{\theta\theta}\theta - \alpha\left(M_\alpha + \frac{M_{\dot{\theta}}L_\alpha}{mU}\right) - \dot{\alpha}(M_{\dot{\alpha}} + M_{\dot{\theta}}) - M_{\dot{\theta}}\frac{K_{ZZ}z}{mU} - \delta\left(M_\delta + \frac{M_{\dot{\theta}}L_\delta}{mU}\right) = 0 \tag{31}$$

Note the similarity in the aerodynamic terms comprising equations (28) and (31). If the dependency derived in the free-flight case were to exist in the mount system analysis, the case where exact data are used would also break down. It has already been demonstrated in Table I that the mount analysis yields each of the aerodynamic derivatives uniquely when exact response is used. It is the added expression $\frac{M_{\dot{\theta}}K_{ZZ}z}{mU}$ which allows us to solve for $M_{\dot{\theta}}$ uniquely and, therefore, solve for each of the aerodynamic derivatives. Hence the mount system restraint K_{ZZ} allows both the vertical translation and pitch equation to be solved separately for the aerodynamic derivatives C_{m_α}, $C_{m_{\dot{\alpha}}}$, $C_{m_{\dot{\theta}}}$, C_{m_δ}, C_{L_δ}, and C_{L_α}.

The analysis fails to separate the terms $C_{m_{\dot{\alpha}}} + C_{m_{\dot{\theta}}}$ when an error is introduced into the response data due to the magnitude of the term $\frac{M_{\dot{\theta}}K_{ZZ}z}{mU}$. For example:

$$\dot{\alpha}(M_{\dot{\alpha}} + M_{\dot{\theta}}) = \frac{qS\bar{c}^2}{2U}(C_{m_{\dot{\alpha}}} + C_{m_{\dot{\theta}}})\left[\dot{\theta} + \frac{\ddot{z}}{U}\right]$$

$$= (C_{m_{\dot{\alpha}}} + C_{m_{\dot{\theta}}})\left[\frac{qS\bar{c}^2}{2U}\left(i\omega\theta_o e^{i\phi_2} - \frac{\omega^2 z_o}{U} e^{i\phi_1}\right)\right]$$

$$\frac{M_{\dot{\theta}}K_{ZZ}z}{mU} = \frac{qS\bar{c}^2}{2U}(C_{m_{\dot{\theta}}})\frac{K_{ZZ}z_o e^{i\phi_1}}{mU}$$

Comparing $\frac{qS\bar{c}^2}{2mU^2} C_{m_{\dot{\theta}}}K_{ZZ}z_o e^{i\phi_1}$ with $C_{m_{\dot{\theta}}} \frac{\omega^2 z_o e^{i\phi_1}}{2U^2} qS\bar{c}^2$ results in approximately $\frac{K_{ZZ}}{m}$ compared to ω^2. For this example K_{ZZ} = 20 lb/ft, m = 2.0 slugs, and ω = 1,2,3, . . . 30 rad/sec. Hence for a large range of ω, the expression defining $C_{m_{\dot{\theta}}}$ separately is small compared to the expression defining $(C_{m_{\dot{\alpha}}} + C_{m_{\dot{\theta}}})$, and the introduction of an error into the response eliminates any accuracy in separating the two terms.

CHAPTER IV

EXPERIMENTAL TECHNIQUE FOR MEASURING AILERON EFFECTIVENESS AND DAMPING-IN-ROLL STABILITY DERIVATIVES

4.1 Introduction

The lateral equations of motion of the two-cable-mount system are given by equations (14c), (14d), and (14e). The problem of determining each of the aerodynamic derivatives has greatly increased over that of the longitudinal case due to the added degree of freedom and its associated derivatives.

The general approach to measuring the three-degree-of-freedom lateral derivatives would be the same as discussed in the previous chapter. However, Etkin (Ref. 1) states that for many conventional airplane configurations, the roll equation in free flight can be simplified and treated as a single degree of freedom. If we assume it is possible to force the model to behave as a single degree of freedom in the wind tunnel, equation (14d) could be simplified as follows:

$$I_X\ddot{\phi} - \left(\frac{qSb^2}{2U} C_{l_p} - 2\zeta_\phi I_X \omega_{n_\phi}\right)\dot{\phi} + K_\phi\phi = \bar{L}_A$$

Letting $\bar{L}_A = qSbC_{l_\delta}\delta_A$ results in

$$I_X\ddot{\phi} - \left(\frac{qSb^2}{2U} C_{l_p} - 2\zeta_\phi I_X \omega_{n_\phi}\right)\dot{\phi} + K_\phi\phi = qSbC_{l_\delta}\delta_A \qquad (32)$$

The aerodynamic derivatives C_{l_δ} and C_{l_p} appearing in equation (32) are referred to as the aileron effectiveness and damping-in-roll stability derivatives, respectively. A brief insight into the physical nature of the derivatives C_{l_δ} and C_{l_p} is necessary.

The primary function of the ailerons is to produce a rolling motion of the aircraft. As the term implies, aileron effectiveness is a measure of the performance of the ailerons in producing this motion. Physically, a differential deflection of the ailerons creates an incremental change in the lift on each wing. Since this lift is in opposite directions on each wing, a rolling moment is produced. However, when dealing with an elastic airplane, a deflection of the ailerons also produces a twist of the wings. This induced twist changes the wing lift in the opposite direction to the lift due to the aileron deflection. Hence, the moment generated by a control input is the difference between the moment produced by the ailerons and that induced by wing twist. An elastic airplane may even experience a phenomenon referred to in the literature as "aileron reversal," if the moment generated by the wing twist is larger than that produced by the imposed aileron deflection.

C_{l_p} is referred to as the damping-in-roll derivative. In most configurations only the wing contributes significantly to this derivative. A rolling moment is generated opposing the rolling motion of an airplane due to the spanwise angle of attack produced by a roll rate. The angle of attack varies linearly across the wing, from a value of $\frac{\dot{\phi}b}{2U}$ at the right wing tip to $-\frac{\dot{\phi}b}{2U}$ at the left wing tip ($+\dot{\phi}$ right

wing down). The angle-of-attack distribution along both wings generates a moment which resists the rolling motion of the airplane.

It will be shown in this chapter that through the proper selection of cable-mount parameters, the roll response of the model to a sinusoidal oscillation of the ailerons can be approximated by a single degree of freedom. A parametric study of the model and its mount system is presented to establish a mount configuration which permits the roll response to be approximated by a single degree of freedom.

Once the single-degree-of-freedom system approach to the problem is established, the equation of motion is solved for the aerodynamic derivatives C_{l_δ} and C_{l_p}, based on the dynamic response technique presented in Chapter III. In this case the ailerons are sinusoidally oscillated through a known frequency range, and the steady-state model response is monitored.

In order to verify the dynamic technique, experimental results are presented for an aeroelastically scaled model of a high-speed jet transport that was tested in the wind tunnel to determine C_{l_δ} and C_{l_p}. Due to the static nature of C_{l_δ} it is possible to measure this derivative without resorting to a dynamic approach so that a static measure of C_{l_δ} can be found for comparison with the dynamic results. The mount system used during the static wind-tunnel tests is also unique and will be described. Since C_{l_p} is a dynamic derivative, no experimental results are available for comparison purposes. A simplified error analysis to determine the accuracy of the dynamic technique is also presented.

4.2 Analytical Aspects

4.2.1 Equations of Motion

The lateral equations of motion on the two-cable-mount system are given by equations (14c), (14d), and (14e). In order to measure the aileron effectiveness and damping-in-roll stability derivatives, it is necessary to show that the model response to a sinusoidal oscillation of the ailerons can be simplified to a single degree of freedom. If we assume that an oscillation of the ailerons only generates a forcing function in roll, then the right-hand side of the lateral equations of motion can be written, as a function of time, in the following manner:

$$\begin{aligned} \bar{L}(t) &= qSbC_{l_\delta}\delta_A e^{i\omega t} \\ \bar{N}(t) &= 0 \\ \bar{Y}(t) &= 0 \end{aligned} \tag{33}$$

Assuming sinusoidal motion, the steady-state response becomes:

$$\phi(t) = \phi_o e^{i(\omega t+\alpha_1)} \qquad \psi(t) = \psi_o e^{i(\omega t+\alpha_2)} \qquad y(t) = y_o e^{i(\omega t+\alpha_3)}$$

$$\dot{\phi}(t) = i\omega\phi_o e^{i(\omega t+\alpha_1)} \qquad \dot{\psi}(t) = i\omega\psi_o e^{i(\omega t+\alpha_2)} \qquad \dot{y}(t) = i\omega y_o e^{i(\omega t+\alpha_3)}$$

$$\ddot{\phi}(t) = -\omega^2\phi_o e^{i(\omega t+\alpha_1)} \qquad \ddot{\psi}(t) = -\omega^2\psi_o e^{i(\omega t+\alpha_2)} \qquad \ddot{y}(t) = -\omega^2 y_o e^{i(\omega t+\alpha_3)}$$

The phase angles relating model response to aileron deflection are α_1, α_2, and α_3.

Substituting equation (33) and the steady-state response into the lateral equations of motion results in the following form of the equations:

Roll:

$$\phi_o e^{i\alpha_1}\left[-I_X\omega^2 + K_{\phi\phi} - i\omega\left(\frac{qSb^2}{2U} C_{l_p} - 2\zeta_\phi I_X \omega_{\phi\phi}\right)\right] + \psi_o e^{i\alpha_2}\left[I_{XZ}\omega^2 + qSbC_{l_\beta}\right.$$

$$\left. + K_{\phi\psi} - i\omega \frac{qSb^2}{2U} C_{l_r}\right] + y_o e^{i\alpha_3}\left[K_{\phi Y} - i\omega \frac{qSb}{U} C_{l_\beta}\right] = qSbC_{l_\delta}\delta_A \tag{34}$$

Yaw:

$$\phi_o e^{i\alpha_1}\left[I_{XZ}\omega^2 + K_{\psi\phi} - i\omega \frac{qSb^2}{2U} C_{n_p}\right] + \psi_o e^{i\alpha_2}\left[-I_Z\omega^2 + qSbC_{n_\beta} + K_{\psi\psi}\right.$$

$$\left. - i\omega\left(\frac{qSb^2}{2U} C_{n_r} - 2\zeta_\phi I_Z \omega_{\psi\psi}\right)\right] + y_o e^{i\alpha_3}\left[K_{\psi Y} - i\omega \frac{qSb}{U} C_{n_\beta}\right] = 0 \tag{35}$$

Side translation:

$$\phi_o e^{i\alpha_1}\left[K_{Y\phi} - qSC_L - i\omega \frac{qSb}{2U} C_{y_p}\right] + \psi_o e^{i\alpha_2}\left[qSbC_{y_\beta} + K_{Y\psi} + i\omega \frac{qSb}{2U} C_{y_r}\right]$$

$$+ y_o e^{i\alpha_3}\left[-m\omega^2 + K_{YY} - i\omega\left[\frac{qS}{U}(C_{y_\beta} - C_D) - 2\zeta_Y m\omega_{YY}\right]\right] = 0 \tag{36}$$

The simplification of equation (34) as a single degree of freedom yields,

$$\phi_o e^{i\alpha_1}\left[-I_x\omega^2 + K_{\phi\phi} - i\omega\left(\frac{qSb^2}{2U} C_{l_p} - 2\zeta_\phi I_x\omega_{\phi\phi}\right)\right] = qSbC_{l_\delta}\delta_A \qquad (37)$$

It has been stated previously that in flight the roll equation can be analyzed in a form similar to equation (37). Since the cable restraints are a function of mount system geometry and other test parameters, it is necessary to compare calculated results based on both single degree and three-degree-of-freedom solutions. Assuming approximate values of the aerodynamic derivatives, equations (34), (35), and (36) are solved simultaneously for the roll response as a function of the forcing frequency ω. These results are then compared with those for the "single degree" equation. A parametric study is presented for a numerical example with physical and mount properties quite similar to the model of the high-speed jet transport tested in the wind tunnel.

4.2.2 Parametric Study of the Model and Its Mount System

Let Mach number = 0.89, q = 225 psf, hence U = 470 ft/sec. The model physical properties, mount configuration, and assumed aerodynamic derivatives[1] are as follows:

---

[1]The aerodynamic derivatives given are estimated through information supplied by the aircraft manufacturer.

m	= 2.18 slugs	C_{l_p}	= -0.401/rad
I_X	= 5.25 slug-ft^2	C_{l_r}	= 0.078/rad
I_Z	= 7.30 slug-ft^2	C_{l_β}	= -0.062/rad
I_{XZ}	= 0	C_{n_p}	= 0.422/rad
S	= 8.94 ft^2	C_{n_r}	= -0.124/rad
b	= 8.46 ft	C_{n_β}	= 0.117/rad
h	= 0.35 ft	C_{y_p}	= 0.105/rad
d	= 0.30 ft	C_{y_r}	= 0.0051/rad
$\beta_F = \beta_R$	= 20.0 deg	C_{y_β}	= -0.725/rad
$L_F = L_R$	= 20.0 ft	C_D	= 0.02
T_F	= 161 lb	C_L	= 0.035
T_R	= 140 lb		
$\zeta_\phi = \zeta_Y = \zeta_\psi$	= 0.05		

The parametric study will deal with the design of a mount configuration based on the fore and aft pulley separation distances a and e (Fig. 3), which permits the roll response to be approximated by a single degree of freedom. The cable restraints for this example are calculated from the mount restraint equations presented in Chapter II. Calculated values of the mount restraints K_{YY} and $K_{\phi\phi}$ are 28.5 lb/ft and 70.6 ft-lb/rad, respectively, since these restraints are not functions of either a or e. Values of the restraints $K_{\psi Y}$ and $K_{\psi\psi}$, as a function of the parameters a and e, are presented in Figure 5. Due to the mount symmetry $K_{Y\phi} = K_{\phi Y} = K_{\psi\phi} = K_{\phi\psi} = 0$.

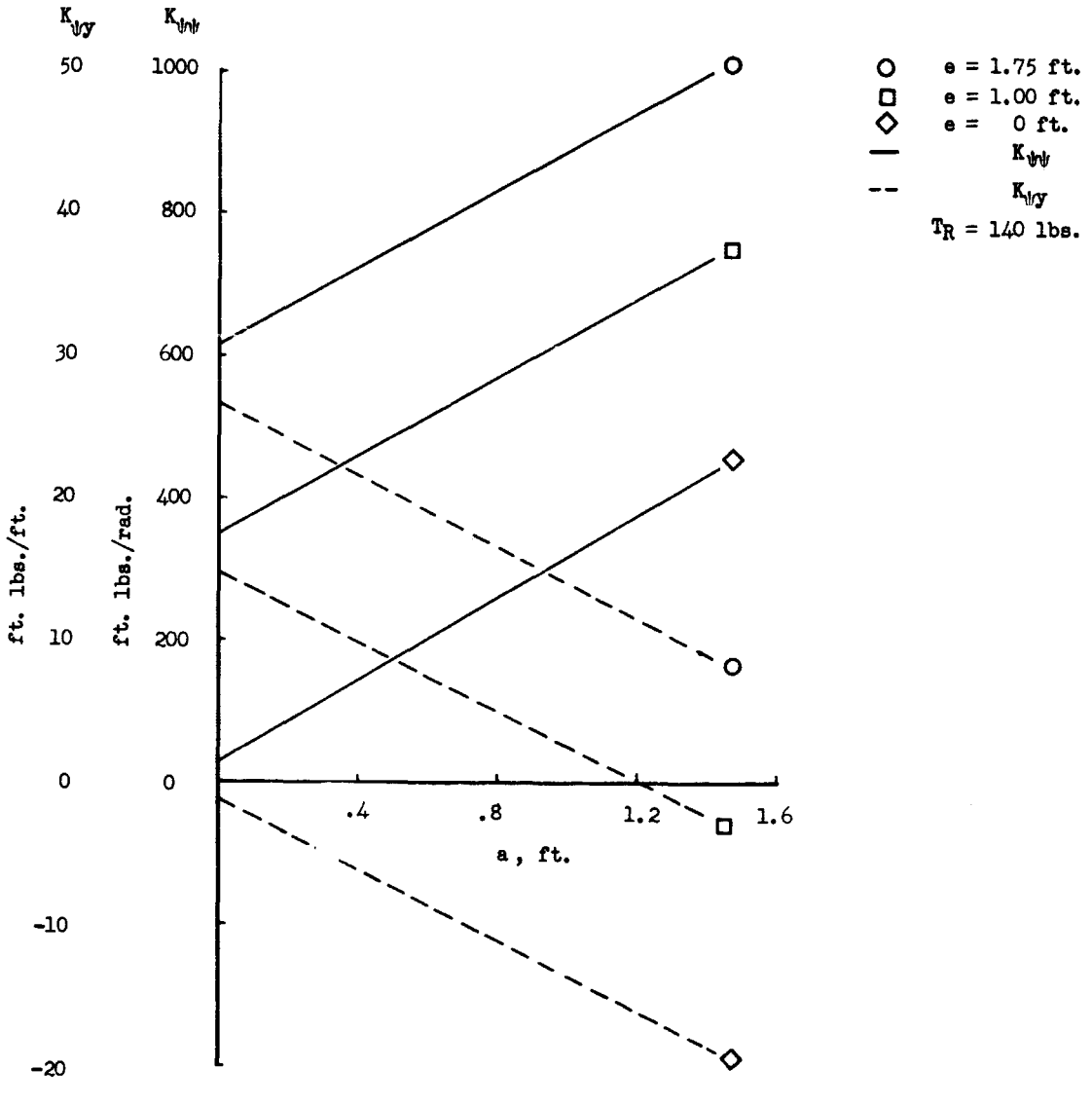

Figure 5.- Cable restraints as a function of fore and aft pulley separation distances, a and e.

Using the physical and aerodynamic properties of the example given, equations (34), (35), and (36) are solved simultaneously for the roll response as a function of the aileron frequency ω. Figure 6 presents results obtained for three sets of a and e values and compares three-degree-of-freedom to single-degree-of-freedom solutions. Since no value of C_{l_δ} is assumed, the results are presented in terms of the magnitude $\frac{1}{C_{l_\delta}}\left|\frac{\phi}{\delta_A}\right|$ and α_1 versus aileron forcing frequency ω. These results should be valid for any nonzero C_{l_δ}.

All three sets of data presented in Figure 6 agree well with the single-degree-of-freedom calculations for frequencies above approximately 8 rad/sec. Below this frequency, a peak response around 4-1/2 rad/sec is apparent for a = 0, e = 1.75 ft, and a = 0, e = 1.0 ft. For the case a = 1.2 ft, e = 1.0 ft, this peak response is much less pronounced and the calculated data compare favorably with the single degree analysis throughout the frequency range given.

$K_{\psi Y}$ for the three sets of a and e values (Fig. 5) are as follows:

	$K_{\psi Y}$ - ft-lb/ft
a = 0, e = 1.75	26.6
a = 0, e = 1.00	14.8
a = 1.2, e = 1.0	0

Comparing the trend in $K_{\psi Y}$ with the results presented in Figure 6, we notice that as the magnitude of $K_{\psi Y}$ diminishes, the single degree and three-degree-of-freedom analysis agree more favorably.

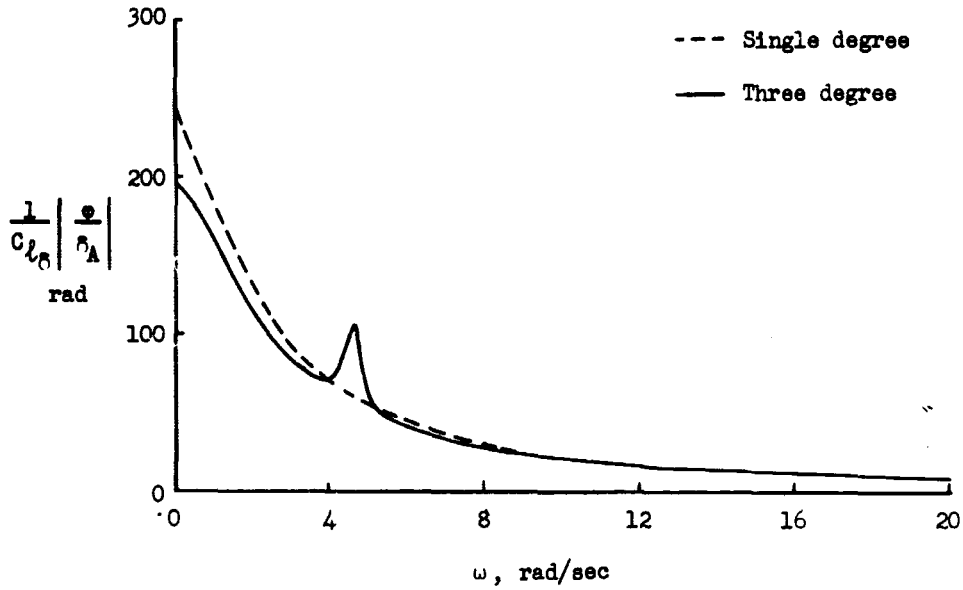

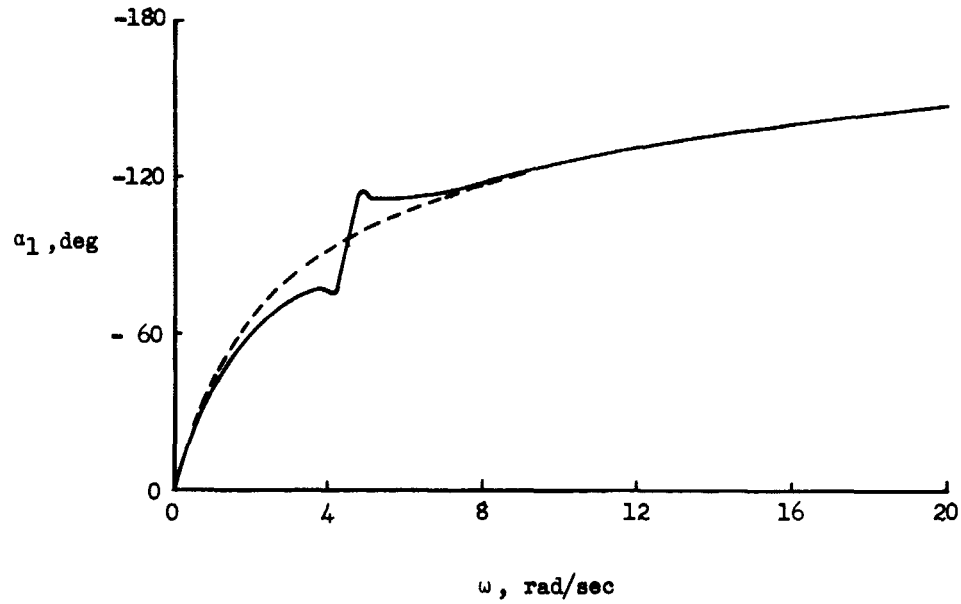

Figure 6(a).- Roll response as a function of aileron frequency. (a = 0; e = 1.75)

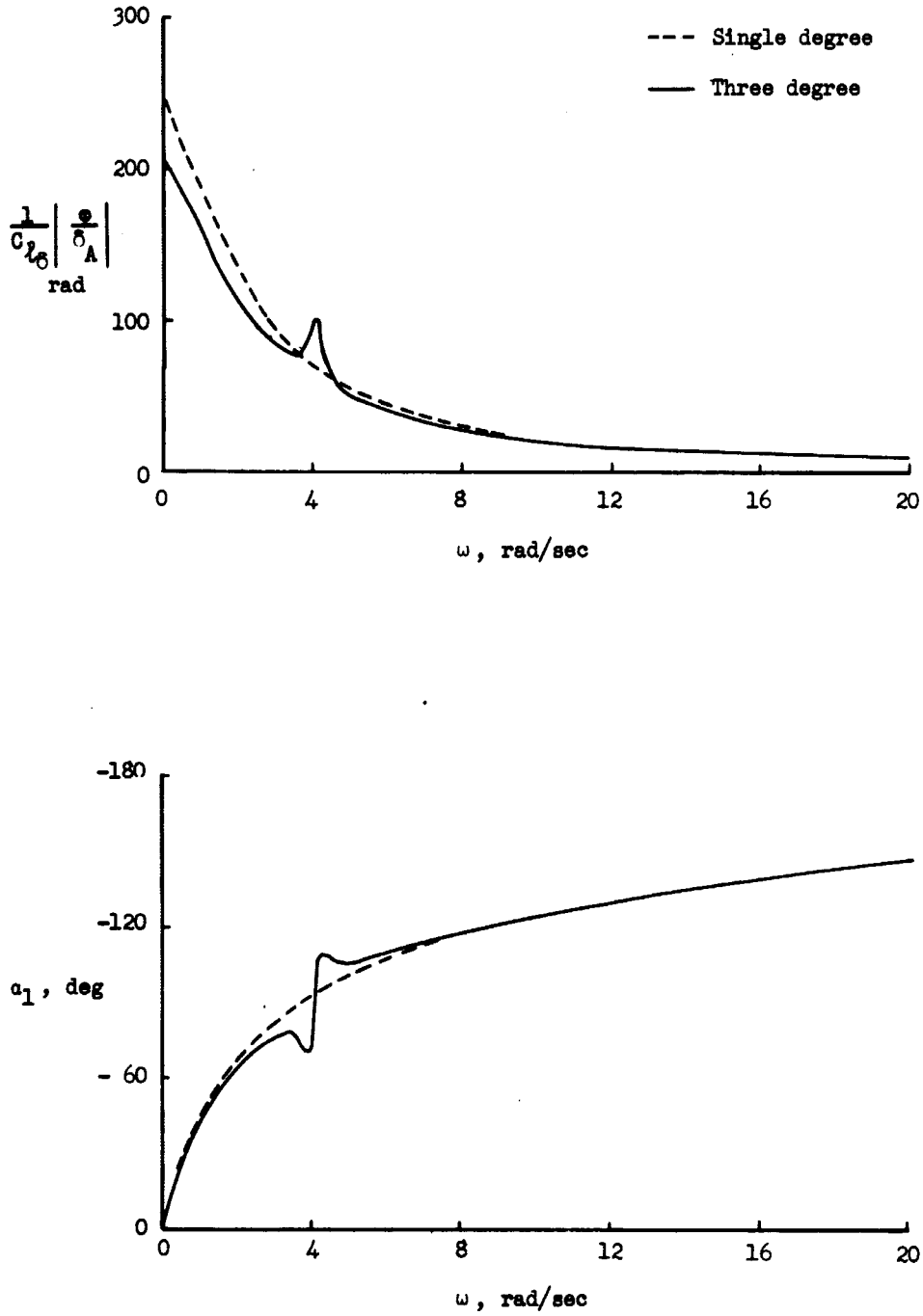

Figure 6(b).- Roll response as a function of aileron frequency. (a = 0; e = 1.00)

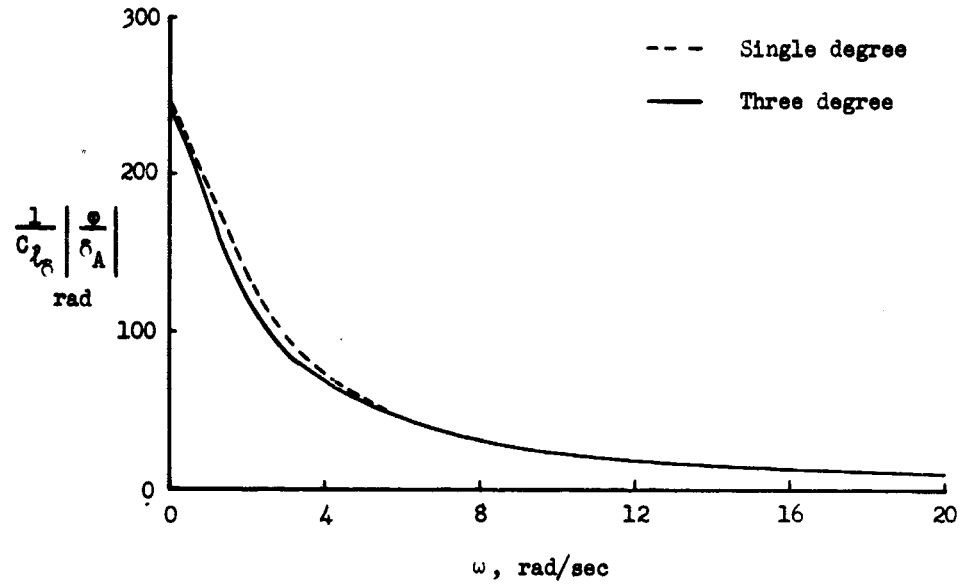

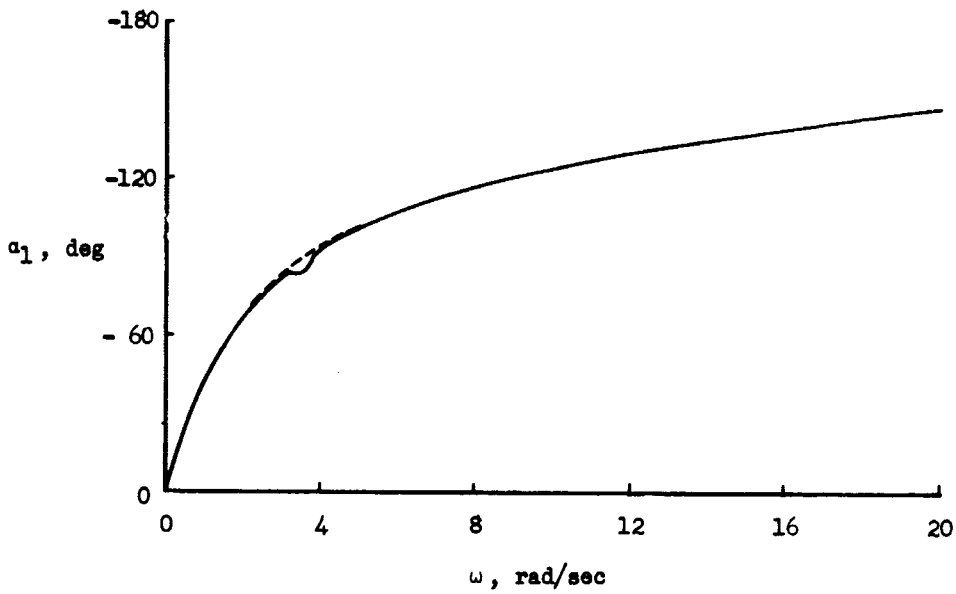

Figure 6(c).- Roll response as a function of aileron frequency. (a = 1.2; e = 1.0)

These results are more apparent if we look at the homogeneous solution of the equations of motion to determine the dynamic behavior of the system. Let $\bar{L}(t) = \bar{N}(t) = \bar{Y}(t) = 0$. Assume $\phi(t) = \phi_o e^{\lambda t}$, $\psi(t) = \psi_o e^{\lambda t}$, and $y(t) = y_o e^{\lambda t}$; where $\lambda = \eta + i\omega$. Hence

$$\dot{\phi}(t) = \lambda\phi_o e^{\lambda t} \qquad \dot{\psi}(t) = \lambda\psi_o e^{\lambda t} \qquad \dot{y}(t) = \lambda y_o e^{\lambda t}$$

$$\ddot{\phi}(t) = \lambda^2\phi_o e^{\lambda t} \qquad \ddot{\psi}(t) = \lambda^2\psi_o e^{\lambda t} \qquad \ddot{y}(t) = \lambda^2 y_o e^{\lambda t}$$

Substituting these terms into equations (34), (35), and (36) results in three homogeneous algebraic equations in the unknowns ϕ_o, ψ_o, y_o, and containing λ.

Therefore

$$\begin{aligned}
&\phi_o\left[A_{11}\lambda^2 + A_{12}\lambda + A_{13}\right] + \psi_o\left[b_{11}\lambda^2 + b_{12}\lambda + b_{13}\right] + y_o\left[C_{12}\lambda + C_{13}\right] = 0 \\
&\phi_o\left[A_{21}\lambda^2 + A_{22}\lambda + A_{23}\right] + \psi_o\left[b_{21}\lambda^2 + b_{22}\lambda + b_{23}\right] + y_o\left[C_{22}\lambda + C_{23}\right] = 0 \\
&\phi_o\left[A_{32}\lambda + A_{33}\right] + \psi_o\left[b_{32}\lambda + b_{33}\right] + y_o\left[C_{31}\lambda^2 + C_{32}\lambda + C_{33}\right] = 0
\end{aligned} \tag{38}$$

$$A_{11} = I_X \qquad A_{21} = -I_{XZ} \qquad A_{32} = -\frac{qSb}{2U} C_{y_p}$$

$$A_{12} = -\frac{qSb^2}{2U} C_{l_p} + 2\zeta_\phi I_X \omega_\phi \qquad A_{22} = -\frac{qSb^2}{2U} C_{n_p} \qquad A_{33} = K_{Y_\phi} - qSC_L$$

$$A_{13} = K_{\phi\phi} \qquad A_{23} = K_{Y\phi} \qquad b_{32} = -\frac{qSb}{2U} C_{y_r}$$

$$b_{11} = -I_{XZ} \qquad b_{21} = I_Z \qquad b_{33} = qSC_{y_\beta} + K_{Y\psi}$$

$$b_{12} = -\frac{qSb^2}{2U} C_{l_r} \qquad b_{22} = -\frac{qSb^2}{2U} C_{n_r} + 2\zeta_\psi I_Z \omega_\psi \qquad C_{31} = m$$

$$b_{13} = qSbC_{l_\beta} + K_{\phi\psi} \qquad b_{23} = qSbC_{n_\beta} + K_{\psi\psi} \qquad C_{32} = -\frac{qS}{U}(C_{y_\beta} - C_D) + 2\zeta_Y m\omega_{YY}$$

$$C_{12} = -\frac{qSb}{U} C_{l_\beta} \qquad C_{22} = -\frac{qSb}{U} C_{n_\beta} \qquad C_{33} = K_{YY}$$

$$C_{13} = K_{\phi Y} \qquad C_{23} = K_{\psi Y}$$

Setting the determinant of the coefficients of equation (38) equal to zero provides the condition for determining the values of λ. This determinant is known as the "stability determinant," and its expansion results in the characteristic equation of the dynamic system. For this example the characteristic equation is of the form

$$A\lambda^6 + B\lambda^5 + C\lambda^4 + D\lambda^3 + E\lambda^2 + F\lambda + G = 0 \qquad (39)$$

The six roots of this equation establish the dynamic characteristics of the system. For the example given the solutions of equation (39) are as follows:

a = 0, e = 1.75	λ_1 = -1.50
	λ_2 = -11.1
	λ_3, λ_4 = -0.16 ± i 4.47
	λ_5, λ_6 = -2.28 ± i 18.79
a = 0, e = 1.0	λ_1 = -1.407
	λ_2 = -11.16
	λ_3, λ_4 = -0.152 ± i 4.15
	λ_5, λ_6 = -2.22 ± i 17.9
a = 1.2, e = 1.0	λ_1 = -1.17
	λ_2 = -11.17
	λ_3, λ_4 = -0.36 ± i 3.6
	λ_5, λ_6 = -2.27 ± i 19.2

Figure 7 presents these results plotted in the complex plane. Since the complex roots appear in conjugate pairs, only the upper half of the complex plane is presented. The radial distance from the origin to a complex root is the undamped natural frequency ω_n. The angle between the radial vector and the $i\omega$ axis is equal to $\sin^{-1} \bar{\zeta}_n$, where $\bar{\zeta}_n$ is the damping ratio of the model in flight relative to critical damping.

Note in Figure 7 that a lightly damped mode exists at 4.47, 4.15, and 3.6 rad/sec for the three cases under consideration. Reed and Abbott (Ref. 4) refer to this as the side translation mount mode. (This can be verified by substituting the roots λ_3, λ_4 into equation (38) and solving for the characteristic mode shape.) If we assume the forced model response at the side translation frequency decreases with increased damping in this mode, the case where $a = 1.2$, $e = 1.0$ would exhibit the least response. Figure 6 confirms this fact since the response at the side translation frequency for $a = 1.2$, $e = 1.0$ is much less pronounced. The cable configuration which allows single degree approximation seems to be one in which the mount restraint $K_{\psi Y} = 0$ since this increases the damping in the side translation mode. Based on this analysis the model pulley locations were fixed at $a = 1.2$ ft, $e = 1.0$ ft, and the model response to a sinusoidal oscillation of the ailerons was assumed to behave as a single degree of freedom in roll.

4.2.3 Single-Degree-of-Freedom Solution

Once it has been assumed that the model behaves essentially as a single degree of freedom in roll, equation (37) can be written in the form

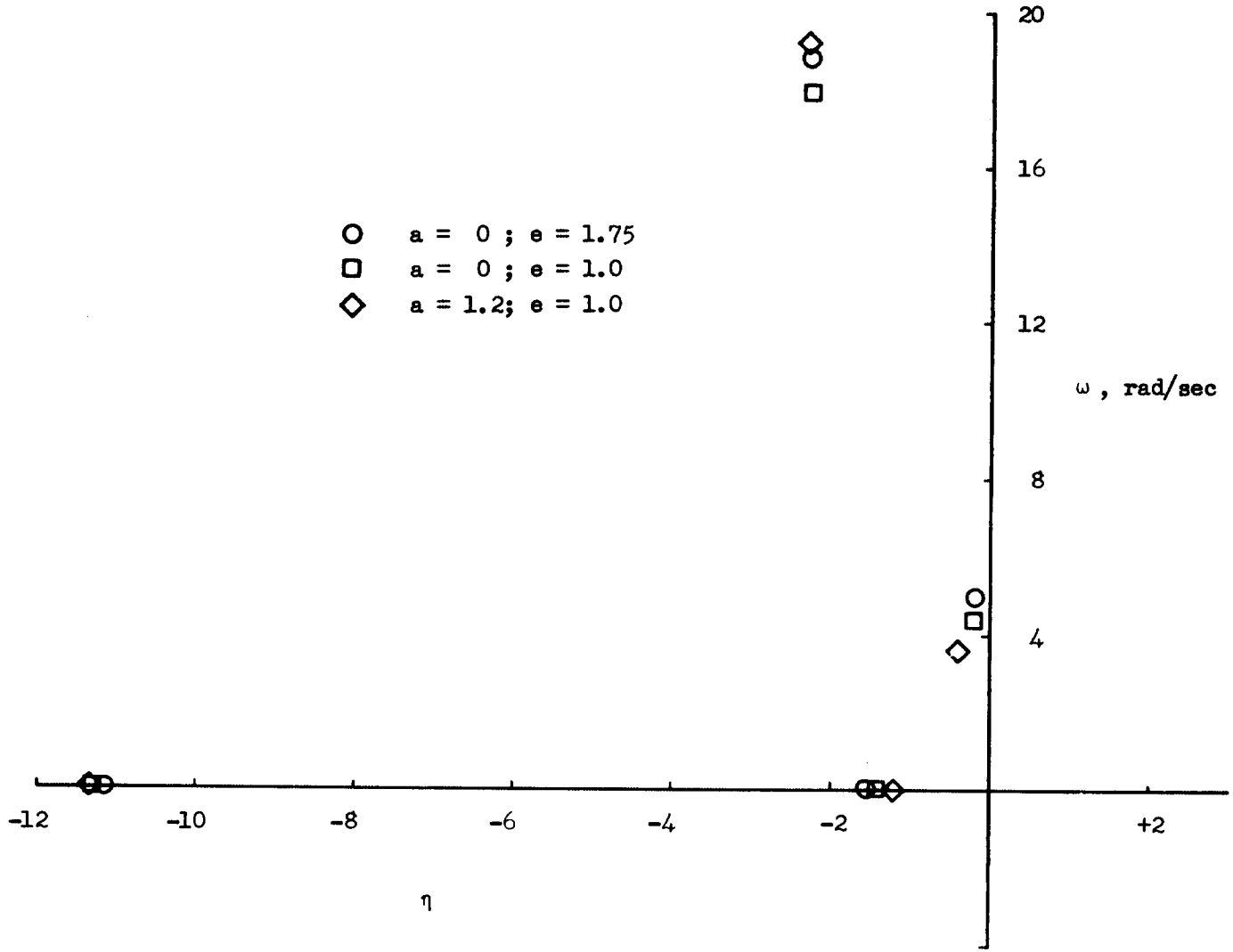

Figure 7.- Dynamic characteristics of lateral modes.

$$i\omega\left(\frac{qSb^2}{2U} C_{l_p} - 2\zeta_\phi I_x \omega_{\phi\phi}\right)\phi_o e^{i\alpha_1} + qSbC_{l_\delta}\delta_A = (-I_x\omega^2 + K_{\phi\phi})\phi_o e^{i\alpha_1} \tag{40}$$

One further simplification is desirable in order to measure the aileron derivative C_{l_δ} and the damping-in-roll derivative C_{l_p}. Looking at the magnitude of the terms $\frac{qSb^2}{2U} C_{l_p}$ and $2\zeta_\phi I_x \omega_{\phi\phi}$ in equation (40), we notice that $\frac{qSb^2}{2U} C_{l_p} >> 2\zeta_\phi I_x \omega_{\phi\phi}$ ($C_{l_p} \approx 0.3$ from estimated data). Therefore, equation (40) can be written approximately as

$$i\omega \frac{qSb^2}{2U} \phi_o e^{i\alpha_1} C_{l_p} + qSbC_{l_\delta}\delta_A = (-I_x\omega^2 + K_{\phi\phi})\phi_o e^{i\alpha_1} \tag{41}$$

Equation (41) can be solved for C_{l_p} and C_{l_δ} using a least-squares solution, by measuring the dynamic amplitude ϕ_o and the phase angle α_1 at N discrete frequencies. Assuming C_{l_δ} and C_{l_p} are independent of frequency, equation (41) becomes

$$A_{j1}C_{l_p} + A_{j2}C_{l_\delta} = b_j$$

where

$$A_{j1} = \frac{qSb^2}{2U}\left[i\omega\phi_o e^{i\alpha_1}\right]_{\omega=\omega_j}$$

$$A_{j2} = qSb\delta_A$$

$$A_{j3} = \left[(-I_x\omega^2 + K_{\phi\phi})\phi_o e^{i\alpha_1}\right]_{\omega=\omega_j} \qquad j = 1,2,3, \ldots N$$

From Appendix B

$$\begin{bmatrix} 2\sum_{j=1}^{N} |A_{j1}|^2 & \sum_{j=1}^{N} (A_{j1}^* A_{j2} + A_{j1} A_{j2}^*) \\ \sum_{j=1}^{N} (A_{j1}^* A_{j2} + A_{j1} A_{j2}^*) & 2\sum_{j=1}^{N} |A_{j2}|^2 \end{bmatrix} \begin{bmatrix} C_{l_p} \\ C_{l_\delta} \end{bmatrix} = \begin{bmatrix} \sum_{j=1}^{N} (A_{j1}^* b_j + A_{j1} b_j^*) \\ \sum_{j=1}^{N} (A_{j2}^* b_j + A_{j2} b_j^*) \end{bmatrix}$$

Hence

$$\begin{bmatrix} \left(\frac{qSb^2}{2U}\right)^2 \sum_{j=1}^{N} (\omega\phi_o)^2_{\omega=\omega_j} & -\frac{q^2S^2b^3\delta_A}{2U} \sum_{j=1}^{N} (\omega\phi_o \sin\alpha_1)_{\omega=\omega_j} \\ -\frac{q^2S^2b^3\delta_A}{2U} \sum_{j=1}^{N} (\omega\phi_o \sin\alpha_1)_{\omega=\omega_j} & (qSb\delta_A)^2 N \end{bmatrix} \begin{bmatrix} C_{l_p} \\ C_{l_\delta} \end{bmatrix}$$

$$= \begin{bmatrix} 0 \\ -qSb\delta_A \sum_{j=1}^{N} \left[(I_X\omega^2 - K_{\phi\phi})(\phi_o \cos\alpha_1)\right]_{\omega=\omega_j} \end{bmatrix}$$

(42)

4.3 Experimental Results

A 1/19-size aeroelastically scaled model of a large, subsonic, multijet cargo airplane was tested in the NASA-Langley transonic dynamics tunnel. The wind tunnel uses Freon-12 gas as the testing medium. The speed of sound in Freon-12 is approximately half that of air. Since many aeroelastic phenomenon are functions of Mach number, this allows testing to higher Mach numbers at reduced dynamic pressures.

Since C_{l_δ} can be measured either statically or dynamically, test results employing both of these methods will be presented. These results will then be compared to establish an evaluation of the dynamic approach. The mount system used during the static tests is also unique and will be briefly described.

4.3.1 Static Wind-Tunnel Tests

Once the model is designed and constructed, static testing is fairly straightforward. Grosser (Ref. 3) presents a testing technique where the model is supported in the wind tunnel on a sting-pylon-spring mount system. A photograph of the model on this mount support is presented in Figure 8.

The support consists of a rigid sting which is attached to the tunnel splitter plate, a pair of pylons which extend from the sting to within the model fuselage contour, and a set of springs which connect the fuselage spar to the pylons. The mount allows the model six degrees of limited freedom. The model is restrained from excessive motion by stops located on the front and rear pylons. Rolling moments generated by a deflection of the ailerons are transmitted by a pair of push-pull

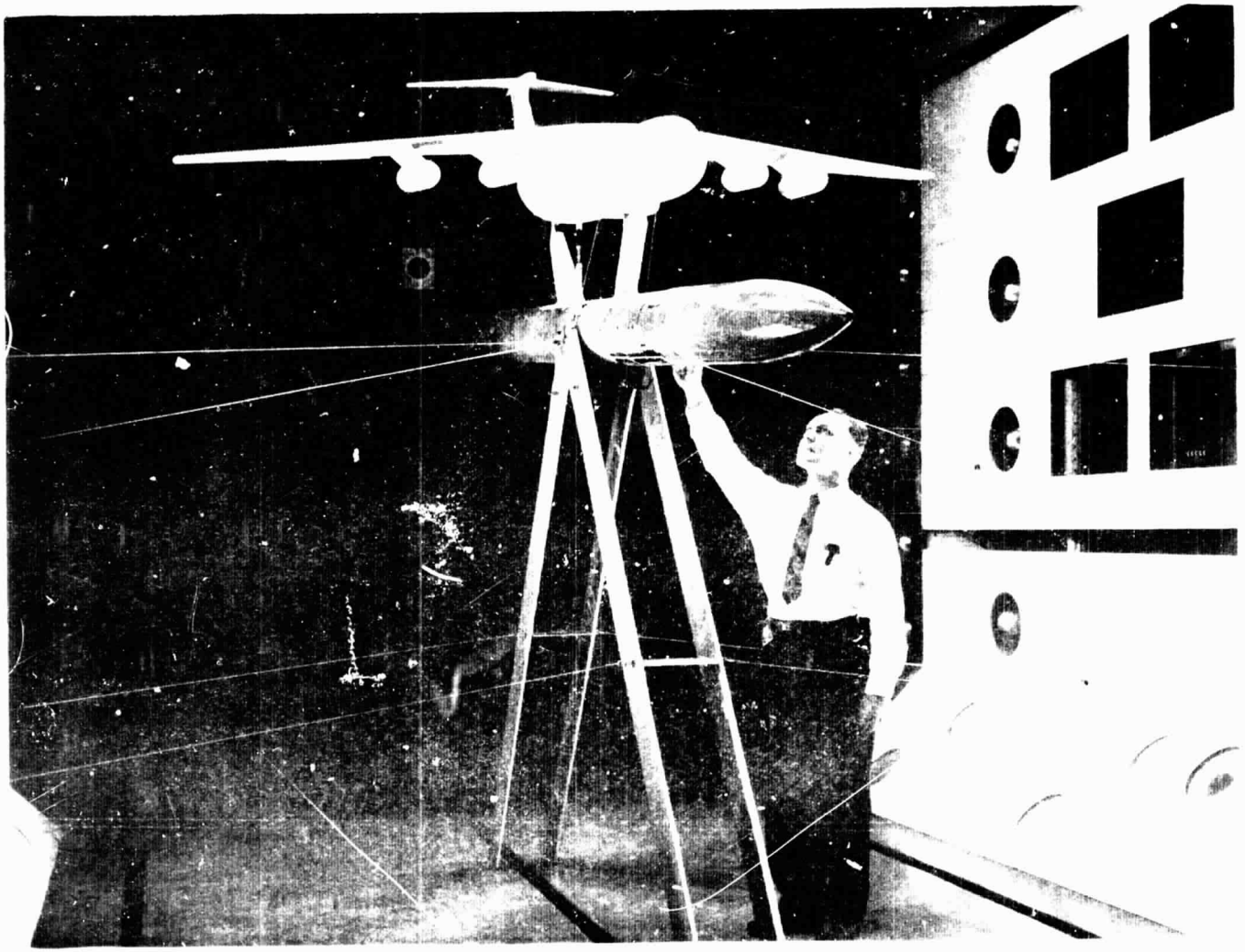

Figure 8.- Photograph of model on sting-pylon-spring mount.

rods extending from the fuselage spar to a strain-gaged beam located in the sting. Roll control for trim, independent of model control surfaces, is provided by a remotely controlled rotation of the entire roll mechanism within the sting.

At selected test points during a run, the ailerons are remotely deflected. Rolling moments and aileron displacements, measured from the strain-gaged beam and position indicators on the ailerons, respectively, are monitored on direct writing recorders. Since rolling moment is defined as $qSbC_{l_\delta}\delta_A$, C_{l_δ} can be determined from the measured data. Static values of C_{l_δ}, determined at the same test conditions as the dynamic tests, will be presented under the comparison of experimental results.

The static wind-tunnel tests were originally designed to establish the aileron reversal boundary of the model. For purely informative purposes the results of this test are presented in Figure 9. Curves representing the measured reversal boundary ($C_{l_\delta} = 0$) and 25 in-lb of rolling moment/degree of aileron deflection are given as a function of model dynamic pressure versus Mach number. The two reversal points measured statically on the cable-mount system will be discussed later. The dashed line representing the estimated boundary is based on positive aileron effectiveness measurements approaching reversal. The reversal boundary could not be attained due to excessive buffeting loads experienced in this region.

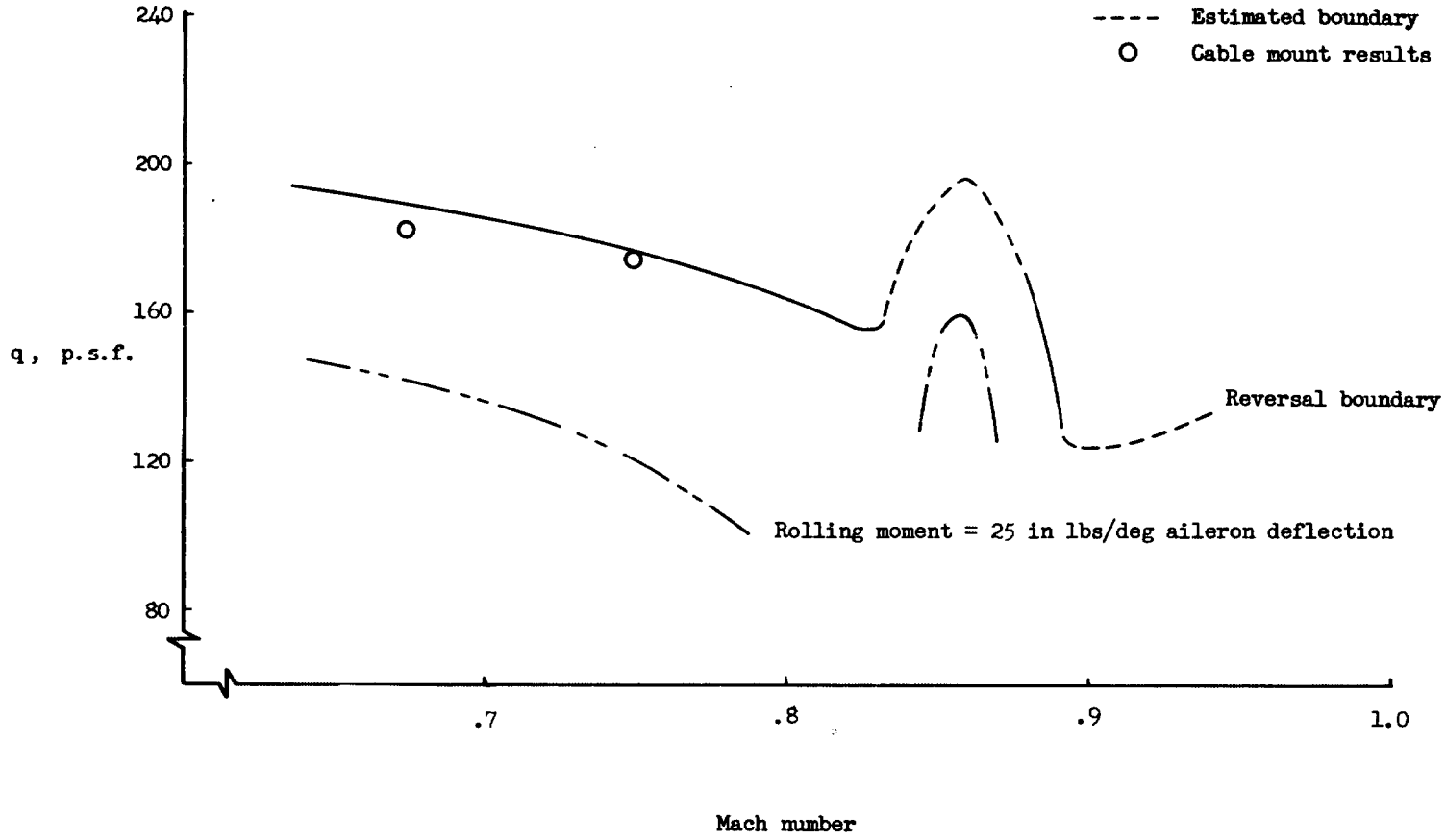

Figure 9.- Aileron effectiveness boundaries.

4.3.2 Dynamic Wind-Tunnel Tests

In order to verify the dynamic technique, the model used in the previously mentioned static tests was tested dynamically to determine the derivatives C_{l_δ} and C_{l_p}. A photograph of the model on the two-cable mount is presented in Figure 10.

The aileron drive mechanism on the model had to be modified in order to provide a sinusoidal fixed amplitude deflection. The aileron drive was modified to consist of a pair of push-pull rods extending from the aileron pivot to the wing attachment structure, a rotating cam, and a variable speed ac motor. The aileron frequency is altered remotely by varying the voltage to the drive motor. A finite torque was required to overcome friction in the drive system, and therefore limited it to a minimum sustained frequency of about 0.5 cps. The maximum frequency was around 4.0 cps. The aileron amplitude could not be altered during a run since this was set by the eccentric attachment of the push-pull rods on the cam. The drive mechanism was designed so that the ailerons would return to zero deflection after the oscillation. The ailerons could also be statically deflected up to the maximum preset dynamic amplitude. Roll control was provided remotely by a pair of spring loaded spoiler panels located inboard on each wing. These panels were opened and closed by means of a torque tube arrangement driven by an electric motor. Longitudinal control was provided by a remotely controlled horizontal stabilizer.

Onboard instrumentation included a miniature rate gyro and a strain-gage position indicator to measure roll rate $\dot{\phi}$ and aileron

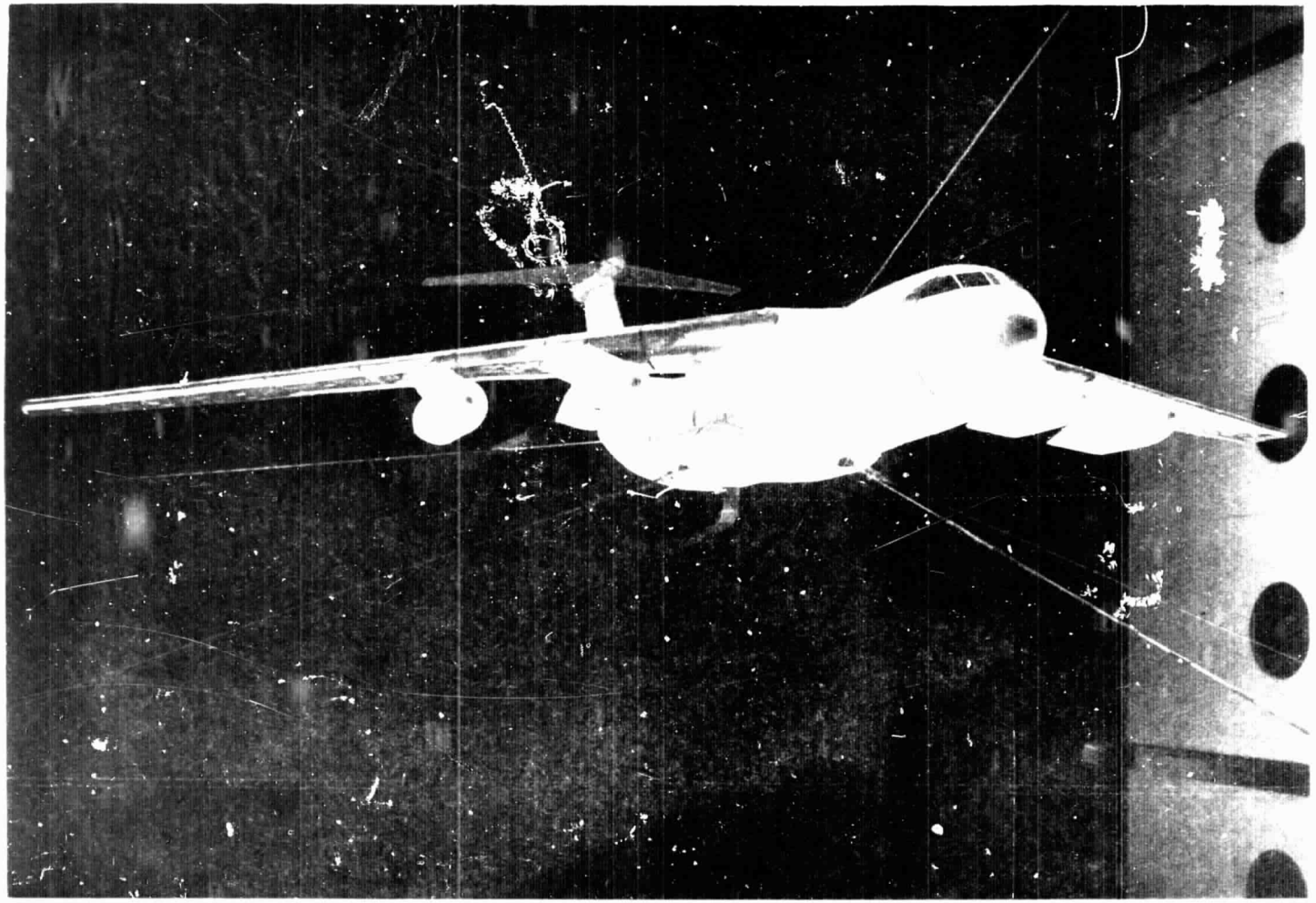

Figure 10.- Photograph of model on two-cable mount.

displacement δ_A, respectively. A servo accelerometer was included to measure static roll angles and provide a level roll reference. Signals from these instruments were displayed on a direct writing recorder for visual monitoring and simultaneously recorded on magnetic tape for further analysis.

The dynamic amplitude is determined by integrating the roll rate signal. For sinusoidal motion this integration results in $|\phi_o| = \left|\frac{\dot{\phi}}{\omega}\right|$. Ideally, a direct comparison between the traces $\dot{\phi}$ and δ_A as a function of time is all that is required to determine the phase angle α_1. Since the model is essentially free and subjected to tunnel turbulence, signal noise, etc., this procedure is quite time consuming and subject to added errors. In lieu of this, an electronic sin-cosine resolver was utilized to determine α_1. This instrument is designed to electronically evaluate the phase angle between two known signals.

Once the dynamic response of the system is known, a value of the mount restraint $K_{\phi\phi}$ is required before solving equation (42) for the derivatives C_{l_δ} and C_{l_p}. This restraint is calculated based on the equation presented in Chapter II. Since $K_{\phi\phi}$ is a function of front and rear cable tensions (geometric properties are known), miniature load cells are installed in these cables and at each test point these tensions are recorded.

The geometric and physical properties of the model and mount are as follows:[1]

---

[1]A response analysis with measured model properties was run to establish that the model behaves essentially as a single degree of freedom.

I_X = 2.16 slug-ft^2

Weight = 47.9 lb

S = 8.94 ft^2

b = 8.46 ft

δ_A = 0.105 rad

$L_F = L_R$ = 23.0 ft

$\beta_F = \beta_R$ = 20 deg

a = 1.2 ft

e = 1.0 ft

h = 0.37 ft

d = 0.39 ft

Tests were run at Mach numbers 0.675 and 0.75 over a range of dynamic pressures from 115 psf to the reversal boundary. At each dynamic pressure, tunnel conditions were held constant while the ailerons were oscillated over a range of frequencies. At each discrete frequency, roll rate, aileron deflection, cable tensions, and the tunnel parameters were recorded.

Theoretically, the model should have no roll response at the reversal boundary. Such is not the case, since this assumption is based on a single-degree-of-freedom analysis. For the areas where the ailerons are quite effective (C_{l_δ} is a function of Mach number and dynamic pressure), the assumption that $\bar{N}(t) = \bar{Y}(t) = 0$ is realiztic. As the ailerons become less effective so does the forcing function $\bar{L}(t)$. In the region near reversal the servo accelerometer was used.

The reversal dynamic pressure was estimated at the point where no roll was evident for a static deflection of the ailerons. The dynamic pressure was then increased slightly above this point, and reversal was noted both on the accelerometer and visually.

Table IV presents the measured model response data as a function of Mach number and dynamic pressure over a range of aileron forcing functions. The dynamic amplitude ϕ_o, the dynamic phase angle α_1, (sin-cosine resolver), the cable-mount tensions, and the tunnel test parameters at each frequency are substituted into equation (42) to determine the aerodynamic derivatives. Figure 11 presents the calculated aerodynamic derivatives as a function of Mach number and dynamic pressure.

4.3.2.1 Error Analysis.- In order to establish the effect of measured response errors on the accuracy of the calculated derivatives, a simpl numerical error analysis is included. Test data obtained at Mach number 0.675 are used in the analysis. At each of the test dynamic pressures a response error was introduced in the following form:

$$\phi_{\epsilon\neq 0} = \phi_{\epsilon=0} + \epsilon_\phi \cdot \phi_{\epsilon=0}$$

$$\alpha_{1_{\epsilon\neq 0}} = \alpha_{1_{\epsilon=0}} + \alpha_{1_\epsilon}$$

where

$\phi_{\epsilon=0}$ = measured dynamic amplitude

ϵ_ϕ = incremental error

$\phi_{\epsilon\neq 0}$ = measured dynamic amplitude with error

TABLE IV.- MEASURED MODEL ROLL RESPONSE

ω, rad/sec	ϕ_o, rad	α_1, deg	M	Q, lb/ft^2	U, ft/sec	T_F, lb	T_R, lb
26.4	0.011	-159	0.675	115	350	130	100
22.8	0.013	-150					
21.4	0.016	-147					
18.3	0.019	-136					
16.6	0.021	-117					
13.8	0.022	-112					
10.8	0.029	-101					
8.9	0.038	-99					
6.7	0.051	-86					
4.3	0.072	-66					
25.5	0.010	-158	0.675	130	350	138	100
22.1	0.013	-147					
20.9	0.014	-143					
17.7	0.018	-116					
15.7	0.018	-107					
13.8	0.021	-111					
11.6	0.024	-109					
9.3	0.031	-99					
5.1	0.055	-72					
3.9	0.064	-62					
2.9	0.076	-53					
26.6	0.0088	-159	0.675	150	350	144	100
24.4	0.0103	-151					
22.9	0.012	-147					
21.6	0.013	-138					
19.4	0.015	-116					
16.7	0.014	-107					
14.8	0.014	-114					
11.6	0.020	-103					
8.8	0.025	-97					
7.4	0.031	-92					
6.6	0.036	-85					
4.1	0.052	-69					

TABLE IV.- Concluded

ω, rad/sec	ϕ_o, rad	α_1, deg	M	Q, lb/ft^2	U, ft/sec	T_F, lb	T_R, lb
26.9	0.009	-162	0.75	117	397	128	100
24.8	0.011	-157					
22.9	0.013	-151					
21.5	0.014	-150					
19.4	0.016	-139					
16.7	0.018	-124					
14.7	0.020	-124					
12.0	0.025	-117					
9.3	0.033	-98					
7.0	0.042	-92					
3.5	0.076	-55					
26.6	0.008	-160	0.75	135	397	138	100
24.2	0.009	-154					
22.4	0.011	-151					
21.4	0.012	-147					
19.4	0.014	-138					
16.7	0.014	-119					
14.3	0.015	-120					
11.5	0.023	-104					
8.6	0.029	-100					
7.3	0.032	-89					
5.7	0.046	-82					
3.4	0.064	-56					
23.9	0.008	-153	0.75	152	397	145	100
22.9	0.009	-151					
21.7	0.009	-147					
20.0	0.010	-132					
17.7	0.011	-121					
15.7	0.012	-115					
13.8	0.012	-118					
11.2	0.016	-104					
8.7	0.021	-93					
7.0	0.026	-85					
6.2	0.030	-83					
5.0	0.040	-69					
3.9	0.043	-63					

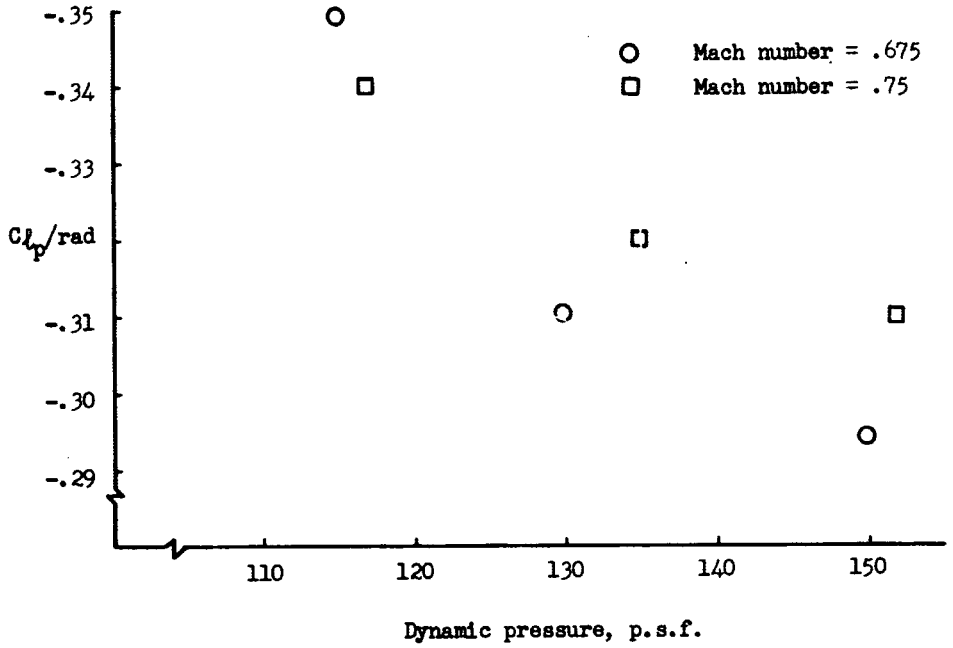

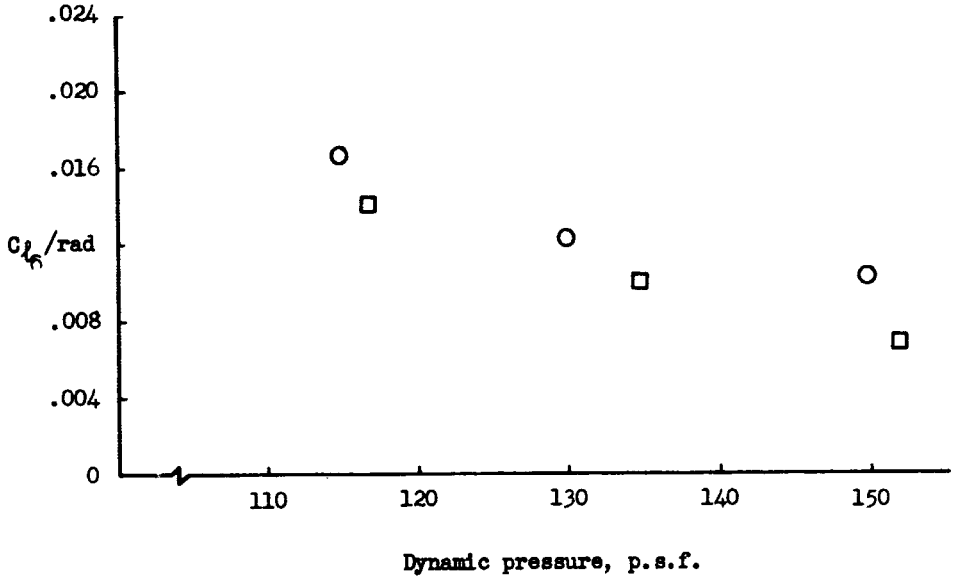

Figure 11.- Dynamic wind-tunnel experimental results.

$\alpha_{l_{\epsilon=0}}$ = measured phase angle

$\alpha_{l_{\epsilon}}$ = error in α_l

$\alpha_{l_{\epsilon\neq0}}$ = measured phase angle with error

and

$$\epsilon_{\phi} = 0.01, 0.02, 0.03, 0.04, 0.05$$

$$\alpha_{l_{\epsilon}} = 1^{\circ}, 2^{\circ}, 2^{\circ}, 4^{\circ}, 5^{\circ}$$

Equation (42) is solved for the aerodynamic derivatives based on the response measurements with errors. These results are presented in Table V. Amplitude errors of the form ϵ_{ϕ} are normally associated with instrument calibration errors. Numerical results show that ϵ_{ϕ} does not affect C_{l_p} and appears to have a one to one effect on C_{l_δ}. $\alpha_{l_{\epsilon}}$ is associated with errors due to the sin-cosine resolver. Phase angles determined with this equipment were repeated several times at each frequency, and the repeatability was normally within 1° to 3°. Numerical results show that phase errors affect C_{l_δ} slightly and C_{l_p} about 2 per cent per degree of error depending on the dynamic pressure. In general, this simplified analysis shows that realistic values of response errors ($\epsilon_{\phi} \leq 0.05$, $\alpha_{l_{\epsilon}} \leq 3^{\circ}$) predict results within about 5 per cent accuracy.

4.3.3 Comparison of Experimental Results

A comparison of the aileron derivative C_{l_δ}, measured both statically and dynamically, is presented in Figure 12. Results are presented in terms of C_{l_δ} versus model dynamic pressures at Mach

TABLE V.- ROLL RESPONSE ERROR ANALYSIS

c_{ϕ}, of ϕ	C_{l_p}/rad	C_{l_δ}/rad	α_{l_ϵ}, deg	C_{l_p}/rad	C_{l_δ}/rad	M	Q, psf
0	-0.349	0.0166	0	-0.349	0.0166	0.675	115
1.0	-0.349	0.0168	1.0	-0.356	0.0168		
2.0	-0.349	0.0169	2.0				
3.0	-0.349	0.0171	3.0	-0.369	0.0171		
4.0	-0.349	0.0173	4.0	-0.375	0.0173		
5.0	-0.349	0.0174	5.0	-0.381	0.0174		
0	-0.310	0.0123	0	-0.310	0.0123	0.675	130
1.0	-0.310	0.0124	1.0	-0.313	0.0123		
2.0	-0.310	0.0125	2.0	-0.316	0.0124		
3.0	-0.310	0.0126	3.0	-0.318	0.0124		
4.0	-0.310	0.0128	4.0	-0.319	0.0124		
5.0	-0.310	0.0129	5.0	-0.321	0.0124		
0	-0.294	0.0104	0	-0.294	0.0104	0.675	150
1.0	-0.294	0.0105	1.0	-0.300	0.0105		
2.0	-0.294	0.0106	2.0	-0.306	0.0106		
3.0	-0.294	0.0107	3.0	-0.311	0.0107		
4.0	-0.294	0.0108	4.0	-0.317	0.0108		
5.0	-0.294	0.0109	5.0	-0.321	0.0109		

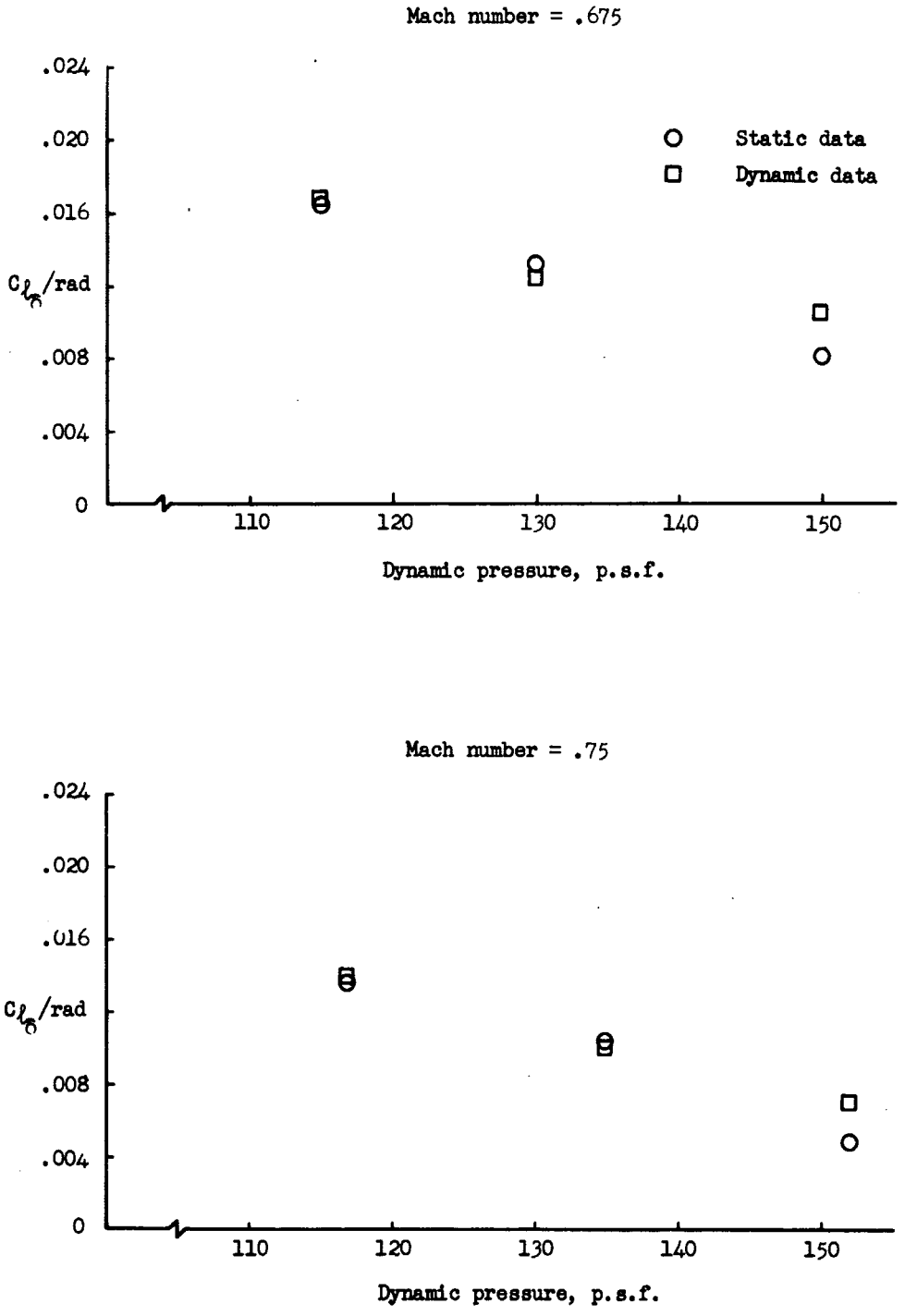

Figure 12.- Comparison of static and dynamic experimental results.

numbers 0.675 and 0.75. Note the close correlation between static and dynamic results at all but the higher dynamic pressures. These results tend to confirm the assumption made earlier: that as the ailerons become less effective, the dynamic motion can no longer be approximated by a single-degree-of-freedom solution. Since C_{l_p} cannot be measured statically, experimental data are not available for a comparison of the damping-in-roll derivative.

The reversal boundary was also determined statically at Mach numbers 0.675 and 0.75 using the two-cable mount. These results are presented in Figure 9 to give comparison of static testing procedures using both the sting-pylon-spring and two-cable mounts. Note the extremely close comparison of results between the two mounts for determining reversal dynamic pressure.

CHAPTER V

SUMMARY AND CONCLUSIONS

A new wind-tunnel technique for measuring various aerodynamic derivatives of an aeroelastic model has been presented. The technique applies free-flight procedures to a model flown in the wind tunnel on the two-cable-mount system. The complete equations of motion have been derived in terms of model properties, mount geometry, and aerodynamic derivatives.

In the case of the longitudinal equations of motion, it is theoretically possible to uniquely determine each of the aerodynamic derivatives by measuring the model response to a steady-state sinusoidal oscillation of the horizontal tail. In the determination of the derivatives from model test data a least-squares procedure is used to solve the set of redundant equations generated. A numerical example has shown that the derivatives can be determined uniquely only if exact response data are analyzed. The derivatives C_{L_α}, C_{m_α}, C_{m_δ}, and $(C_{m_{\dot\alpha}} + C_{m_\vartheta})$ can be predicted with significant accuracy using this technique. An alternate static method to measure C_D has been presented. The assumption that $C_{L_\delta} = -\frac{C_{m_\delta}\bar{c}}{L_t}$ provides an estimate for C_{L_δ}. A comparison between flight and wind-tunnel equations shows that, due to the added mount system restraints, the equations can be solved for each of the derivatives uniquely. However, introduction of an error into the model response causes the solution to become ill-conditioned resulting in equations quite similar to those used for determining the aerodynamic derivatives in free flight.

In the lateral equations of motion a basic free-flight assumption of single-degree-of-freedom response in roll allows the experimental verification of the dynamic approach to derivative measurements. The model in the wind tunnel can be forced to behave in a similar fashion by the proper selection of mount system parameters. The derivatives C_{l_δ} and C_{l_p} can be determined by measuring the dynamic model response to a steady-state sinusoidal oscillation of the ailerons. Experimental results obtained on a 1/19-size aeroelastically scaled model, tested both statically and dynamically in the wind tunnel to determine C_{l_δ}, verifies the application of this new testing procedure.

It has been shown that by means of a rather simple two-cable-mount system the dynamic characteristics of an aircraft can be closely simulated, allowing the use of free-flight techniques to estimate the aerodynamic derivatives of an aircraft in the early design stages. Application of the analysis presented in this thesis should assist in developing testing techniques required to satisfy specific research programs.

REFERENCES

1. Etkin, B.: Dynamics of Flight, Stability, and Control. John Wiley and Son, Inc., 1959.

2. Greenburg, H.: A Survey of Methods for Determining Stability Parameters of an Airplane From Dynamic Flight Measurements. NACA TN 2340, 1951.

3. Grosser, W. F.: A Transonic Speed Wind Tunnel Investigation of the Rolling Effectiveness of a Large Swept Wing Transport Aircraft With Conventional Type Ailerons and Various Spoiler Configurations. AIAA Paper No. 65-787, November 1965.

4. Reed, W. H., III and Abbott, F. T., Jr.: A New "Free-Flight" Mount System for High Speed Wind-Tunnel Flutter Models. Proceedings of the Symposium on Aeroelastic Dynamic Modeling Technology, U.S. Air Force Systems Command, RTD-TDR-63-2197, Part I (1964).

5. Seckel, E.: Stability and Control of Airplanes and Helicopters. Academic Press, 1964.

APPENDIX A

MOUNT RESTRAINT INFLUENCE COEFFICIENTS

Vertical Translation

As shown in Figure 3 the cable configuration analyzed has a vertical forward cable and horizontal rear cable. The linearized mount stiffness due to small perturbations about a trim point will be determined. A diagram of the forward pulley configuration is shown in sketch (1A).

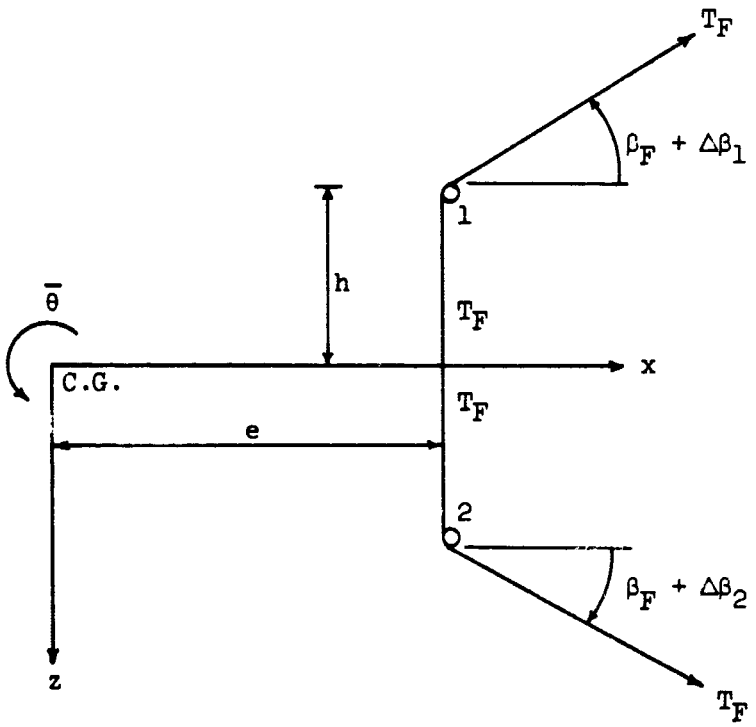

Sketch (1A)

The Z force at each pulley due to a z displacement is

$$Z_1 = -T_F \sin(\beta_F + \Delta\beta_1) + T_F$$

$$Z_2 = T_F \sin(\beta_F + \Delta\beta_2) - T_F \qquad \text{(A-1)}$$

Since all displacements are small perturbations about the trim point

$$Z_1 + Z_2 = T_F(\Delta\beta_2 - \Delta\beta_1)\cos\beta_F \qquad \text{(A-2)}$$

$\Delta\beta_1$ and $\Delta\beta_2$ are composed of angular changes due to displacements in the x and z directions.

x displacement:

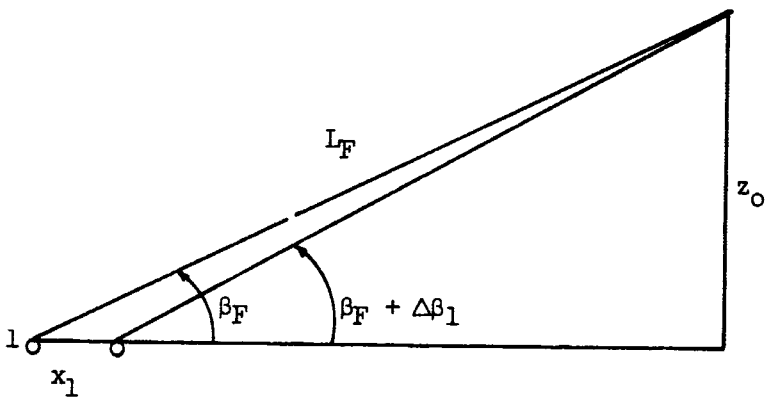

$$x_1 << L_F$$

From the geometry

$$z_o = \frac{x_1 \sin\beta_F \sin(\beta_F + \Delta\beta_1)}{\sin(\beta_F + \Delta\beta_1 - \beta_F)}$$

$$z_o = \frac{x_1 \sin\beta_F \sin(\beta_F + \Delta\beta_1)}{\sin(\Delta\beta_1)}$$

For small perturbations

$$\sin \Delta\beta_1 = \Delta\beta_1$$

$$\sin(\beta_F + \Delta\beta_1) = \frac{z_o}{L_F}$$

hence,

$$\Delta\beta_1 = \frac{x_1}{L_F} \sin \beta_F \qquad \text{(A-3)}$$

z displacement:

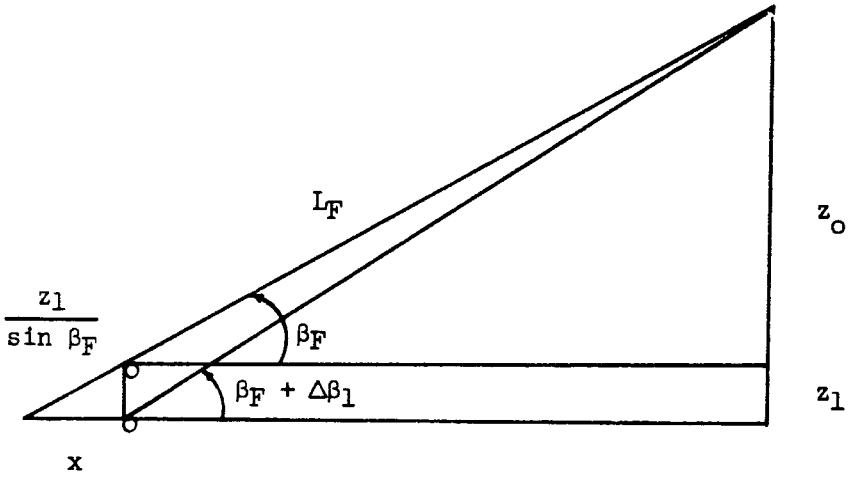

$$z_1 << z_o$$

From the geometry

$$z_o + z_1 = \frac{x \sin \beta_F \sin(\beta_F + \Delta\beta_1)}{\sin \Delta\beta_1}$$

and

$$\cos \beta_F = \frac{x}{z_1} \sin \beta_F$$

For small perturbations

$$\sin(\beta_F + \Delta\beta_1) = \frac{z_o + z_1}{L_F}$$

hence

$$\Delta\beta_1 = \frac{z_1}{L_F} \cos \beta_F \tag{A-4}$$

Therefore, the total $\Delta\beta_1$ due to an x and z displacement is

$$\Delta\beta_1 = \frac{x_1 \sin \beta_F + z_1 \cos \beta_F}{L_F} \tag{A-5}$$

In a similar manner it can be shown that

$$\Delta\beta_2 = \frac{x_2 \sin \beta_F - z_2 \cos \beta_F}{L_F} \tag{A-6}$$

Pulley movements due to z and $\bar{\theta}$ displacement (sketch(1A)) are as follows:

$$\begin{aligned} x_1 &= -h\bar{\theta} & z_1 &= z - e\bar{\theta} \\ x_2 &= h\bar{\theta} & z_2 &= z - e\bar{\theta} \end{aligned} \tag{A-7}$$

Substituting equations (A-5), (A-6), and (A-7) into (A-2) gives

$$Z_1 + Z_2 = - \frac{2T_F}{L_F} \cos \beta_F \left[-h\bar{\theta} \sin \beta_F + z \cos \beta_F - e\bar{\theta} \cos \beta_F\right] \tag{A-8}$$

A diagram of the rear pulleys is given in sketch (2A)

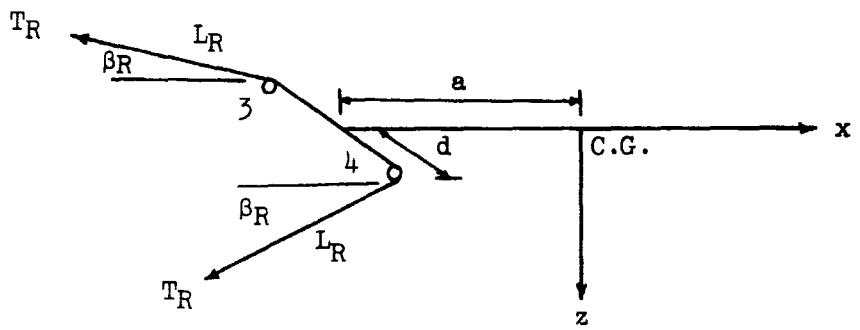

Sketch (2A)

The vertical force at each of the rear pulleys due to a z displacement is

$$Z_3 = -\frac{T_R z_3}{L_R} \qquad Z_4 = -\frac{T_R z_4}{L_R} \tag{A-9}$$

The rear pulley displacements are (sketch (2A))

$$z_3 = z + a\bar{\theta} \qquad z_4 = z + a\bar{\theta} \tag{A-10}$$

Therefore,

$$Z_3 + Z_4 = -\frac{2T_R}{L_R}(z + a\bar{\theta}) \tag{A-11}$$

The sum of the vertical forces at each of the pulleys ((A-11) and (A-8)) due to a z and $\bar{\theta}$ displacement is

$$Z_C = Z_1 + Z_2 + Z_3 + Z_4$$

or

$$Z_C = -2z\left[\frac{T_F}{L_F}\cos^2\beta_F + \frac{T_R}{L_R}\right] + 2\bar{\theta}\left[\frac{T_F}{L_F}\, h \cos\beta_F \sin\beta_F + \frac{T_F}{L_F}\, e \cos^2\beta_F - a\,\frac{T_R}{L_R}\right] \tag{A-12}$$

Since $\bar{\theta} = \theta + \theta_t$, we can express equation (A-12) in stiffness-influence coefficient form as

$$Z_C = Z_{C_o} - K_{ZZ}z - K_{Z\theta}\theta \tag{A-13}$$

Where

$$K_{ZZ} = 2\left[\frac{T_F}{L_F}\cos^2\beta_F + \frac{T_R}{L_R}\right] \tag{A-14}$$

$$K_{Z\theta} = 2\left[a\,\frac{T_R}{L_R} - h\,\frac{T_F}{L_F}\cos\beta_F \sin\beta_F - e\,\frac{T_F}{L_F}\cos^2\beta_F\right] \tag{A-15}$$

$$Z_{C_o} = -K_{\theta Z}\theta_t \tag{A-16}$$

Pitch

The forces producing moments about the center of gravity from the forward cable are (sketch (1A)):

$$Z_1 = -T_F \sin(\beta_F + \Delta\beta_1)$$

$$Z_2 = T_F \sin(\beta_F + \Delta\beta_2)$$

$$X_1 = T_F \cos(\beta_F + \Delta\beta_1) \qquad \text{(A-17)}$$

$$X_2 = T_F \cos(\beta_F + \Delta\beta_2)$$

For a positive z, $\bar{\theta}$ displacement, the moment produced by the forward cable is

$$M_{C_F} = -Z_1(e - h\bar{\theta}) - Z_2(e + h\bar{\theta}) - X_1(h + e\bar{\theta}) + X_2(h - e\bar{\theta}) \qquad \text{(A-18)}$$

Substituting equations (A-5), (A-6), (A-7), and (A-17) into equation (A-18) and simplifying gives

$$M_{C_F} = 2T_F\bar{\theta}\left[-h \sin \beta_F - e \cos \beta_F - \frac{(e \cos \beta_F + h \sin \beta_F)^2}{I_F}\right] + \frac{2T_F z}{L_F}\left[e \cos^2\beta_F + h \sin \beta_F \cos \beta_F\right] \qquad \text{(A-19)}$$

The forces producing moments about the center of gravity from the rear cable are (sketch (2A)):

$$Z_3 = -\frac{T_R z_3}{L_R}$$

$$Z_4 = -\frac{T_R z_4}{L_R} \qquad \text{(A-20)}$$

$$X_3 = -T_R \cos \beta_R$$

$$X_4 = -T_R \cos \beta_R$$

The pulley displacements due to a positive z, $\bar{\theta}$ displacement are

$$z_3 = z_4 = z + a\bar{\theta}$$

$$x_3 = x_4 = a \qquad \text{(A-21)}$$

The moment about the center of gravity produced by the rear cable is

$$M_{C_R} = Z_3 a + Z_4 a + X_3 a\bar{\theta} + X_4 a\bar{\theta} \qquad \text{(A-22)}$$

Substituting (A-20), (A-21), into (A-22) and simplifying, results in

$$M_{C_R} = 2\bar{\theta}\left[-\frac{a^2 T_R}{L_R} - aT_R \cos \beta_R\right] + 2z\left[-\frac{aT_R}{L_R}\right] \qquad \text{(A-23)}$$

The total moment

$$M_C = M_{C_F} + M_{C_R}$$

Hence,

$$M_C = 2\bar{\theta}\left[-\frac{a^2T_R}{L_R} - aT_R\cos\beta_R - T_F\left[h\sin\beta_F + e\cos\beta_F + \frac{1}{L_F}(e\cos\beta_F + h\sin\beta_F)^2\right]\right] + 2z\left[-\frac{aT_R}{L_R} + \frac{T_F}{L_F}(e\cos^2\beta_F + h\sin\beta_F\cos\beta_F)\right] \tag{A-24}$$

As before, $\bar{\theta} = \theta + \theta_t$ and we can express equation (A-24) in stiffness-influence coefficient form as

$$M_C = M_{C_o} - K_{\theta Z}z - K_{\theta\theta}\theta \tag{A-25}$$

Where

$$M_{C_o} = -K_{\theta\theta}\theta_t$$

$$K_{\theta Z} = \frac{2aT_R}{L_R} - \frac{2T_F}{L_F}(e\cos^2\beta_F + h\sin\beta_F\cos\beta_F)$$

$$K_{\theta\theta} = \frac{2a^2T_R}{L_R} + 2aT_R\cos\beta_R + 2T_F\left[h\sin\beta_F + e\cos\beta_F + \frac{1}{L_F}(e\cos\beta_F + h\sin\beta_F)^2\right]$$

Note that for small perturbation theory $K_{Z\theta} = K_{\theta Z}$. Equations (A-13) and (A-25) completely define the mount system restraints in terms of

known and measured quantities. Therefore, it has been shown that in the longitudinal case the cable restraints can be defined as follows:

$$Z_C = Z_{C_o} - K_{ZZ}z - K_{Z\theta}\theta$$

$$M_C = M_{C_o} - K_{\theta Z}z - K_{\theta\theta}\theta$$

where

$$K_{ZZ} = 2\left(\frac{T_F}{L_F}\cos^2\beta_F + \frac{T_R}{L_R}\right)$$

$$K_{Z\theta} = 2\left(\frac{aT_R}{L_R} - \frac{hT_F}{L_F}\cos\beta_F \sin\beta_F - \frac{eT_F}{L_F}\cos^2\beta_F\right)$$

$$K_{\theta\theta} = \frac{2a^2T_R}{L_R} + 2aT_R\cos\beta_R + 2T_F\left[h\sin\beta_F + e\cos\beta_F + \frac{1}{L_F}(e\cos\beta_F + h\sin\beta_F)^2\right]$$

$$Z_{C_o} = -K_{Z\theta}\theta_t$$

$$M_{C_o} = -K_{\theta\theta}\theta_t$$

In a similar manner (Ref. 4) the lateral restraints can be derived in the form

$$L_C = -K_{\phi Y}y - K_{\phi\phi}\phi - K_{\phi\psi}\psi$$

$$N_C = -K_{\psi Y}y - K_{\psi\phi}\phi - K_{\psi\psi}\psi$$

$$Y_C = -K_{YY}y - K_{Y\phi}\phi - K_{Y\psi}\psi$$

Where

$$K_{YY} = \frac{2T_F}{L_F} + \frac{2T_R}{L_R}\cos^2\beta_R$$

$$K_{Y\phi} = 0$$

$$K_{Y\psi} = \frac{2eT_F}{L_F} - \frac{2T_R}{L_R}\cos\beta_R(d\sin\beta_R + a\cos\beta_R)$$

$$K_{\phi Y} = K_{Y\phi} = 0$$

$$K_{\phi\phi} = 2hT_F\left(\frac{h}{L_F} + \sin\beta_F\right) + 2dT_r\left(\frac{d}{L_R} + \sin\beta_R\right)$$

$$K_{\phi\psi} = 0$$

$$K_{\psi\phi} = K_{\phi\psi} = 0$$

$$K_{\psi Y} = K_{Y\psi}$$

$$K_{\psi\psi} = 2eT_F\left(\frac{e}{L_F} + \cos\beta_F\right) + 2T_R\left[a\cos\beta_R + d\sin\beta_R + \frac{1}{L_R}(a\cos\beta_F \cdot d\sin\beta_R)^2\right]$$

APPENDIX B

LEAST-SQUARES SOLUTION OF REDUNDANT LINEAR EQUATIONS

General Solution

Given at set of N equations in M unknowns

$$\begin{aligned} Y_1 &= A_{11}X_1 + A_{12}X_2 + A_{13}X_3 + \ldots A_{1m}X_m \\ Y_2 &= A_{21}X_1 + A_{22}X_2 + A_{23}X_3 + \ldots A_{2m}X_m \\ &\vdots \\ Y_N &= A_{N1}X_1 + A_{N2}X_2 + A_{N3}X_3 + \ldots A_{NM}X_M \quad N > M \end{aligned} \tag{B-1}$$

Equations (B-1) can be written in the form

$$Y_i = \sum_{m=1}^{M} A_{im}X_m \qquad i = 1,2,3, \ldots N \tag{B-2}$$

We wish to solve for $(X_1, X_2, \ldots X_m)$ given $(Y_i, i = 1,2, \ldots N;$ $A_{im}, m = 1,2, \ldots M)$. Choose $(X_1, X_2, \ldots X_m)$ so that the sum of the squares of the deviations is as small as possible. Where

$$V_i = \sum_{m=1}^{M} (A_{im}X_m - Y_i)$$

is the deviation. Therefore,

$$E = \sum_{i=1}^{N} (V_i)^2 = \sum_{i=1}^{N} \left[\sum_{m=1}^{M} A_{im}X_m - Y_i \right]^2$$

is to be minimized. Hence,

$$\frac{\partial E}{\partial X_k} = 0$$

where

$$k = 1,2,3, \ldots M$$

$$\frac{\partial E}{\partial x_k} = 2 \sum_{i=1}^{N} \left[\sum_{m=1}^{M} (A_{im}X_m - Y_i) \right] \frac{\partial X_m}{\partial x_k} A_{im} = 0$$

Therefore,

$$\sum_{i=1}^{N} \left[\sum_{m=1}^{M} A_{im}X_m \right] \frac{\partial X_m}{\partial X_k} A_{im} = \sum_{i=1}^{N} Y_i \frac{\partial X_m}{\partial X_k} A_{im}$$

$$\frac{\partial X_m}{\partial X_k} = 1 \qquad m = k$$

$$= 0 \qquad m \neq k$$

Hence

$$\sum_{i=1}^{N} \left[\sum_{m=1}^{M} A_{im}X_m \right] A_{ik} = \sum_{i=1}^{N} Y_i A_{ik} \qquad \text{(B-3)}$$

Equation (B-3) results in M equations which are solved simultaneously for $X_1, X_2, X_3, \ldots X_m$.

Complex Solution

If the Y's and A's are complex, define

$$E = \sum_{i=1}^{N} |V_i|^2 = \sum_{i=1}^{N} \left| \sum_{m=1}^{M} A_{im}X_m - Y_i \right|^2 \qquad \text{(B-4)}$$

where

$$Y_i = Y_{i_{real}} + iY_{i_{imag}}.$$

$$A_{im} = A_{im_{real}} + iA_{im_{imag}}.$$

also, the complex conjugates of these quantities are

$$Y_i^* = Y_{i_{real}} - iY_{i_{imag}}.$$

$$A_{im}^* = A_{im_{real}} - iA_{im_{imag}}.$$

Therefore, equation (B-4) is written

$$E = \sum_{i=1}^{N} \left(\sum_{m=1}^{M} A_{im}X_m - Y_i \right) \left(\sum_{m=1}^{M} A_{im}^* X_m - Y_i^* \right)$$

which is to be minimized. Therefore,

$$\frac{\partial E}{\partial X_k} = 0 \qquad k = 1,2,3, \ldots M$$

$$\frac{\partial X_m}{\partial X_k} = 0 \qquad m = k$$

$$= 0 \qquad m \neq k$$

Hence,

$$\sum_{i=1}^{N}\left[\left(\sum_{m=1}^{M} A_{im}X_m\right)A_{ik}^* + \left(\sum_{m=1}^{M} A_{im}^*X_m\right)A_{ik}\right] = \sum_{i=1}^{N}\left(Y_i^*A_{ik} + Y_i^*A_{ik}\right) \tag{B-5}$$

Equation (B-5) results in M <u>real</u> equations which are solved for $X_1, X_2, X_3, \ldots X_M$.

Example: M = 3

k = 1

$$\sum_{i=1}^{N}\left[(A_{i1}X_1 + A_{i2}X_2 + A_{i3}X_3)A_{i1}^* + (A_{i1}^*X_1 + A_{i2}^*X_2 + A_{i3}^*X_3)A_{i1}\right] = \sum_{i=1}^{N}\left(Y_iA_{i1}^* + Y_iA_{i1}^*\right)$$

$$\therefore 2X_1\sum_{i=1}^{N}|A_{i1}|^2 + X_2\sum_{i=1}^{N}\left(A_{i1}^*A_{i2} + A_{i1}A_{i2}^*\right) + X_3\sum_{i=1}^{N}\left(A_{i1}^*A_{i3} + A_{i1}A_{i3}^*\right) = \sum_{i=1}^{N}\left(Y_i^*A_{i1} + Y_iA_{i1}^*\right)$$

Similarly for $k = 2$, $k = 3$

$$X_1 \sum_{i=1}^{N} (A_{i1}^* A_{i2} + A_{i1} A_{i2}^*) + 2X_2 \sum_{i=1}^{N} |A_{i2}|^2 + X_3 \sum_{i=1}^{N} (A_{i2}^* A_{i3} + A_{i2} A_{i3}^*) = \sum_{i=1}^{N} (Y_i^* A_{i2} + Y_i A_{i2}^*)$$

$$X_1 \sum_{i=1}^{N} (A_{i1}^* A_{i3} + A_{i1} A_{i3}^*) + X_2 \sum_{i=1}^{N} (A_{i2}^* A_{i3} + A_{i2} A_{i3}^*) + 2X_3 \sum_{i=1}^{N} |A_{i3}|^2 = \sum_{i=1}^{N} (Y_i^* A_{i3} + Y_i A_{i3}^*)$$

In determinant form

$$\begin{bmatrix} 2\sum_{i=1}^{N} |A_{i1}|^2 & \sum_{i=1}^{N} (A_{i1}^* A_{i2} + A_{i1} A_{i2}^*) & \sum_{i=1}^{N} (A_{i1}^* A_{i3} + A_{i1} A_{i3}^*) \\ \sum_{i=1}^{N} (A_{i1}^* A_{i2} + A_{i1} A_{i2}^*) & 2\sum_{i=1}^{N} |A_{i2}|^2 & \sum_{i=1}^{N} (A_{i2}^* A_{i3} + A_{i2} A_{i3}^*) \\ \sum_{i=1}^{N} (A_{i1}^* A_{i3} + A_{i1} A_{i3}^*) & \sum_{i=1}^{N} (A_{i2}^* A_{i3} + A_{i2} A_{i3}^*) & 2\sum_{i=1}^{N} |A_{i3}|^2 \end{bmatrix} \begin{bmatrix} X_1 \\ X_2 \\ X_3 \end{bmatrix} = \begin{bmatrix} \sum_{i=1}^{N} (Y_i^* A_{i1} + Y_i A_{i1}^*) \\ \sum_{i=1}^{N} (Y_i^* A_{i1} + Y_i A_{i1}^*) \\ \sum_{i=1}^{N} (Y_i^* A_{i3} + Y_i A_{i3}^*) \end{bmatrix}$$

APPENDIX C

COMPUTER PROGRAMS

Model Response

Assuming sinusoidal motion in the form $z(t) = z_o e^{i(\omega t+\phi_1)}$, $\theta(t) = \theta_o e^{i(\omega t+\phi_2)}$ equations (17a) and (17b) can be written.

Vertical translation:

$$z_o e^{i\phi_1}\left[(-\omega^2 m + K_{ZZ}) + i\omega \frac{qS}{U}(C_{L_\alpha} + \text{-}D)\right] + \theta_o e^{i\phi_2} qSC_{L_\alpha} = -qSC_{L_\delta}\delta_o$$

Pitch:

$$z_o e^{i\phi_1}\left[\frac{qS\bar{c}^2\omega^2}{2U^2} C_{m_{\dot\alpha}} - i\omega \frac{qS\bar{c}}{U} C_{m_\alpha}\right] + \theta_o e^{i\phi_2}\left[-I_Y\omega^2 - qS\bar{c}C_{m_\alpha} + K_{\theta\theta}\right.$$

$$\left. - i\omega \frac{qS\bar{c}^2}{2U}(C_{m_{\dot\alpha}} + C_{m_{\dot\vartheta}})\right] = qS\bar{c}C_{m_\delta}\delta_o$$

The equations above can be written in the form

$$z_o e^{i\phi_1}\left[A_1 + iB_1\right] + \theta_o e^{i\phi_2}\left[A_2\right] = F_o \qquad \text{(C-1)}$$

$$z_o e^{i\phi_1}\left[A_3 + iB_3\right] + \theta_o e^{i\phi_2}\left[A_4 + iB_4\right] = M_o \qquad \text{(C-2)}$$

Where

$$A_1 = -\omega^2 m + K_{ZZ} \qquad A_3 = \frac{qS\bar{c}^2\omega^2}{2U^2} C_{m_{\dot{\alpha}}}$$

$$B_1 = \omega \frac{qS}{U}(C_{L_\alpha} + C_D) \qquad B_3 = -\omega \frac{qS\bar{c}}{U} C_{m_\alpha}$$

$$A_2 = qSC_{L_\alpha} \qquad A_4 = -I_Y\omega^2 - qS\bar{c}C_{m_{\dot{\alpha}}} + K_{\theta\theta}$$

$$F_o = -qSC_{L_\delta}\delta_o \qquad B_4 = -\omega \frac{qS\bar{c}^2}{2U}(C_{m_{\dot{\alpha}}} + C_{m_{\dot{\theta}}})$$

$$M_o = qS\bar{c}C_{m_\delta}\delta_o$$

Applying Kramer's rule results in

$$z_o e^{i\phi_1} = \frac{\begin{vmatrix} F_o & A_2 \\ M_o & A_4 + iB_4 \end{vmatrix}}{D_r + iD_i}$$

$$\theta_o e^{i\phi_2} = \frac{\begin{vmatrix} A_1 + iB_1 & F_o \\ A_3 + iB_3 & M_o \end{vmatrix}}{D_r + iD_i}$$

Where

$$D_r = A_1A_4 - A_2A_3 - B_1B_4$$

$$D_i = A_1B_4 + A_4B_1 - A_2B_3$$

Each of the terms $z_o e^{i\phi_1}$ and $\theta_o e^{i\phi_2}$ can then be divided into the real and imaginary parts z_o, θ_o, ϕ_1, and ϕ_2. A_1, A_2, A_3, A_4, B_1, B_3, and B_4 are defined in the program listing. Once the values of the aerodynamic derivatives, model physical properties, and test conditions are selected equations (C-1) and (C-2) are solved simultaneously to determine the dynamic response z_o, θ_o, ϕ_1, and ϕ_2 as a function of ω. A sample program listing is presented.

Definition of terms:

M - mass of model, slugs

KZZ - vertical spring restraint, lb/ft

Q - dynamic pressure, psf

S - wing area, ft^2

U - wind-tunnel flow velocity, ft/sec

C - mean-aerodynamic chord, ft

IY - pitch inertia, $slug\text{-}ft^2$

CLA - lift curve slope C_{L_α}/rad

DC - drag coefficient C_D

CMADOT - $C_{m_{\dot{\alpha}}}$/rad

CMA - C_{m_α}/rad

CMQ - $C_{m_{\dot{\theta}}}$/rad

FO - $-qSC_{L_\delta}\delta_o$, lb

MO - $qS\bar{c}C_{m_\delta}\delta_o$, ft-lb

N - number of frequencies at which response is calculated

WW(I) - values of ω to be used to calculate response

A1 - A_1

A2 - A_2, etc.

Error Analysis

Equations (20) and (21) are programed in the following manner:

$$\begin{bmatrix} B(1,1) & B(1,2) & B(1,3) \\ B(2,1) & B(2,2) & B(2,3) \\ B(3,1) & B(3,2) & B(3,3) \end{bmatrix} \begin{bmatrix} C_{L_\alpha} \\ C_D \\ C_{L_\delta} \end{bmatrix} = \begin{bmatrix} B(1,4) \\ B(2,4) \\ B(3,4) \end{bmatrix} \qquad \text{(C-3)}$$

Where

$$B(1,1) = \sum_{j=1}^{N} \left|A_{j1}\right|^2 = (qS)^2 \sum_{j=1}^{N} \left[\theta_o^2 + \left(\frac{\omega z_o}{U}\right)^2 + \frac{2\omega z_o \theta_o}{U} \sin(\phi_2 - \phi_1)\right]_{\omega=\omega_j}$$

$$B(1,2) = \sum_{j=1}^{N} (A^*_{j1}A_{j2} + A_{j1}A^*_{j2}) = \frac{2(qS)^2}{U} \sum_{j=1}^{N} \left[\frac{(\omega z_o)^2}{U} + \omega z_o \theta_o \sin(\phi_2 - \phi_1)\right]_{\omega=\omega_j}$$

$$B(1,3) = \sum_{j=1}^{N} (A^*_{j1}A_{j3} + A_{j1}A^*_{j3}) = 2q^2S^2\delta_o \sum_{j=1}^{N} \left[\theta_o \cos\phi_2 - \frac{\omega z_o}{U} \sin\phi_1\right]_{\omega=\omega_j}$$

$$B(1,4) = \sum_{j=1}^{N} (b^*_j A_{j1} + b_j A^*_{j1}) = 2qS \sum_{j=1}^{N} \left[(m\omega^2 - K_{ZZ}) z_o \theta_o \cos(\phi_2 - \phi_1)\right]_{\omega=\omega_j}$$

$$\begin{bmatrix} A(1,1) & A(1,2) & A(1,3) & A(1,4) \\ A(2,1) & A(2,2) & A(2,3) & A(2,4) \\ A(3,1) & A(3,2) & A(3,3) & A(3,4) \\ A(4,1) & A(4,2) & A(4,3) & A(4,4) \end{bmatrix} \begin{bmatrix} C_{m_{\dot{\theta}}} \\ C_{m_{\dot{\alpha}}} \\ C_{m_{\alpha}} \\ C_{m_{\delta}} \end{bmatrix} = \begin{bmatrix} A(1,5) \\ A(2,5) \\ A(3,5) \\ A(4,5) \end{bmatrix} \qquad (C\text{-}4)$$

Where

$$A(1,1) = \sum_{j=1}^{N} \left| g_{j1} \right|^2 = \left(\frac{qS\bar{c}^2}{2U} \right)^2 \sum_{j=1}^{N} \left[\omega\theta_o \right]^2_{\omega=\omega_j}$$

$$A(1,2) = \sum_{j=1}^{N} \left(g^*_{j1} g_{j2} + g_{j1} g^*_{j2} \right) = 2\left(\frac{qS\bar{c}^2}{2U} \right)^2 \sum_{j=1}^{N} \left[\theta_o^2 + \frac{\omega\theta_o z_o}{U} \sin(\phi_2 - \phi_1) \right]_{\omega=\omega_j} (\omega_j)^2$$

$$A(1,3) = \sum_{j=1}^{N} \left(g^*_{j1} g_{j3} + g_{j1} g^*_{j3} \right) = \frac{2q^2 S^2 \bar{c}^3}{2U^2} \sum_{j=1}^{N} \left[\omega^2 \theta_o z_o \cos(\phi_1 - \phi_2) \right]_{\omega=\omega_j}$$

$$A(1,4) = \sum_{j=1}^{N} \left(g^*_{j1} g_{j4} + g_{j1} g^*_{j4} \right) = - \frac{2q^2 S^2 \bar{c}^3 \delta_o}{2U} \sum_{j=1}^{N} \left[\omega\theta_o \sin \phi_2 \right]_{\omega=\omega_j}$$

$$A(1,5) = \sum_{j=1}^{N} \left(h^*_j g_{j1} + h_j g^*_{j1} \right) = 0$$

The program generates the coefficients A(i,j), B(i,j) based on the test conditions, model properties, and model dynamic response. The effect of an error in response is introduced by considering

$$z_{o_{\epsilon\neq 0}} = z_{o_{\epsilon=0}}(1 + \Delta\epsilon_Z)$$

$$\theta_{o_{\epsilon\neq 0}} = \theta_{o_{\epsilon=0}}(1 + \Delta\epsilon_\theta)$$

$$\phi_{1_{\epsilon\neq 0}} = \phi_{1_{\epsilon=0}} + \Delta\epsilon\phi_1$$

$$\phi_{2_{\epsilon\neq 0}} = \phi_{2_{\epsilon=0}} + \Delta\epsilon\phi_2$$

Next, the program solves equations (C-3) and (C-4) separately for the value of each aerodynamic derivative with response errors included. (The equations are solved by a library subroutine called MATRIX.)
A sample program listing is presented.
Definition of terms:

U - wind-tunnel flow velocity, fps

Q - dynamic pressure, psf

S - wing area, ft^2

M - model mass, slugs

C - mean aerodynamic chord, ft

IY - pitch inertia, $slug\text{-}ft^2$

KZZ - vertical mount restraint, lb/ft

KTT - pitch mount restraint $K_{\theta\theta}$, ft-lb/rad

DELT - tail angle δ_o, rad

ZE - $\Delta\epsilon_Z$

TE - $\Delta\epsilon_\theta$

PIE - $\Delta\epsilon_{\phi_1}$

P2E - $\Delta\epsilon_{\phi_2}$

K - program code
- 0 new test case
- 1 new error function
- 2 stop

N - number of response data to be analyzed

W(I) - values of tail frequency

ZO(I) - values of response z_o

THETAO(I) - values of response θ_o

PHI1(I) - values of phase angle ϕ_1

PHI2(I) - values of phase angle ϕ_2

MATRIX - solves equations (C-3) and (C-4)

MODEL RESPONCE PROGRAM

```
      DIMENSION WW(100)
      REAL KZZ,KTT,M,M0,IY
    1 FORMAT(10F8.0)
      READ(5,1) M,KZZ,Q,S,U,C,IY,KTT,CLA,CD,CMADOT,CMA,CMQ
      PRINT 2
    2 FORMAT(25H I ABEL    AIL STOP  340//)
      READ(5,1) F0,M0
      PRINT 3,F0,M0
    3 FORMAT(/5H F0 =F10.4/5H M0 =F10.4//)
      PRINT 4
    4 FORMAT(16H OMEGA - RAD/SEC,8X,7HZ0 - FT,10X,12HTHETA0 - RAD,
     16X,10HPHI1 - DEG,6X,10HPHI2 - DEG//)
    5 FORMAT(I4)
    6 FORMAT(10F8.2)
      READ(5,5)N
      READ(5,6)(WW(I),I=1,N)
      I=0
    7 I=I+1
      W=WW(I)
      A1=KZZ-M*W**2
      B1=(CLA+CD)*W*Q* :/U
      A2=Q*S*CLA
      A3=Q*S*C**2*W**2*CMADOT/2.0/U**2
      B3=-W*Q*S*C*CMA/U
      A4=-IY*W**2+KTT-Q*S*C*CMA
      B4=-(CMADOT+CMQ)*W*Q*S*C**2/2./U
      DR=A1*A4-A2*A3-B1*B4
      DI=A1*B4+A4*B1-A2*B3
      Z0=SQRT((DR*(F0*A4-M0*A2)+DI*F0*B4)**2+(DR*F0*B4-DI*(F0*A4-M0*A2))
     1**2)/(DR**2+DI**2)
      PHI1=57.295780*ATAN2(DR*F0*B4-DI*(F0*A4-M0*A2),DR*(F0*A4-M0*A2)+DI
     1*F0*B4)
      THETA0=SQRT((DR*(M0*A1-F0*A3)+DI*(M0*B1-F0*B3))**2+(DR*(M0*B1-F0*
     1B3)-DI*(M0*A1-F0*A3))**2)/(DR**2+DI**2)
      PHI2=57.295780*ATAN2(DR*(M0*B1-F0*B3)-DI*(M0*A1-F0*A3),DR*(M0*A1-
     1F0*A3)+DI*(M0*B1-F0*B3))
      PRINT 8,W,Z0,THETA0,PHI1,PHI2
    8 FORMAT(4XF6.2,8X4E18.8)
      PUNCH 9,W,Z0,THETA0,PHI1,PHI2
    9 FORMAT(5E15.8)
      IF(I.LT.N) GO TO 7
      STOP
      END
```

ERROR ANALYSIS PROGRAM

```
      DIMENSION W(50),Z0(50),THETA0(50),PHI1(50),PHI2(50)
      DIMENSION A(4,5),B(3,4)
      REAL KZZ,KTT,M,IY
    1 FORMAT(5F15.8)
    3 FORMAT(30X,42H LONG. LEAST SQUARES SOLUTION - TAIL INPUT////)
    4 FORMAT(5H   U=F10.4,4X,5H   Q=F10.4,4X,5H   S=F10.4,4X,5H   M=F10.
     14,4X,5H   C=F10.4//5H  IY=F10.4,4X,5H KZZ=F10.4,4X,5H KTT=F10.4,4X
     2,5HDELT=F10.6,4X,5H  ZE=F10.4//5H  TE=F10.4,4X,5H P1E=F10.4,4X,5H
     3P2E=F10.4////)
    5 FORMAT(I4)
    6 FORMAT(5E15.8)
      PRINT 3
   20 READ(5,5)K
      IF(K.EQ.0) GO TO 14
      IF(K.EQ.1) GO TO 16
      IF(K.EQ.2) GO TO 1500
   14 READ(5,5)N
      DO 15 I=1,N
   15 READ(5,6) W(I),Z0(I),THETA0(I),PHI1(I),PHI2(I)
   16 READ(5,1) U,Q,S,M,C,IY,KZZ,KTT,DELT,ZE,TE,P1E,P2E
      PRINT 4,U,Q,S,M,C,IY,KZZ,KTT,DELT,ZE,TE,P1E,P2E
      N=1
      J=30
   11 DO 101 I1=1,4
      DO 101 J1=1,5
  101 A(I1,J1)=0.
      DO 102 I1=1,3
      DO 102 J1=1,4
  102 B(I1,J1)=0.
      PRINT 9,N,J
    9 FORMAT(3H N=I2,6X,2HJ=I2///)
      DO 100 I=N,J
      Z0(I)=(1.0+ZE)*Z0(I)
      THETA0(I)=(1.0+TE)*THETA0(I)
      PHI1(I)=P1E+PHI1(I)
      PHI2(I)=P2E+PHI2(I)
      A(1,1)=A(1,1)+(W(I)*THETA0(I))**2
      A(1,2)=A(1,2)+(THETA0(I)**2+W(I)*THETA0(I)*Z0(I)/U*SIN((PHI2(I)-PH
     1I1(I))/57.2958))*W(I)**2
      A(1,3)=A(1,3)+W(I)**2*THETA0(I)*Z0(I)*COS((PHI1(I)-PHI2(I))/57.295
     18)
      A(1,4)=A(1,4)+W(I)*THETA0(I)*SIN(PHI2(I)/57.2958)
      A(2,2)=A(2,2)+(THETA0(I)**2+(W(I)*Z0(I)/U)**2+2.0*THETA0(I)*Z0(I)*
     1W(I)/U*SIN((PHI2(I)-PHI1(I))/57.2958))*W(I)**2
```

```
      A(2,4)=A(2,4)+W(I)*THETA0(I)*SIN(PHI2(I)/57.2958)+W(I)**2*Z0(I)/U*
     1COS(PHI1(I)/57.2958)
      A(2,5)=A(2,5)+(IY*W(I)**2-KTT)*W(I)**2*Z0(I)*THETA0(I)/U*COS((PHI2
     1(I)-PHI1(I))/57.2958)
      A(3,3)=A(3,3)+THETA0(I)**2+(W(I)*Z0(I)/U)**2+2.0*THETA0(I)*Z0(I)*
     1W(I)/U*SIN((PHI2(I)-PHI1(I))/57.2958)
      A(3,4)=A(3,4)+THETA0(I)*COS(PHI2(I)/57.2958)-W(I)*Z0(I)/U*SIN(PHI1
     1(I)/57.2958)
      A(3,5)=A(3,5)+(IY*W(I)**2-KTT)*(THETA0(I)**2+W(I)*Z0(I)*THETA0(I)/
     1U*SIN((PHI2(I)-PHI1(I))/57.2958))
      A(4,4)=A(4,4)+(Q*S*C*DELT)**2
      A(4,5)=A(4,5)+(IY*W(I)**2-KTT)*THETA0(I)*COS(PHI2(I)/57.2958)
      B(1,1)=B(1,1)+THETA0(I)**2+(W(I)*Z0(I)/U)**2+2.0*W(I)*THETA0(I)*
     1Z0(I)/U*SIN((PHI2(I)-PHI1(I))/57.2958)
      B(1,2)=B(1,2)+W(I)**2*Z0(I)**2/U+W(I)*THETA0(I)*Z0(I)*SIN((PHI2(I)
     1-PHI1(I))/57.2958)
      B(1,3)=B(1,3)+THETA0(I)*COS(PHI2(I)/57.2958)-W(I)*Z0(I)/U*SIN(PHI1
     1(I)/57.2958)
      B(1,4)=B(1,4)+(M*W(I)**2-KZZ)*Z0(I)*THETA0(I)*COS((PHI2(I)-PHI1(I)
     1)/57.2958)
      B(2,2)=B(2,2)+(W(I)*Z0(I))**2
      B(2,3)=B(2,3)+W(I)*Z0(I)*SIN(PHI1(I)/57.2958)
      B(3,3)=B(3,3)+(Q*S*DELT)**2
      B(3,4)=B(3,4)+(M*W(I)**2-KZZ)*Z0(I)*COS(PHI1(I)/57.2958)
      Z0(I)=Z0(I)/(1.0+ZE)
      THETA0(I)=THETA0(I)/(1.0+TE)
      PHI1(I)=PHI1(I)-P1E
  100 PHI2(I)=PHI2(I)-P2E
      A(1,1)=A(1,1)*(Q*S*C**2/2.0/U)**2
      A(1,2)=A(1,2)*(Q*S*C**2/2.0/U)**2
      A(1,3)=A(1,3)*(Q**2*S**2*C**3/2.0/U**2)
      A(1,4)=A(1,4)*(-Q**2*S**2*C**3*DELT/2.0/U)
      A(2,1)=A(1,2)
      A(2,2)=A(2,2)*(Q*S*C**2/2.0/U)**2
      A(2,4)=A(2,4)*(-Q**2*S**2*C**3*DELT/2.0/U)
      A(2,5)=A(2,5)*Q*S*C**2/2.0/U
      A(3,1)=A(1,3)
      A(3,3)=A(3,3)*(Q*S*C)**2
      A(3,4)=A(3,4)*(Q*S*C)**2*DELT
      A(3,5)=A(3,5)*(-Q*S*C)
      A(4,1)=A(1,4)
      A(4,2)=A(2,4)
      A(4,3)=A(3,4)
      A(4,5)=A(4,5)*(-Q*S*C*DELT)
      B(1,1)=B(1,1)*(Q*S)**2
      B(1,2)=B(1,2)*(Q*S)**2/U
      B(1,3)=B(1,3)*(+Q*S)**2*DELT
```

```
      B(1,4)=B(1,4)*Q*S
      B(2,1)=B(1,2)
      B(2,2)=B(2,2)*(Q*S/U)**2
      B(2,3)=B(2,3)*(-Q*S)**2*DELT/U
      B(3,1)=B(1,3)
      B(3,2)=B(2,3)
      B(3,4)=B(3,4)*(Q*S*DELT)
      PRINT 400
  400 FORMAT(//9H A MATRIX//)
      PRINT 8,((A(I1,J1),J1=1,5),I1=1,4)
    8 FORMAT(5E16.8)
      PRINT 401
  401 FORMAT(//9H B MATRIX//)
      PRINT 10,((B(I1,J1),J1=1,4),I1=1,3)
   10 FORMAT(4E16.8)
      CALL MATRIX(10,4,5,0,A,4,DETERM)
      CALL MATRIX(10,3,4,0,B,3,DETERM)
      PRINT 7,A(1,5),A(2,5),A(3,5),A(4,5),B(1,4),B(2,4),B(3,4)
    7 FORMAT(5H CMQ=F10.4//8H CMADOT=F10.4//5H CMA=F10.4//7H CMDEL=F10.4
     1//5H CLA=F10.4//4H CD=F10.4//7H CLDEL=F10.4///)
      IF(J.GE.30) GO TO 20
 1500 STOP
      END
```